Scuola Universitaria Superiore IUSS Pavia

In proximity to DNA polymerase λ: discovering novel interactors through the BioID approach

And

Revealing Ellagitannins as potent and selective SGK1 inhibitors for targeted therapy

A Thesis Submitted in Partial Fulfilment of the Requirements
for the Degree of Doctor of Philosophy in

BIOMOLECULAR SCIENCES AND BIOTECHNOLOGY

Obtained in the framework of the Doctoral Programme in
Biomolecular Sciences and Biotechnology

by

Elena Bianchi

August, 2025

Scuola Universitaria Superiore IUSS Pavia

In proximity to DNA polymerase λ: discovering novel interactors through the BioID approach

And

Revealing Ellagitannins as potent and selective SGK1 inhibitors for targeted therapy

A Thesis Submitted in Partial Fulfilment of the Requirements
for the Degree of Doctor of Philosophy in

BIOMOLECULAR SCIENCES AND BIOTECHNOLOGY

Obtained in the framework of the Doctoral Programme in
Biomolecular Sciences and Biotechnology

by

Elena Bianchi

Supervisor: Dr. Emmanuele Crespan

Istituto di Genetica Molecolare, CNR, Via Abbiategrasso 207, 27100 Pavia, Italy

August, 2025

ABSTRACT

DNA polymerase λ (Pol λ) is a specialised enzyme involved in different DNA repair pathways, including classical Non-Homologous End Joining (NHEJ) and alternative double-strand break repair pathways, as well as in faithful Translesion synthesis (TLS) over 8-oxo-dG. The identification of Pol λ interactors poses significant challenges due to its transient interactions within repair/TLS pathways and the lack of specific and effective antibodies for IF and co-IP. To address this challenge, we have adopted a proximity-dependent biotinylation (BioID) approach. This exploits the activity of a mutant *A. aeolicus* biotin ligase BirA, which promiscuously biotinylates proximity proteins. A BirA_Pol λ construct was expressed in U2OS cells and biotinylated proteins were collected using streptavidin-coated beads and identified by mass spectrometry. As expected, we identified both known and novel Pol λ interactors involved in DNA repair and replication processes, as well as in telomeres metabolism and Alternative Lengthening of Telomeres (ALT) process, confirming our previous finding. In unperturbed conditions, we also identified several Pol λ interactors involved in nucleolar metabolism. These interactions were lost upon etoposide and hydroxyurea (HU) treatment, suggesting Pol λ re-localization at the lesions upon damage.

Distinct classes of enzymes are implicated in the initiation and progression of tumours. Kinases are involved in the onset and progression of many diseases, including cancer. Protein kinases play a pivotal role in cellular signalling under both physiological and pathological conditions. Serum- and glucocorticoid-inducible kinase 1 (SGK1) is a serine/threonine kinase implicated in various biological processes and diseases. SGK1 is found overexpressed in several types of cancer and its expression is dysregulated in conditions such as hypertension, diabetic neuropathy, ischaemia, and neurodegenerative disorders. Given its involvement in multiple pathologies, SGK1 represents a promising target for drug development.

Through *in silico* analyses, we have screened a panel of potential SGK1 inhibitors including several ellagitannins. These are polyphenolic compounds derived from pomegranate with known anti-inflammatory and anticancer properties. Among these compounds, we identified hits showing potency of inhibition in the nanomolar range and highly selectivity toward SGK1. The ability of these compounds to reach their molecular target within living cells was also confirmed using nanogels nanoparticle carriers to overcome cell membrane permeability issues.

These active molecules represent a new class of highly potent and selective SGK1 inhibitors, providing a solid foundation for the development of next-generation analogues with superior potency and improved pharmacokinetic properties.

TABLE OF CONTENTS

LIST OF FIGURES

LIST OF TABLES

LIST OF BOXES

LIST OF ACRONYMS

Pol: DNA polymerase

FEN1: Flap endonuclease 1

LIG1: DNA Ligase I

dsDNA: double-stranded DNA

PAD: Polymerase-Associated Domain

ROS: Reactive Oxygen Species

DDR: DNA Damage Response

BER: Base Excision Repair

NER: Nucleotide Excision Repair

TLS: translesion synthesis

DSBs: Double-Strand DNA breaks

NHEJ: Non-Homologous End Joining

HR: Homologous Recombination

alt-EJ: Alternative-End Joining

SSA: Single-Strand Annealing

MMEJ: Microhomology-Mediated End Joining

PolXs: X-family polymerases

TdT: Terminal deoxynucleotidyl Transferase

BRCT: BRCA1 c-terminal protein-protein interaction

ALT: Alternative Lengthening of Telomere

8-oxodG: Guanine oxidized at position 8

OGG1: Glycosylase 8-Oxoguanine Glycosylase

MUTYH: MutY DNA glycosylase

T-loop: Telomeric loop

TPE: Telomere Position Effect

TERRA: Telomeric repeat-containing RNAs

ATR: Ataxia Telangiectasia and Radiation 3 (ATR) related protein

ATM: Ataxia Telangiectasia Mutated

TERT: Telomerase reverse transcriptase

TERC: Telomerase RNA component

TMMs: Telomere Maintenance Mechanisms

APBs: ALT-associated PML bodies

ECTC: extrachromosomal telomeric circular DNA

TIFs: Telomere damage Induced Foci

γH2AX: phosphorylated histone 2A.X

BIR: Break-Induced Replication

RPA: Replication Protein A

BLM: Bloom Helicase

PPIs: Protein-Protein Interactions

PL: Proximity Labelling

BioID: Biotin-ligase Identification approach

PI: Phosphatidylinositol

PKs: Protein Kinases

SGK1: Serum and Glucocorticoid-regulated Kinase 1

PDK1: 3-phosphoinositide-dependent protein kinase-1

PIP3: phosphatidylinositol 3,4,5-triphosphate

MR: Mineralocorticoid Receptor

Th: T helper

ENaC: Epithelial Sodium Channel

NDRG1: N-myc Downstream-Regulated Gene family member 1

GLUT: Glucose Transporter 1

SGLT1: Sodium-Glucose cotransporter 1

ETs: Ellagitannins

EA: Ellagic Acid

MAPK: Mitogen-Activated Protein Kinase

pBirA: myc-BioID2-13XLinker-MCS

pBirA_Pol λ: myc-BioID2-13XLinker-MCS_Pol λ

IF: Immunofluorescence

WB: Western Blot

HU: Hydroxyurea

MS: Mass Spectometry

GO: Gene ontology

BP: Biological Process

CCL: Cellular Component Localization

DAve: Differential Average

DCI: Differential Confidence Index

PEG: polyethylene glycol

PEI: linear polyethyleneimine

NG: Nanogel

BRET: Bioluminescence Resonance Energy Transfer

1. INTRODUCTION – 1st Part

1.1. DNA POLYMERASES

Maintaining genomic integrity is essential for the optimal functioning of living cells. For this reason, repair DNA polymerases (Pols) are crucial factors in all organisms. The human genome encodes for 16 different DNA polymerases, which are divided into seven families A, B, C, D, X, Y, RT, and PrimPol (Díaz-Talavera et al., 2022; W. Yang & Gao, 2018) (Figure 1). All Pols share a general structure that is similar to a human right hand, composed of three main domains: the palm, the thumb and the fingers. When these enzymes form a complex with the DNA substrate, the fingers of the "hand" engage the incoming nucleotide, thereby coordinating interaction with the single-stranded template. The catalytic core is located within the palm, engaging with both the incoming nucleotide and the double-stranded DNA portion, while the thumb domain holds the double-stranded DNA upstream of the catalytic site (Hoitsma et al., 2020; Kuznetsova et al., 2022).

The majority of DNA polymerases belonging to the A, B, C and D families are involved in the synthesis of DNA during DNA replication and include enzymes with 3'-5' exonuclease proof-reading activity, a characteristic that is absent in the X, Y, RT and PrimPol families (Johansson & Dixon, 2013; Reha-Krantz, 2010). DNA replication initiates at specific sites along the DNA sequence, known as replication origins. During replication, these sites are recognized by the pre-replication complex which separates the two DNA strands allowing the recruitment of replication factors that constitute the replication fork complex. In eukarya, RNA/DNA primers are synthesised at both strands by DNA polymerase α-primase complex. Since DNA replication progress from 3' to 5' direction, DNA synthesis proceeds continuously at one strand (leading strand) by Pol ε, in contrast multiple rounds of primer synthesis and extension (by Pol δ) occur at the other strand (lagging strand), forming Okazaki fragments (Jain et al., 2018). The maturation of Okazaki fragments generates a continuous lagging strand DNA from thousands to millions of short intermediates through a highly coordinated series of sequential reactions catalysed by DNA polymerases, nucleases, and DNA ligases. In this process, the nascent DNA synthesized

by Pol δ displaces the RNA-DNA primer of the downstream fragment, leading to the formation of a 5' flap structure. This flap is subsequently cleaved by Flap Endonuclease 1 (FEN1), producing a nick. That is finally sealed by DNA ligase I (Lig I) (Sun et al., 2023). At the conclusion of the DNA replication process, two identical double-stranded DNA (dsDNA) molecules are produced, composed of a parental strand and a newly synthesised one. Notably, other than their roles in DNA replication, A, B, C and D Pols play a role in specific DNA repair pathways (Dewar & Walter, 2017; van Loon et al., 2015).

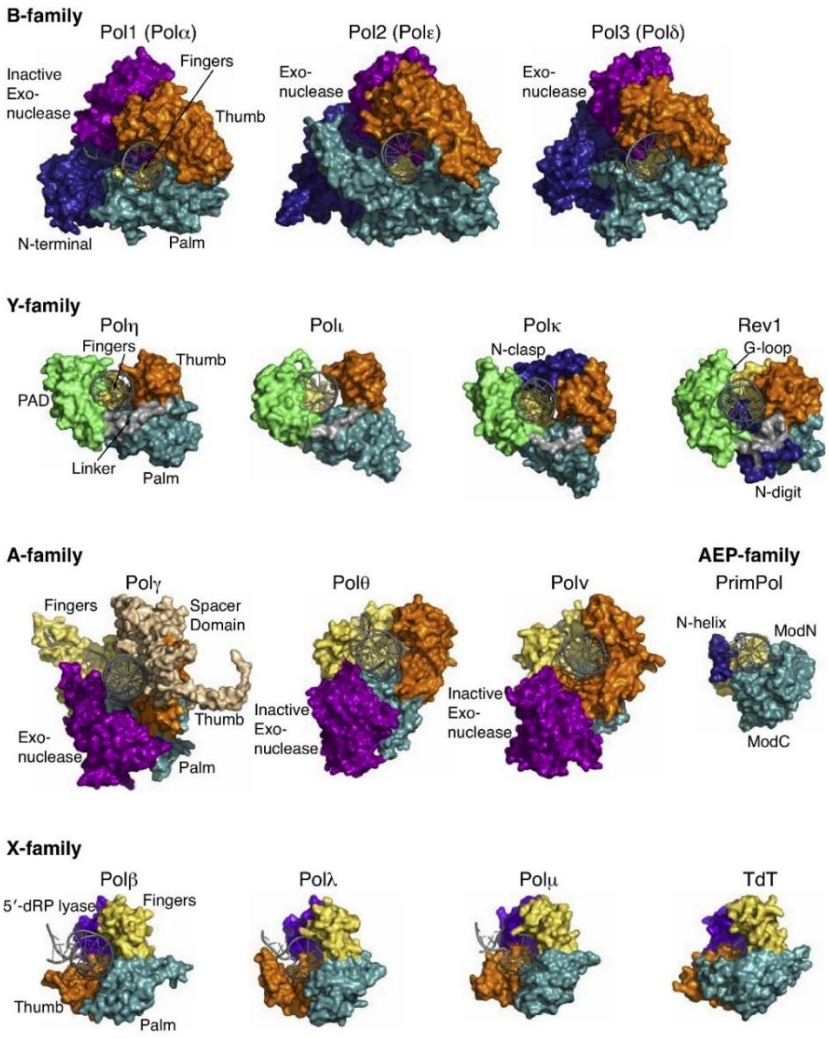

Figure 1. DNA Polymerases family's catalytic core. B-family Pols shown the N-terminal domain in dark blue, exonuclease domain in purple, palm in cyan, fingers in yellow and thumb in orange. The structure of Pol ζ remain unclear. Y-family exposed in green the PAD (Polymerase-Associated Domain) in green, this domain is joined by a linker (in grey) with the thumb. Pol γ belonging to A-family has in beige an additional spacer domain. Prim-Pol possesses the N-terminal domain in yellow, and the C-terminal in cyan and a N-terminal N-helix in dark blue. X-family polymerases show the lyase domain in violet (Jain et al., 2018)

1.1.1. Repair DNA Polymerases and DNA Damages

Repair Pols are specialized enzymes that function in the maintenance of genomic information repairing DNA damage. A multitude of sources cause damage to DNA, including endogenous factors and exogenous agents such as reactive oxygen species (ROS), ultraviolet radiation, ionising radiation, and chemicals (Lange et al., 2011). The Base Excision Repair (BER) pathway is responsible for the restoration of small, non-helix-distorting base lesions. In contrast, the Nucleotide Excision Repair (NER) mechanism is responsible for the resolution of bulker lesions, such as those induced by UV damage, which generate nucleotide dimers (Kaminski et al., 2021). Lesions that escape these pathways and persist in the S phase are bypassed by translesion synthesis (TLS). Double-Strand DNA Breaks (DSBs) are produced both spontaneously and by physiological processes. These latter include coiling relaxation coupled to DNA unwinding in DNA replication and transcription, crossing-over during meiosis, and in immunoglobulin gene rearrangement and V(D)J recombination. On the other hand, spontaneous DSBs are caused by topoisomerases inhibition, collapsed replication forks, or by ionizing radiation. These lesions are primarily repaired by Non-Homologous End Joining (NHEJ) and Homologous Recombination (HR) (Scully et al., 2019; W. Yang & Gao, 2018) (Box 1). While DNA replication consists in a high-speed, high-processivity, and high-fidelity process, DNA repair mechanisms often required Small Gap-filling Repair Synthesis (sGRS), which is characterized by low accuracy, low processivity, and low efficiency, reflecting a tolerance of damage (W. Yang & Gao, 2018). X and Y families comprise Pols involved in DNA repair and translesion synthesis processes. In particular, X-family members are implicated in sGRS processes associated with BER and NHEJ, while A, and B Pols are involved in DNA repair pathways requiring synthesis of longer DNA tracts. Conversely, Y-family polymerases are responsible for TLS. This process is generally error-prone and is responsible for a significant number of point mutations, playing a role in cancer onset and progression (Lange et al., 2011).

Additionally, tumour cells often exhibit elevated levels of DNA repair factors, including different Pols. Many tumour resistance mechanisms are controlled by DNA repair pathways. The factors involved in these processes represent a promising avenue for therapeutic intervention in cancer and immunotherapy. These observations pose DNA Pols as a highly effective therapeutic targets in cancer treatment (Lange et al., 2011; van Loon et al., 2015).

Box 1

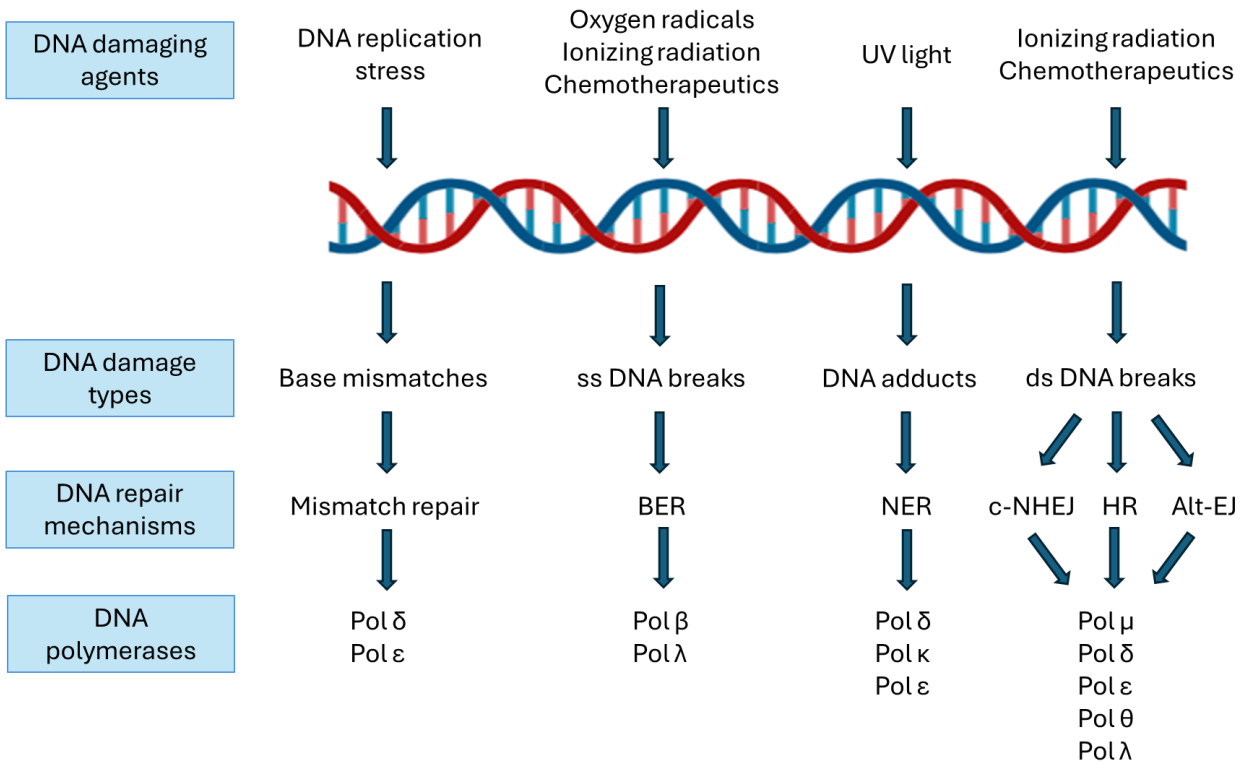

DNA damages and DNA Damage Response (DDR). DNA lesions can arise from a variety of exogenous and endogenous sources and are repaired by specific DNA repair pathways. Together, these mechanisms constitute the DDR. Different DNA polymerases contribute to multiple repair pathways, reflecting their functional versatility. Single-base lesions caused by oxidation, deamination, alkylation, or abasic site formation, destabilise the DNA helix and are mainly repaired by BER or NER. DSBs induced by ionizing radiation, chemotherapeutic agents, or physiological processes such as meiosis and immunoglobulin gene rearrangement, are repaired by different pathways, two of which are canonical: HR and c-NHEJ. In addition, alternative end-joining (alt-EJ) pathways, such as single-strand annealing (SSA) and microhomology-mediated end joining (MMEJ), have been identified. These alt-EJ are minor processes in normal cells but are fundamental in cancer, promoting therapy resistance (M. Jiang et al., 2021; Sallmyr & Tomkinson, 2018; W. Yang & Gao, 2018)

1.1.2. X-family DNA polymerases

The X-family polymerases (PolXs) constitute a class of specialised DNA polymerases that are distributed across various species. Indeed, PolXs variants have been identified in plants, animals and viruses (Uchiyama et al., 2009; Yamtich & Sweasy, 2010). The primary function of these proteins is to perform GRS during the process of repairing single- or double-stranded DNA breaks. PolX members include DNA polymerase β (Pol β), DNA polymerase λ (Pol λ), DNA polymerase μ (Pol μ) and Terminal deoxynucleotidyl Transferase (TdT) (Uchiyama et al., 2009; Yamtich & Sweasy, 2010). Notwithstanding the differences in amino acid sequence, PolXs share a common structural fold. The catalytic domain is comprised of two Helix-Harping-Helix motifs, which interact with DNA (Moon et al., 2007). The catalytic site, composed by the thumb, palm and fingers subdomains, is localised in the 31 kDa polymerase fragment and shows a 43.5% identity between Pol μ and TdT, a 22.8% identity between TdT and Pol λ. These enzymes display limited processivity, exhibiting an incorporation error rate of 1 x 10^{-4} with no 3'-5' exonuclease activity. All PolXs possess a conserved domain of 8 kDa, which, in Pol β and Pol λ, exhibits a dRP lyase activity. Except for Pol β, the other PolXs are characterised by the presence of a BRCA1 c-terminal protein-protein interaction (BRCT) domain at their N-terminal region, which shows an identity of 39.2% between Pol μ and TdT and 16.3% between Pol λ and TdT. This domain is important for binding of interacting factors during NHEJ and V(D)J. Moreover, Pol λ, Pol μ, and TdT have an extended N-terminus that includes additional domains, which are absent in Pol β (Uchiyama et al., 2009; W. Yang & Gao, 2018) (Figure 2). As previously stated, eukaryotic PolXs are involved in BER, DSBs repair during NHEJ pathways and V(D)J recombination of immunoglobulins, as well as during TLS of specific DNA damages (M. J. Howard & Wilson, 2017; Yamtich & Sweasy, 2010). It has been observed that Pol β is the only polymerase that undergoes a change in conformation from an "open" to a "closed" state upon binding to a nucleotide substrate. The interaction of DNA and the incoming dNTP in Pol β, like other Pols, leads to substrate-induced

conformational changes within the active site to ensure substrate specificity, a mechanism known as "induced fit". dNTP binding triggers structural rearrangements within the catalytic domain, in particular involving the fingers and thumb subdomains, which shift their positions relative to each other. In contrast, other PolXs display greater structural rigidity and a permanently "closed" conformation. For instance, in Pol λ the template strand undergoes a shift in its position within the catalytic site when a new dNTP is bound, but this does not result in a concomitant movement of shift interacting domains (Belousova & Lavrik, 2015; W. Yang & Gao, 2018).

Pol β is involved in BER, a mechanism devoted to the repair of small lesions at nucleobases, such as alkylation, oxidation or deamination. The BER pathway can be subdivided into two distinct processes: Short Nucleotide (SN) and Long Patch (LP) BER. In the SN-BER, after the removal of the damaged nucleobase and the incision of the phosphate-sugar backbone, Pol β incorporates a single nucleotide within the neo-formed gap. In this process, the 8 kDa domain is essential for interacting with the downstream 3'-phosphate moiety, accommodating the polymers. This enables the completion of the BER process through DNA ligation (Krokan & Bjørås, 2013; Visnes et al., 2018). The LP-BER resembles SN-BER, with the exception that the recruited polymerase is Pol δ, which synthesises 2-8 nucleotides displacing the downstream strand (W. Yang & Gao, 2018).

It has been hypothesised that also Pol β could also play a specialised role in alternative pathways of NHEJ, filling gaps that are generated after the joining of palindromic sequences. Eventually, it has also been suggested the participation of Pol β in V(D)J pathway (Ray et al., 2018).

Pol μ contains a high number of flexible loops, Loop1 in the C-terminal domain being of particular relevance for its activity. Within the catalytic structure, this loop resembles the position of the template strand This enables the enzyme to extend a single-stranded DNA molecule, thereby functioning as a terminal transferase (Kaminski et al., 2020; Yamtich & Sweasy, 2010). Pol μ was the first Pols to be identified as implicated in NHEJ,

demonstrating the ability to bridge and extend DNA ends that are not fully complementary (Ghosh & Raghavan, 2021; Moon et al., 2014). This extension, being independent from the eventual presence of template strand, is error prone. Pol μ is predominantly expressed in lymphoid tissue, where it plays a crucial role in V(D)J recombination, facilitating the joining of DNA ends. Indeed, Pol μ-deficient mice showed impaired IgG light chain rearrangement and an aberrant B-cell differentiation (Bertocci et al., 2003).

TdT shares common features with Pol μ. It is a fully template-independent polymerase that generates portions of random sequences of DNA after DSBs at immunoglobulin gene junctions during V(D)J recombination (Moon et al., 2007).

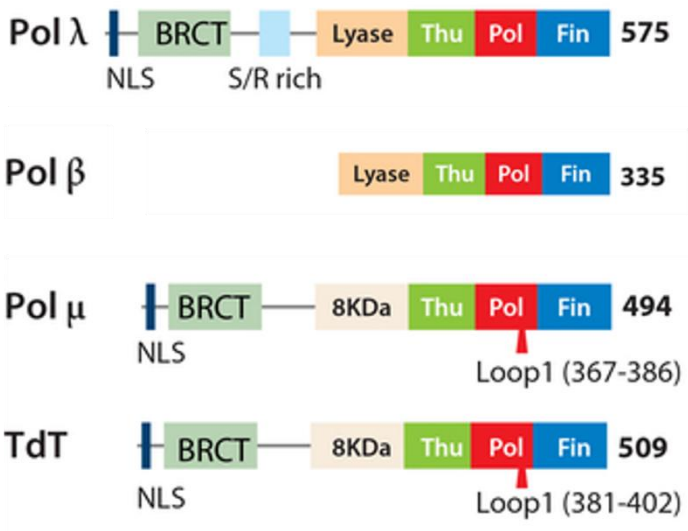

Figure 2. Schematic representation of X family Polymerase. The catalytic subdomains thumb, palm and fingers are coloured in green, red and blue, respectively. The 8 KDa in salmon encodes for a lyase activity (in orange) present only in Pol λ and Pol β. Only Pol λ contains a Serine-Proline rich domain in light blue (Adapted from W. Yang & Gao, 2018)

1.1.3. DNA Polymerase λ

Pol λ is a monomeric single-subunit enzyme comprising 575 amino acids and a molecular weight of 63.5 kDa. It is the largest enzyme within the Pol X family in mammals, encompassing all enzyme activities peculiar to the other members. Pol λ is considered to be the most ancient of the X-family polymerases in mammals. This hypothesis is supported by the fact that Pol IV (also known as PolX), the only X-family polymerase present in budding yeast, exhibits all the core enzymatic activities found in mammalian X-family members, similarly to Pol λ (Bebenek et al., 2003; Bienstock et al., 2014; García-Díaz et al., 2002). The structure of Pol λ comprises an N-terminal nuclear localisation sequence, a BRCT domain, a Ser-Pro rich region and a C-terminal catalytic domain (Bebenek et al., 2014; García-Díaz et al., 2002; Lieber, 2023) (Figure 3). Pol λ displays several activities, including template-dependent DNA polymerisation, terminal transferase activity, dRP lyase and polynucleotide synthetase. The polymerase domain of Pol λ shares a high amino acid sequence homology (34%) with Pol β, and in 30% with Pol μ's catalytic domain. Given this similarity, Pol λ can substitute Pol β in BER and Pol μ in NHEJ and V(D)J recombination (Bebenek et al., 2014; Kaminski et al., 2021). Due to its high affinity for dNTPs, Pol λ is particularly efficient in DNA synthesis outside the S-phase, when the concentration of dNTPs is lower. The Ser/Pro-rich region is a target for post-translational modifications and, like the BRCT domain, is essential for Pol λ interaction with different factors, encompassing proteins implicated in NHEJ. It has also been suggested that this region plays a role in modulating the fidelity of Pol λ (Bebenek et al., 2014; Fiala et al., 2006; Kaminski et al., 2024; Maltseva et al., 2023).

Other than its involvement in NHEJ, Pol λ has been suggested to participate in the alternative DSBs repair pathway Microhomology-Mediated End Joining (MMEJ). This pathway emerged in the absence of classical NHEJ factors and involved 5'-ends resection up to the exposure of short homologous sequences (2-25 nucleotides) on both strands.

Subsequent to this, the broken ends are then annealed, any existing gaps are filled, and the strands are ligated (Seol et al., 2018; Truong et al., 2013). In a recent paper, Pol λ was described as a major player in this pathway in living cells, confirming precedent in vitro results obtained by our laboratory (Chandramouly et al., 2023; Crespan et al., 2012). In addition, research conducted by our laboratory has identified a correlation between this polymerase and the Alternative Lengthening of Telomere (ALT) pathway. Pol λ may play a role in the annealing of a single G-rich telomeric repeat to its complementary strand, which could then be used to train DNA synthesis (Mentegari et al., 2021).

Pol λ is also involved in TLS of specific DNA lesions. Guanine oxidized at position 8 (8-oxodG) is a prevalent DNA damage elicited by Reactive Oxygen Species (ROS). This lesion has the capacity to pair with both a correct cytosine or with an adenine, generating GC to TA transversions (Maga et al., 2007). The 8-oxodG:C base pair is recognised by the specific glycosylase 8-Oxoguanine Glycosylase (OGG1), which removes the oxidised base, leaving a gap that is then filled by Pol β. When this lesion escapes DNA repair and is present in the template strand during DNA replication, replicative Pols misincorporate an A, forming A:8-oxodG pairs. This is recognised by the glycosylase MutY DNA glycosylase (MUTYH), which removes the newly incorporated A, leaving a single nucleotide gap with the 8-oxodG in the template strand. Pol λ is recruited at this structure, being the solely polymerase that incorporates a cytosine over 8-oxodG in a faithful manner, thus restoring the 8-oxodG:C base pair and allowing BER to proceed in a faithful manner (Svilar et al., 2011; Shengyuan Zhao et al., 2021). Moreover, Pol λ can act as a scaffold protein for Pol ζ, substituting REV1 during TLS (Yoon et al., 2021).

The deregulation of Pol λ has been associated with the onset and progression of malignant tumours. Pol λ has been found to be overexpressed in 24% of several human solid tumours. Furthermore, a cancer-related natural variant of Pol λ (R438W) has been identified, exhibiting lower expression, reduced efficiency in NHEJ and being associated with chromosomal instability (Albertella et al., 2005).

This evidence, when considered alongside the central role of Pol λ in processes critical to the maintenance of genomic stability, suggests that this enzyme represents an significant target for cancer therapy (Albertella et al., 2005; Mentegari et al., 2016).

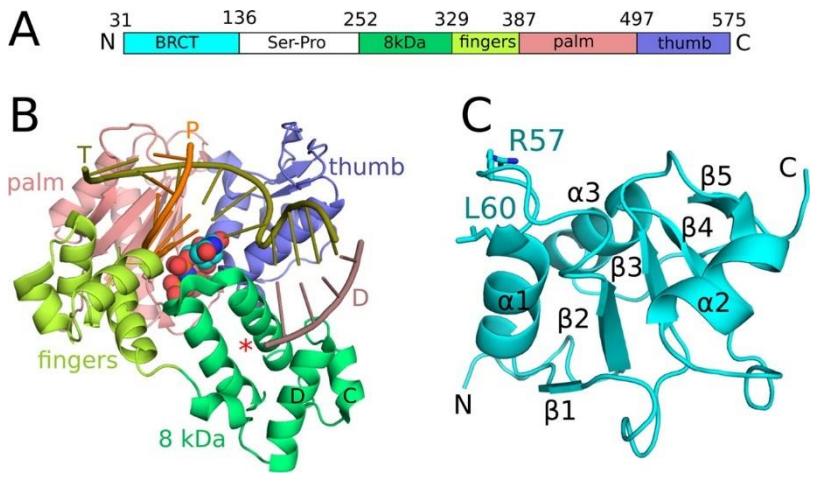

Figure 3. Structure and domains of DNA polymerase λ (A) The BRCT domain is located at the N-terminal end of the protein and is separated from the catalytic core of Pol λ by a Serine-Proline-rich domain that plays a crucial role in mediating protein interactions between the polymerase and other proteins. **(B)** The crystal structure of the ternary complex of the catalytic domains of Pol λ with bound one-nucleotide gapped DNA and an incoming nucleotide. The fingers, palm and thumb are coloured lemon, salmon and slate, respectively. The 8 kDa domain is indicated in lime green. The primer (P) is represented by the orange strand, the DNA template strand is shown in olive, and the downstream strand is represented by the violet one. The 5'-phosphate is indicated by a red asterisk. The incoming nucleotide is shown in cyan. **(C)** Nuclear magnetic resonance solution structure of the BRCT domain of Pol λ. Secondary structural elements, as well as the potential protein-interacting residues Arg57 and Leu60, are labelled (Bebenek et al., 2014)

1.2. TELOMERES AND TELOMER MAINTENANCE MECHANISMS (TMM)

Telomeres are the extremities of linear chromosomes that, in humans, span for 10-15 Kilobases. They are constituted by the exanucleotide sequence 5'-TTAGGG-3' repeated in tandem which terminates with a single stranded 3' overhangs of 25-200 nucleotides. This 3'-overhang foldback, invading the telomere double-stranded region by displacing the G-rich strand, forming a D-loop structure that is defined as telomeric loop (T-loop) (W. Lu et al., 2013; Muoio et al., 2022). T-loop is bound by the Shelterin complex, which is composed of six factors (TRF1, TRF2, POT1, TIN2, TPP1 and RAP1) that protects the telomere extremity to be recognized as a DSB (Reddel, 2014). TRF1 and TRF2 interact with double-stranded DNA, whereas POT1 binds to the single-strand overhang. The binding of these three proteins is mediated by TIN2, TPP1 and RAP1 (Shay & Wright, 2019) (Figure 4).

Telomeres are enriched in silent heterochromatin, characterized by H3K9me3 histones markers. However, the overall organisation of telomeric heterochromatin remains to be fully elucidated (Blasco, 2005; Mendez-Bermudez et al., 2020). Heterochromatic status alters the three-dimensional telomeric architecture, influencing gene expression through an epigenetic process known as Telomere Position Effect (TPE) that represses or reduces gene expression in sub-telomeric regions, achieved through reversible alterations in the structure of chromatin, encompassing histone modifications and DNA methylation (K.-H. Lee et al., 2021). Telomeric repeat-containing RNAs (TERRA) are long non-coding telomeric RNA transcripts that are generated by RNA polymerase II from the C-rich strand. It has been observed that their downregulation is associated with a reduction in telomeric heterochromatin signature, suggesting that TERRA plays a role in the regulation of telomeric heterochromatic status (Giardini et al., 2014; Udroiu & Sgura, 2019).

Telomeres have evolved to prevent the loss of genetic information due to shortening of chromosomal ends during DNA replication and to protect chromosomes end from being recognized as DSBs.

In fact, when the lagging strand of DNA is used as a template during the replication, the synthesis progresses in the reverse direction of the replication fork, precluding the possibility of continuous DNA synthesis. The requirement of RNA priming in Okazaki fragment maturation precludes the possibility to synthesise DNA at the chromosomal ends, leading to chromosomal ends erosion at each replication cycle (Stroik & Hendrickson, 2020; Turner et al., 2019). Somatic cells shorten their telomeres with each cell division up to a critical length, defined as the Hayflick limit, when the function of the Shelterin complex is impaired. In this condition, cellular division is arrested to prevent erosion of genetic information (Hayflick, 1965; Hayflick & Moorhead, 1961). The cells remain in the G0 phase, entering in senescence, a state of programmed quiescence (Shay, 2016). This process is mediated by the inhibition of cyclin-dependent kinases, which is induced by the Ataxia Telangiectasia Mutated (ATM) or the Ataxia Telangiectasia and Radiation 3 (ATR)-related protein (ATR) pathway (Maciejowski & de Lange, 2017; Muñoz-Espín & Serrano, 2014). During development, and in stem cells, which possess the capacity for infinite replication, the length of telomeres is sustained by the activity of telomerase (Blasco, 2005; Nguyen et al., 2019). This is a ribonucleoprotein complex composed by a catalytic subunit with reverse transcriptase activity (telomerase reverse transcriptase, TERT), and an RNA strand (telomerase RNA component, TERC) that pairs with the G-rich strand and protrudes to the 5'-end, serving as a template for the reverse transcription activity that produces a long G-rich overhang. This is subsequently covered by the Cdc13-Stn1-Ten1 (CST) complex, which recruits primase-pol α to synthesise complementary primers and synthesise the C-strand, generating the double-stranded telomeric DNA (Nguyen et al., 2019). Subsequent to the displacement of telomerase, a 3' overhang end is produced by the resection of the C-rich strand (Lue et al., 2014; Y. Wang et al., 2019; Shuang Zhao et al., 2019).

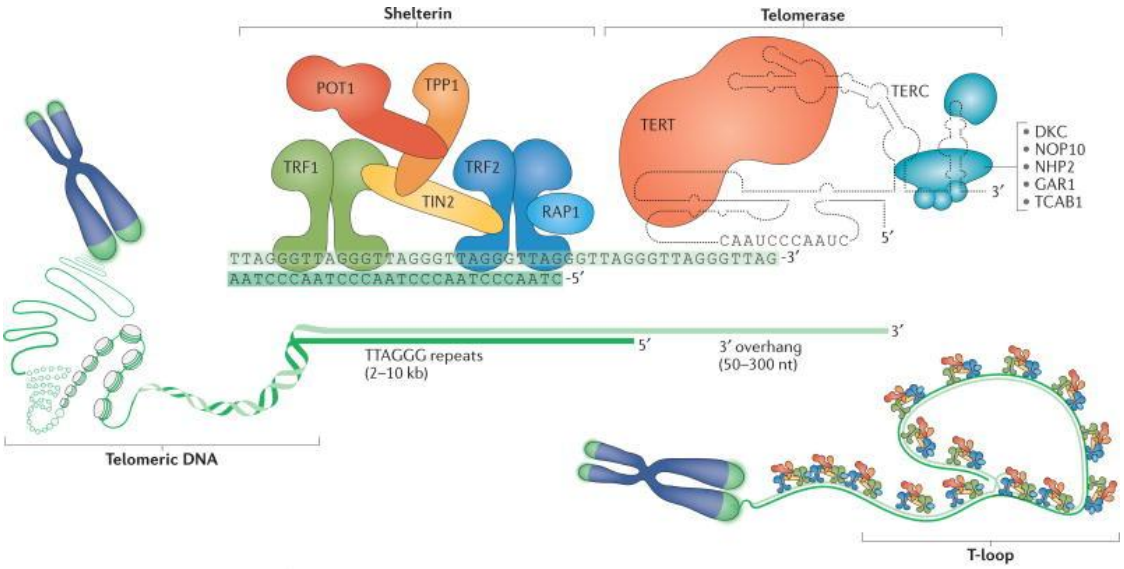

Figure 4. Human telomeres associated with Shelterin complex and Telomerase. Telomeric DNA, Shelterin complex, and the telomerase complex are represented. The telomeric DNA is constituted by double-stranded TTAGGG repeats that culminates in a protruding single-stranded 3' ss strand. This strand invades the telomeric double-stranded repeats and forms the T-loop (bottom left), which, in conjunction with the six-subunit Shelterin complex, protects the chromosomal ends. Telomerase expands the length of the protruding 3' telomere strand in association with accessory factors (light blue) (Maciejowski & de Lange, 2017)

1.2.1. Alternative Lengthening of Telomere (ALT) Pathway and Hallmarks

To circumvent replicative senescence and achieve immortality, cancer cells must maintain telomeres during the process of proliferation. Consequently, cancer cells activate Telomere Maintenance Mechanisms (TMM) pathways. These processes include telomerase expression in 85% of cancers, while the rest of tumours activate the Alternative Lengthening of Telomeres (ALT) pathway (Gao & Pickett, 2022; Maciejowski & de Lange, 2017). The precise mechanisms underlying the selection of specific TMM in cancer cells remain unclear (Cesare & Reddel, 2010). The incidence of ALT cancer depends on the specific tumour type. ALT is more frequent in bone tumours (62%), neuroendocrine system tumours (40%), soft tissue tumours (32%), peripheral (23%), and central nervous system tumours (15%). Some ALT-related tumours exhibit aggressive characteristics, resulting in a reduced survival rate, as observed in sarcomas (Dilley & Greenberg, 2015; Rose et al., 2023).

The synthesis of telomeres in ALT cells is carried out in ALT-associated PML bodies (APBs) in G2 cells or APB-like foci in mitotic cells. APBs represent a defining feature of ALT and have been observed to promote telomere clustering, as well as serving as platforms for proteins involved in telomere maintenance. Other hallmarks of ALT include a heterogeneous range of telomere sizes, from less than 1 Kb to more than 20 Kb, the presence of extrachromosomal telomeric circular DNA (ECTC), particularly C-circles and G-circles, which may be the products of telomere trimming or self-replicating templates for telomeric DNA lengthening, and a high level of insertion at chromosome ends and sister chromatin exchange (J. J. Lee et al., 2021; Shuang Zhao et al., 2019).

C-circles are present at a frequency 750 times higher in ALT cells and thus serve as the most readily detectable biomarker for diagnostic testing (Sohn et al., 2023).

Upon DSBs, long non-coding RNAs are generated at the broken strands. C-rich telomeric damage-induced long non-coding RNAs (TeloC dilncRNAs) are present at high levels in ALT cells. TeloC dilncRNAs have been shown to regulate replication stress at ALT telomeres recruiting replication stress-relieving factors, and their inhibition reduces Rad51 and 53BP1 levels at telomeres (Rosso et al., 2023).

Another characteristic of ALT activity is the increased replication stress and the accumulation of DNA damage signals at telomeres, with the formation of Telomere damage Induced Foci (TIFs) which are constituted by DNA damage markers such as γH2AX, 53BP1 and phospho-ATM (Rose et al., 2023).

ALT is a process that involves telomere sequence-specific homologous recombination (HR). Two main mechanisms have been suggested to participate in ALT: a Rad52-dependent process driven by Break-Induced Replication (BIR) at telomeres and active during the G2 and M phases, and a Rad51-dependent mechanism, confined to the S phase and resembling canonical HR pathway (Gao & Pickett, 2022; T. Zhang et al., 2019).

In the Rad52-dependent mechanism, Rad52 is recruited by RPA (Replication Protein A) bound to the ss-DNA overhang. The extension of the C-rich 3'-overhang occurs via Rolling Circle Amplification (RCA) using ECTCs as a template (Kent & Clynes, 2021; Sobinoff & Pickett, 2017). Telomers synthesis is sustained by the activity of Pol δ subunits POLD3 and POLD4, which are coordinated by the BTR complex. This structure is formed by Bloom Helicase (BML), topoisomerase III, and RMI1/2 scaffold protein. ECTCs are thought to originate from BIR intermediates in APBs, where BLM play a crucial role in their generation. The precise molecular steps underlying this mechanism remain to be fully elucidated. However, different DDR and DNA repair factors have been suggested to

contribute to the regulation of ECTCs formation from BIR intermediates in APBs (J.-M. Zhang et al., 2021) (Figure 5).

In the RAD51-dependent process the ss 3' overhang moiety is coated with RPA, which is then substituted by Rad51, forming a Rad51-ss DNA complex. In this complex, Rad51 facilitates strand invasion of the presynaptic filament to search the homologous telomeric sequence. This process ultimately results in the accumulation of telomeres to form clusters, providing sites for the occurrence of HR (Ackerson et al., 2021; Kent & Clynes, 2021).

Notably, RAD51-interacting Protein (RAD51AP1) plays a crucial role in both RAD51- and RAD52-dependent telomere extension mechanisms, and its knocking out in ALT cells leads to telomere shortening (Barroso-González et al., 2019).

A recent study conducted by our laboratory demonstrated that the deregulation of Pol λ resulted in a perturbation of C-circles levels, a form of ECTCs enriched of by telomeric C-rich DNA, in ALT cells, suggesting its involvement in the ALT mechanism (Mentegari et al., 2021).

It has been shown that the ALT process can be elicited by therapies targeting telomerase (Gao & Pickett, 2022). Therefore, the identification of the precise mechanism underlying ALT is of utmost importance to identify new pharmaceutical targets to be exploited together with telomerase (J. J. Lee et al., 2021).

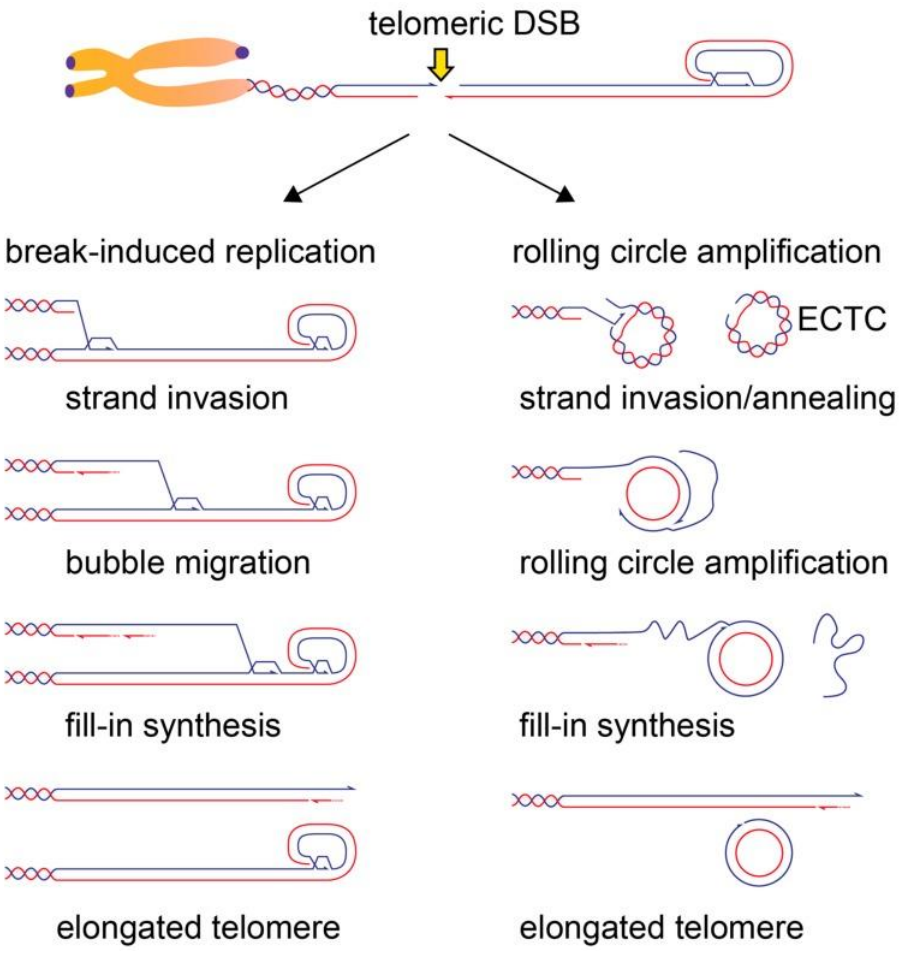

Figure 5. Schematic representation of DSB-induced ALT human pathways. Telomeric DSB can initiate telomere synthesis. In both models the G-rich protruding strand (red) must invade a complementary C-rich strand (blue). In the RAD51-dependent pathway on the left, the telomere is elongated with a BIR-mediated mechanism after the invasion of the G-rich strand into a complementary telomeric region. In the RAD52-dependent model on the right, telomere elongation occurs through RCA, where the G-rich strand invades C-circles, which contain both a continuous strand and a nicked strand (Doksani, 2019; Mazzucco et al., 2020)

1.3. PROXIMITY-DEPENDET BIOTIN IDENTIFICATION (BIOID) LABBELING

The study of Protein-Protein Interactions (PPIs) in living cells with traditional biochemical approaches is subject to a number of limitations. These include the presence of contaminants, the inability to detect weak or fast interactions, loss of material and loss of subcellular regions that cannot be purified by canonical methods (Cho et al., 2020; Roux et al., 2012; Schopp et al., 2017). In light of these limitations, novel and alternative approaches have emerged to detect PPIs utilising Proximity Labelling (PL). These methods include antibody-based approaches, such as Selective Proteomic Proximity Labelling Assay using Tyramide (SPPLAT), Enzyme-Mediated Activation of Radical Source (EMARS), the Ascorbate Peroxidase-based approach (APEX), the Biotin-ligase Identification approach (BioID), the Ancestral BirA for proximity-dependent biotin identification (AirID) and, lastly, the Pupylation-based approach (PUP-IT). In these methods, the protein of interest is tagged with an enzyme that converts a small molecule to a highly reactive intermediate labelling interacting moieties (Kido et al., 2020; May et al., 2020). This approach preserves the native state of PPIs and spatial relationships, as the molecular complex and cellular membranes remain unaltered (Cho et al., 2020).

Since its development, the BioID method has been employed to investigate PPIs within the nuclear envelope and centromeres, as well as to explore the spatiotemporal dynamics of epigenetic regulation, cancer progression, and host–virus interactions (D. I. Kim et al., 2016). BioID is based on a humanised version of the Escherichia coli biotin ligase BirA. This protein functions as a transcriptional repressor for the biotin biosynthetic operon, which in turn regulates the biotinylation of a subunit of acetyl-CoA carboxylase (Chapman-Smith & Cronan, 1999). The biotin ligase BirA adenylates biotin generating a reactive intermediate, biotin-adenosine monophosphate (biotin-5'-AMP), which binds in a covalent manner to the lysine residues present in proximal proteins (Roux et al., 2012). The BirA R118G mutant displays an enhanced affinity for free biotin and a reduced affinity for

biotin-5'-AMP. Consequently, a cloud of biotin-5'-AMP is released in the proximity of the enzyme, reacting with lysine residues within an estimated range of 10 nm. To explain, the binding of biotin at the biotin-binding loop of BirA ligase causes a conformational change within the loop, that promotes the subsequent binding of ATP and a rearrangement of the structure of the adenylate-binding loop, resulting in ATP stabilisation. The lysine 183 of BirA initiates a nucleophilic substitution reaction, which results in the biotin carboxylate's attack on the alpha phosphate of ATP, ultimately leading to the production of biotinyl-5'-AMP. This product forms a hydrogen bond with the arginine 118 of the enzyme thereby establishing a stable association through a salt bridge with the amino acids of the BirA. In the final transfer reaction, this complex attacks the interactor factors in the epsilon amine of lysine, resulting in the covalent biotinylation of the interacting substrate protein (D. I. Kim et al., 2014; Samavarchi-Tehrani et al., 2020) (Figure 6).

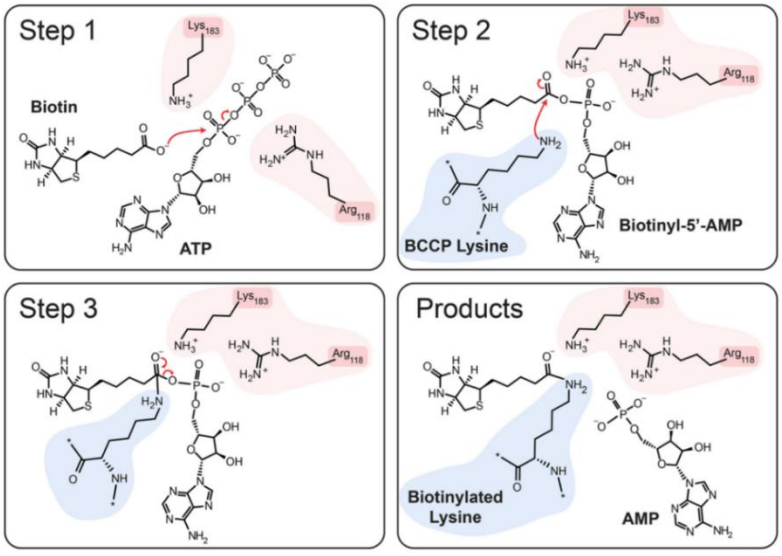

Figure 6. BirA reactions. The binding of biotin to BirA promotes the binding of ATP **(Step 1)**. The lysine 183 of BirA leads the biotin carboxylate's attack on ATP, resulting in the production of biotinyl-5'-AMP **(Step 2)**. biotinyl-5'-AMP forms a stable association mediated by a hydrogen bond with the arginine 118 of the enzyme **(Step 3).** The product of step 3 attacks the lysine of the interactor factors, resulting in their covalent biotinylation **(Products)** (Samavarchi-Tehrani et al., 2020).

Roux and colleagues developed a smaller and more promiscuous biotin ligase (BioID2) showing higher affinity toward biotin and thus operating at a lower biotin concentration. This enzyme was identified in *Aquifex aeolicus*, and, due to the absence of a DNA-binding domain, is smaller than *E. coli* biotin ligase (233 aa versus 321 aa). The substitution of the conserved residue R40G within the catalytic domain is essential to confer biotinylation promiscuity (D. I. Kim et al., 2016; Sears et al., 2019) (Figure 7).

The BioID and BioID2 methods require a period of 12-24 hours to label proximal proteins. A faster BioID approach, designated TurboID, was developed using engineered BirA exhibiting greater affinity for biotin and was able to function in subcellular compartments that were not suitable for other BioID methods (May et al., 2020).

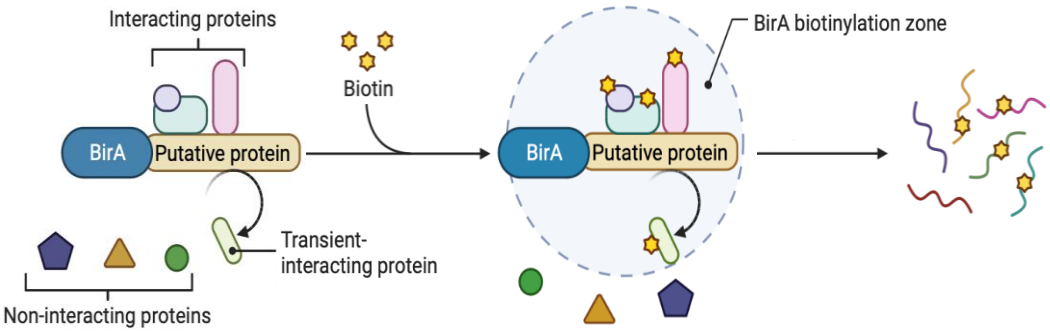

Figure 7. Schematic BioID working. In the presence of biotin, BirA exhibits promiscuous activity, biotynilating all accessible proteins, including those that interact with the studied protein within a range of 10 nm (Image created with Biorender.com).

2. INTRODUCTION – 2nd Part

2.1. KINASES

A vertebrate genome encodes as many as 1001 kinases, with approximately 1.7% of human genes encoding for 518 protein kinases. These enzymes are crucial in cell metabolism and signalling and their activities are fundamental for a number of cellular functions including cell cycle progression, differentiation, genome duplication and maintenance, transcription, translation, cell–matrix and cell–cell interaction, and survival (G Manning et al., 2002). Giving their roles within the cell, it is unsurprising that mutations or deregulation occurring at kinases play a pivotal role in the pathogenesis of a multitude of human diseases, including cancer, diabetes, inflammatory disorders, and neurodegenerative and metabolic diseases (Krupa & Srinivasan, 2002; Middelbeek et al., 2010; Xerxa & Bajorath, 2024). For this reason, kinases represent highly valuable pharmaceutical targets. The investigation of the regulation and function of kinases is of fundamental importance to the identification of novel inhibitors that can be translated into the development of new drugs (Middelbeek et al., 2010).

Depending on their reaction substrate, kinases are classified in three groups: carbohydrate kinases, protein kinases, and lipid kinases. Carbohydrate kinases transfer the terminal phosphate group from a nucleoside triphosphate, most commonly ATP, to a free deprotonated sugar hydroxyl. This process of phosphorylation is crucial to saccharide utilisation and the regulation of carbohydrate metabolism (Roy et al., 2019). Lipids kinases are able to phosphorylate different lipids present at plasma or organelles membranes. The main targets of these enzymes are hydroxyl groups on the inositol moiety of phosphatidylinositol (PI), generating molecules that are important second messengers in cellular signalling and cellular remodelling (Burke et al., 2023). Protein kinases represent the largest group and are further categorised into serine/threonine (Ser/Thr) kinases and tyrosine (Tyr) kinases, depending on the target amino acids. All kinases are divided into 209 subfamilies. In humans, protein kinases alone are classified in 189 distinct subfamilies

(Figure 8), with 51 of these family being conserved in all eukaryotic kinomes from yeast to mammal (Kalaivani et al., 2018; Gerard Manning et al., 2002).

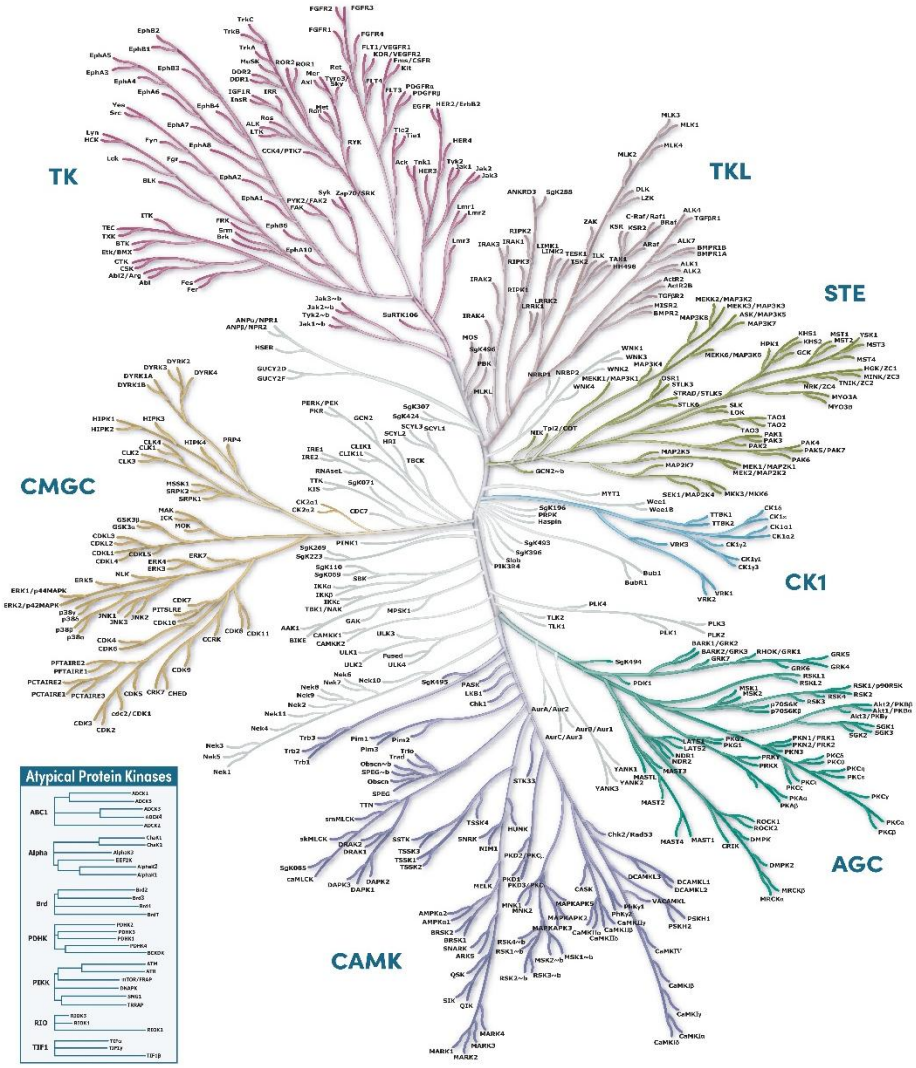

Figure 8. Human Kinome. The human kinome represents the entire set of human kinases. (*Kinase.Com*, n.d.; Taylor & Kornev, 2011)

2.1.1. Protein Kinases

Protein kinases (PKs) catalyse the transfer of γ-phosphate from ATP to the -OH group of serine, threonine or tyrosine employing a conserved residue of located within the catalytic domain of the enzyme (Kalaivani et al., 2018; Ubersax & Ferrell Jr, 2007).

In eukarya (ePKs), protein phosphorylation is the prevalent post-translational modification utilised for signal transduction. With approximately 10,000 distinct proteins in a eukaryotic cell, with an average length of nearly 400 amino acids, of which 8.5% are serine, 5.7% are threonine, and 3% are tyrosine, there are nearly 700,000 potential phosphorylation sites (Ubersax & Ferrell Jr, 2007).

The general architecture of the active domain of protein kinases is conserved. It is composed of two lobes. The catalytic amino acids are located in the N-terminal one, which is constituted by β-strands, this region is also reinforced by a hydrogen bond, which serves to stabilise the structure of the catalytic site. Conversely, the C-terminal lobe is rich in α-helices. The two lobes form both ATP- and substrate-binding sites (Krupa & Srinivasan, 2002) (Figure 9).

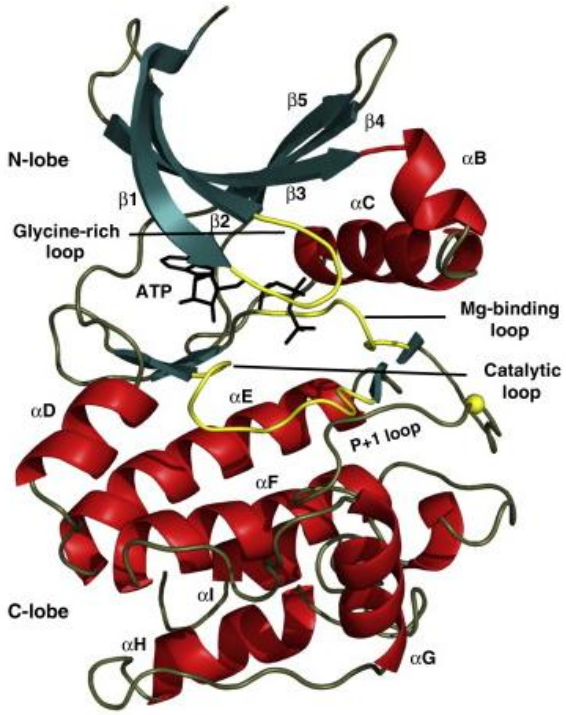

Figure 9. Structure of protein kinase core. The conserved kinase core is composed of 5 β-strands at N-terminal lobe (β1 to β5 in teal) and 2 αC-helix (red). The C-lobe is constituted by α-helices. Between the two lobes an ATP molecule is bound, between β1 and β2 the glycine rich loop coordinates the ATP phosphates. In yellow are coloured the catalytically important loops. The P+1 loop accommodates the P+1 residue of the peptide substrate, which is docked to the peptide-binding site (Taylor & Kornev, 2011)

Protein kinases are classified into distinct classes based on their sequence and structural characteristics, which frequently, though not exclusively, correlate with their biological functions (G Manning et al., 2002) (Figure 8):

- Tyrosine Kinases (TK) constitute a unique class characterised by the phosphorylation of tyrosine residues.

- Tyrosine Kinase-Like (TKL) class exhibits activities typically associated with serine/threonine substrates, yet they exhibit high homology with TKs.

- AGC group that is named after the discovery of protein kinase A, G, and C (PKA, PKC, PKG) families and includes intracellular kinases involved in cell cycle regulation signalling pathways modulated by cyclic nucleotides, phospholipids, and calcium. For instance, members of this group regulate apoptosis process. Protein Kinase A (PKA) type I has been shown to have an antiapoptotic effect, whereas type II has been observed to promote proapoptotic events. Whereas, the Protein Kinase B (PKB) has been demonstrated to inhibit the apoptosis pathway, thereby regulating caspase activation (Cross et al., 2000).

- CMGC class comprise kinases involved in the signalling of different cellular functions, including cell cycle control, metabolic control, and splicing.

- Calmodulin/Calcium-regulated kinases (CAMK) encompasses non-calcium-regulated kinases.

- Cell kinase 1 (CK1), originally designated as Casein Kinase 1 (CK1), constitutes a small group of enzymes closely related. However, this is the most divergent kinase class, showing a certain genetic distance and lacking structural motifs that are conserved among other ePKs.

- STE class is composed by enzymes responsible for transducing signals from the surface of the cell to the nucleus and includes the Mitogen-Activated Protein Kinases (MAPK) cascade. MAPKs family is involved in cell proliferation, survival, and differentiation. The members p42/44 Extracellular signal-Related Kinases (ERK), c-Jun N-terminal protein Kinase (JNK), and p38 MAP play a pivotal role in the process of apoptosis. The activation of JNK and p38 MAP kinases represent the final stages of the signalling cascades, initiated by the binding of a survival factor or death receptor and culminating in the promotion of apoptosis (Biondi & Nebreda, 2003; Cross et al., 2000).

- Receptor Guanylate Cyclases (RGC), a small group of kinases that generate cGMP as second messenger.

- Protein Kinase-Like (PKL) class contains families of kinases sharing a Protein Kinase-Like fold but exhibit low homology sequence with other kinases classes. Additionally, this group encompasses lipid, sugar, and other kinases targeting small molecules (Baranowski et al., 2024; Hanks, 2003; Middelbeek et al., 2010).

- Atypical class is constitute by kinases that do not exhibit structural similarity to ePKs. For example, ATM and ATR belong to this group and serve as the primary regulators of the DDR. In its inactive state, ATM exists as a homodimer. Following the occurrence of a DSB, ATM undergoes autophosphorylation at three distinct serine residues: 367, 1893, and 1981. Upon activation, ATM phosphorylates substrates involved in DNA repair, cell cycle regulation, and DNA replication, thereby orchestrating the cellular response to DNA damage (Rozpędek et al., 2019).

The most populous classes are CAMK (comprising 81 kinases), TK (94 members), CMGC (72 kinases) and AGC (69 enzymes) (Krupa & Srinivasan, 2002).

ePKs play a role in a number of different pathways, and mutations in these enzymes have been linked to a variety of human diseases. In normal cells, kinases could act as both tumour

suppressors and proto-oncogenes. Mutations in kinases have been observed to promote oncogenic processes, including the activation of angiogenesis, the inhibition of DDR and the inhibition of apoptosis causing a wide variety of human diseases, including, but not limited to, cancer, autoimmune diseases, neurodegenerative diseases and cardiovascular disorders (Torkamani et al., 2009). A comprehensive study conducted on all human protein kinases divided the effect of disease-related mutations according to their relevance in different diseases. The findings indicate that the majority of mutations occurring in the catalytic site and activation loops are associated with cancer. In contrast, mutations occurring outside these regions are generally correlated with non-cancer diseases (Medvedev et al., 2023) (Figure 10).

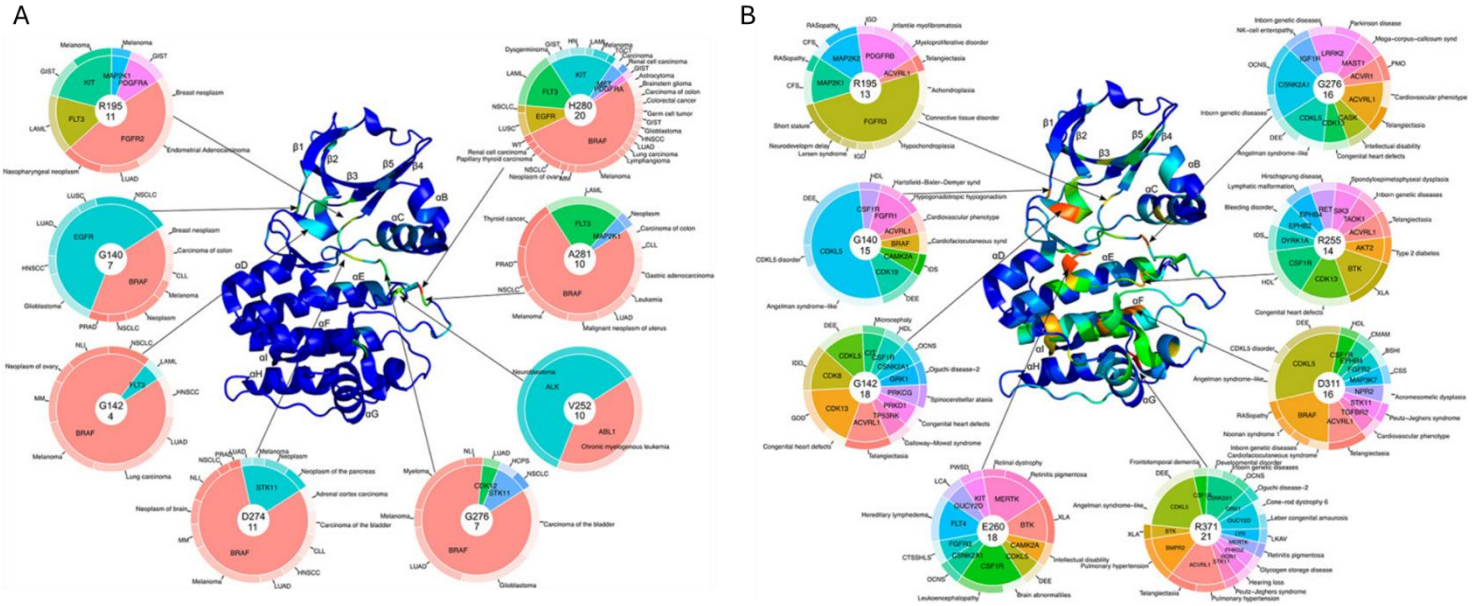

Figure 10. Cancer-associated and other diseases-associated mutations in kinases. Mutations in Ser/Thr kinase domain of Aurora Kinase A (AURKA) are reported. Single mutations are reported in the inner layer of the pie charts. Outer layers show the related diseases. **(A)** Cancer-related mutations of AURKA. CLL, B-cell chronic lymphocytic leukaemia; GIST, gastrointestinal stromal tumour; HCPS, hereditary cancer-predisposing syndrome; HN, hematologic neoplasm; HNSCC, squamous cell carcinoma of the head and neck; LAML, acute myeloid leukaemia; LUAD, lung adenocarcinoma; LUSC, squamous cell lung carcinoma; MM, multiple myeloma; NLI, neoplasm of the large intestine; NSCLC, non-small cell lung carcinoma; PRAD, prostate adenocarcinoma; TGCT, germ cell tumour of testis; WT, nephroblastoma (Wilms tumour). **(B)** Non-cancer-related mutations of AURKA. SHI, bilateral sensorineural hearing impairment; CFS, cardiofaciocutaneous syndrome; CMAM, capillary malformation-arteriovenous malformation; CSS, cardiospondylocarpofacial syndrome; CTSSHLS, camptodactyly-tall stature-scoliosis-hearing loss syndrome; DEE, developmental and epileptic encephalopathy; GDD, global developmental delay; HDL, hereditary diffuse leukoencephalopathy; IDD, intellectual developmental disorder; IDS, intellectual disability syndrome; IGD, inborn genetic diseases; LCA, Leber congenital amaurosis; LKAV, LYN kinase-associated vasculopathy; OCNS, Okur-Chung neurodevelopmental syndrome; PMO, progressive myositis ossificans; PWSD, piebaldism with sensorineural deafness; XLA, X-linked agammaglobulinemia (Medvedev et al., 2023)

Given their roles, ePKs are identified as pharmacological targets of many diseases. Different types of molecules have been developed to treat human diseases and cancers. Notwithstanding the fact that over 400 human diseases have been linked to many protein kinases, only a small number of ePKs are targets of approved drugs (Melnikova & Golden, 2004). As of 2024, the FDA had approved the use of more than 80 small molecules to inhibit the activity of over 20 different ePKs. 58 of these drugs have been approved for the treatment of cancer (Roskoski, 2024). Approximately 180 orally effective protein kinase inhibitors are currently undergoing clinical trials worldwide (Roskoski Jr., 2022). The strategies to target kinases include the inhibition of the catalytic activity, the impairment of protein-protein interaction, and the modulation of the expression of the target gene through the use of antisense oligonucleotides or by RNA interference approaches (Melnikova & Golden, 2004). ePK inhibitors that bind the ATP-binding site can be classified into three main categories. Type I molecules form reversible bonds with the ATP-binding site in an active conformation, as well as with proximal regions, while type II inhibitors bind the ATP-binding site in its inactive configuration. Type III drugs do not interact with the ATP-binding site, but rather with an allosteric site. As a result, they are more selective than other classes of inhibitors (Riegel et al., 2022). Selectivity is a crucial factor in reducing the adverse effects of kinase targeting drugs, together with adequate pharmacokinetic and pharmacodynamic properties (L. N. Johnson, 2009; Sawyer et al., 2013).

2.1.2. Serine/Threonine Protein Kinases.

A total of six subfamilies are associated with Ser/Thr kinases, namely CMGC, TKL, CAMK, AGC, STE and CK1. These are involved in a range of different pathways (J. L. Johnson et al., 2023). The Ser/Thr protein kinase family comprises over 300 members. These kinases are characterised by their ability to phosphorylate the hydroxyl group of serine and threonine residues present in their substrates. These are constituted by other kinases, receptors, cell cycle regulators, transcriptional factors, and other regulatory proteins (Goldsmith et al., 2007). Despite being able to phosphorylate both Serine and Threonine, individual Ser/Thr kinases possess a high degree of selectivity for the nature of the target amino acid. For instance, 90% of cAMP-dependent protein kinase (PKA) substrates are phosphorylated in a serine residue. Conversely, the Liver Kinase B1 (LKB1) substrates are phosphorylated exclusively on threonine residues. The precise mechanisms underlying this specificity remain unclear, but it has been demonstrated that the flexible kinase activation segment contains a residue that is crucial for the discrimination of the target amino acid (C. Chen et al., 2014).

While several Ser/Thr kinases play a pivotal role in cancer onset, progression, metastasis and therapeutic resistance. A study utilising in situ hybridisation-tissue microarray methodology identified 21 Ser/Thr kinases with significantly misregulated expression across diverse cancer types. The findings indicate that Ser/Thr kinases are commonly overexpressed in tumours, supporting their involvement in promoting proliferation and proliferation-related processes (Capra et al., 2006; Jiang et al., 2024). Notably, ten of the overexpressed Ser/Thr kinases in tumour tissue exhibited low or absent levels of expression in normal tissues (Capra et al., 2006). Moreover, alterations in Ser/Thr kinases of specific families are also associated with specific diseases. For instance, the dysregulation of Death-Associated Protein Kinase (DAPK), which are CAMK members, has been

identified as a critical factor in the development of neurodegenerative diseases (L. Zhang et al., 2023). AGC and CMGC kinases alterations have been found to be associated with various cardiovascular diseases, including heart failure, ischaemia, myocardial hypertrophy and infarction, and diabetic cardiomyopathy (Wu et al., 2024).

2.1.3. Serum and Glucocorticoid-regulated Kinase 1 (SGK1)

Glucocorticoids play a pivotal role in the differentiation and development of animal tissues, the regulatory effects of these hormones are achieved through the mediation of intracellular receptors, which function as transcriptional regulators of gene expression. In 1993, a novel Ser/Thr protein kinase was identified through a screen for glucocorticoid-inducible regulated transcripts in a rat mammary tumour, Serum and Glucocorticoid-regulated Kinase 1 (SGK1). This is a 49 kDa enzyme with 45 to 55% homology with the protein kinase C family, ribosomal protein S6 kinase and cyclic AMP-dependent protein kinase (Webster et al., 1993).

Later, other two strictly related kinases were identified, SGK2 and SGK3. SGKs are members of the AGC family, which is among the most conserved classes in the evolutionary history of the animal kingdom, constituting 15% of the human kinome. The genes codifying for SGKs are localised on distinct chromosomes and show high homology (Arencibia et al., 2013). Structurally, SGKs lack the phosphoinositide-binding Pleckstrin Homology (PH) domain that is present in other AGC kinases. This domain is responsible for recruiting the enzyme to phosphatidylinositol 3,4,5-triphosphate (PIP3) bound to the inner cellular membrane. However, SGK3 possesses an N-terminal phosphoinositide-binding Phox homology (PX) domain that interacts with PIP3, which is fundamental for the phosphorylation and activation of SGK3 by 3-Phosphoinositide-Dependent protein Kinase-1 (PDK1) (Di Cristofano, 2017; Pearce et al., 2010). SGKs are intracellular soluble

kinases, SGK1 and SGK3 are ubiquitously expressed, while SGK2 expression is constitutive, but restricted to the liver, pancreas, brain, and kidney proximal tubules (Di Cristofano, 2017).

The regulation of SGKs is achieved through the combined action of transcriptional and enzymatic processes. The activation of these kinases is dependent on the phosphorylation of two specific residues: a threonine within the catalytic domain and a serine situated within the activation loop in C-lobe. Extracellular stimuli activate Phosphoinositide-3 Kinase (PI3K), which converts Phosphatidylinositol 4,5-bisphosphate (PIP2) into PIP3. Subsequently, PIP3 recruits and activates PDK1, which in turn phosphorylates SGKs in the threonine residue in the catalytic site (Jang et al., 2022). The activation loop is included in the C-lobe of the enzymes and contains a DFG motif which directs the positioning of ATP in the active site. The phosphorylation of the activation loop by specific kinases initiates the conformational changes that facilitate the formation of hydrogen bonds between the active site and the ATP, which are essential for the full activation of all SGKs (Pearce et al., 2010).

SGK1 activation and regulation.

In the case of SGK1, the initial phosphorylation event is the phosphorylation of serine 422 by mTORC2. This causes a conformational change in the C-lobe, which is subsequently recognised by PDK1 that phosphorylates the threonine 256 in the catalytic domain, fully activating the enzyme (Figure 11). Additionally, extracellular stimuli have the potential to induce the migration of transcription factors, including glucocorticoid receptor, mineralocorticoid receptor (MR), and tumour suppressor p53, into the nucleus, where they activate SGK1 transcription increasing its expression by a factor of 5-10 fold (Di Cristofano, 2017; Jang et al., 2022). The stability of SGK1 is regulated by post-translational modifications, including polyubiquitination, which results in rapid turnover of the protein. The ubiquitinase target residues are located in the first 60 N-terminal amino acids (Belova et al., 2006; Casamayor et al., 1999; Di Cristofano, 2017).

AKT is another AGC kinase that was considered the prototypical effector of the PI3K signalling cascade. Like SGK1, it is activated by PDK1, but its full activation requires the binding of PIP3 to its PH domain. Both AKT and SGK1 share the target motif arginine-X-argine-X-X-serine/threonine, resulting in a degree of target overlap and a challenge in experimentally attributing specific biological functions to either enzyme. Under physiological conditions, few AKT targets can also be phosphorylated by SGK1 (Di Cristofano, 2017; Lang et al., 2018). However, in specific conditions, SGK1 can compensate for AKT loss or inhibition, particularly in cancer cells where AKT is targeted by target therapy. This compensatory effect is clinically relevant in resistance to AKT-targeted treatments, especially in breast and prostate cancers (Sommer et al., 2013).

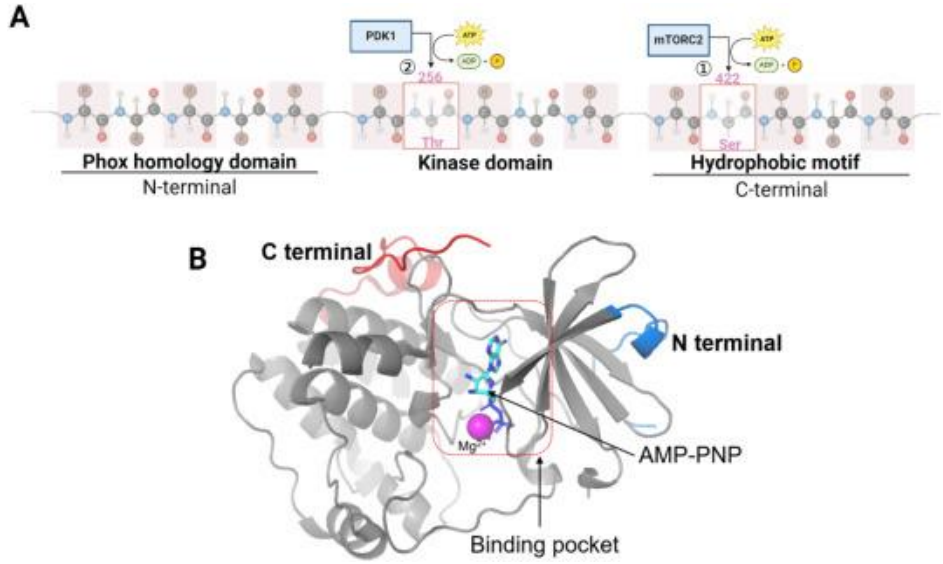

Figure 11. SGK1 structure and activation. (A) Activation of SGK1. Firstly, mTORC2 phosphorylates Ser 422, which is located in the C-terminus of SGK1. Consequently, PDK1 phosphorylates Thr 256, which is located within the activation loop of SGK1. These modifications result in an increase in the volume of the ATP-binding site of SGK1. (B) SGK1 binding domain. The C-terminal is coloured in red and the N-terminal in blue. The pocket is composed of a magnesium ion in magenta and an ATP analogue, an AMP-PNP molecule, in light blue (P. G. Howard et al., 2024)

2.1.3.1. *SGK1 Roles*

SGK1 function is linked to cell proliferation, development, signal transduction and ion channel regulation. Moreover, it plays a pivotal role in apoptosis and inflammation, and has been found dysregulated in diabetes, neurological diseases, cardiovascular diseases, and cancers such as prostate cancer, cervical cancer and oesophageal adenocarcinoma (Jang et al., 2022; M. Wang et al., 2019).

SGK1 in Immune System.

SGK1 plays a multifaceted role in immune response. T helper 2 (Th2) cells are indispensable for B cell proliferation and isotype switching in immune response. It has been demonstrated that SGK1, through the phosphorylation of the ubiquitin ligase NEDD4-2, leads to the differentiation of Th cells into Th2 cells. SGK1 exerts a similar role also in Th9 cells, which, together with Th2 are implicated in the pathogenesis of asthma and allergic diseases (Bian et al., 2023; Di Cristofano, 2017). Th17 cells are pro-inflammatory cells that are crucial in the pathogenesis of chronic Graft-versus-Host Disease (cGVHD) and fibrosis. SGK1 plays a regulatory role in the differentiation of these cells by activating cell sodium channels (R.-Q. Lu et al., 2022). SGK1 has a pivotal role in the recruitment, activation and polarization of macrophages during inflammation. Furthermore, SGK1 is highly expressed in neutrophils, where it promotes cell survival. Conversely, other evidence indicates an anti-inflammatory role suppressing the inflammatory response in CD11 cells (Bian et al., 2023; R.-Q. Lu et al., 2022).

SGK1 in Neuronal System

SGK1 regulates the Epithelial Sodium Channel (ENaC), which is permeable to sodium but also regulates transient H^+-gated currents in neurons. It has been demonstrated that the kinase With No Lysine −1 protein (WNK1) interacts with SGK1 promoting its binding to mTORC2 promoting SGK1 activation.

SGK1 also modulates the Kv7 channels family, which is involved in the maintenance of neuronal membrane potentials and the regulation of potassium ion transport. Long-term potentiation (LTP) is crucial for the formation and maintenance of the memory. SGK1 activation by mTORC increases following tetanisation, with activated-SGK1 upregulating the expression of Postsynaptic Density Protein-95 (PSD-95) in the hippocampus. Moreover, SGK1 modulates glutamate receptors, such as AMPA, enhancing the excitatory effects of glutamate. This is a crucial process in synaptic transmission and plasticity in the hippocampus (Arteaga & Canessa, 2005; P. G. Howard et al., 2024). The loss of SGK1 results in the accumulation of extracellular glutamate, which is caused by the downregulation of glutamate transporters. The accumulation of glutamate in the extracellular space exerts neurotoxic effects, leading to the death of neurons (P. G. Howard et al., 2024).

SGK1 plays a role in the regulation of Brain-Derived Neurotrophic Factor (BDNF), which is important in neuropsychiatric disorders such as Alzheimer's disease, Parkinson's disease, Huntington's disease, depression, and schizophrenia. In Huntington's disease, SGK1 plays a neuroprotective role. It phosphorylates huntingtin at serine 421, which protects striatal neurons from the toxic effects of the mutated protein. In Alzheimer's disease, SGK1 exerts a dual role. On the one hand, it phosphorylates N-myc Downstream-Regulated Gene family member 1 (NDRG1), promoting myelin regeneration. On the other hand, SGK1 interacts with the Tau protein and the Tau-kinase protein GSK-3β, forming a complex that causes the disintegration of microtubules in neurons (P. G. Howard et al., 2024; Lang, Strutz-Seebohm, et al., 2010). In Parkinson's disease, SGK1 plays a pivotal role in the initiation and progression of the pathological process. The inhibition of SGK1 has been demonstrated to safeguard dopamine neurons from degeneration and impedes the aggregation of synuclein (Kwon et al., 2021). Eventually, SGK1 transcription is increased during cerebral ischemia by stimulating the depletion of energy through Na^+/K^+-ATPase stimulation. Moreover, SGK1 inhibits apoptosis, thereby preventing the loss of K^+ and cell swelling (P. G. Howard et al., 2024; Lang, Strutz-Seebohm, et al., 2010).

SGK1 and Diabetes

SGK1 is activated by insulin and involved in the regulation of glucose homeostasis. A common splicing variant of the SGK1 gene (I6CC/E8CC/CT haplotype) has been identified as a potential risk factor for the development of type 2 diabetes, hyperglycaemia, obesity, and high blood pressure (Lang et al., 2009; Schwab et al., 2008). In patients with diabetes, SGK1 enhances fluid retention, hypertension, and coagulation, which in turn leads to the deposition of matrix proteins and fibrosis, as well as diabetic nephropathy (Lang et al., 2009). SGK1 plays a role in the development of obesity, which in turn increases the likelihood of developing type 2 diabetes (Lang et al., 2009; Lang & Stournaras, 2013). The intestines and kidneys, which are responsible for the absorption and reabsorption of glucose, are subject to modulation by SGK1. Within the intestine, the kinase has the capacity to enhance the expression of the Glucose Transporter 1 (GLUT1) and Sodium-Glucose cotransporter 1 (SGLT1) in response to the ingestion of sugar. The overactivation of SGK1 in diabetic patients results in an increased expression of SGLT1, which in turn leads to an augmentation of postprandial blood glucose levels. In the kidney, elevated levels of SGK1 and SGLT1 result in a reduction in glycosuria in diabetic patients (C. Yang et al., 2020). The enhanced uptake of glucose in the intestine, resulting from SGK1 overexpression, provides a conducive environment for the development of obesity. The absorption of glucose results in a significant release of insulin and the accumulation of fat, which subsequently leads to a reduction in glucose levels. Genetic polymorphisms in the 3'-UTR region of SGK1 have been linked to the regulation of insulin secretion, indicating a potential involvement of SGK1 in islet β cell function. In physiological conditions, the expression levels of SGK1 are low in islet β cells; however, they increase in the presence of glucocorticoids. Upon activation, SGK1 upregulates the Kv1.5 potassium channel, which hyperpolarises the membrane of β cells and blocks insulin secretion. Moreover, SGK1 modulates the Na^+/K^+-ATPase during membrane repolarisation, thereby limiting insulin secretion (C. Yang et al., 2020).

Furthermore, SGK1 has been linked to the progression of diabetic complications, including retinopathy, cardiomyopathy and nephropathy associated with diabetes and for all these reasons has been proposed as a possible target in in the treatment of diabetes (Lang et al., 2009; C. Yang et al., 2020).

Other Functions of SGK1

SGK1 plays a crucial role in maintaining skeletal muscle integrity, preventing muscle atrophy (Di Cristofano, 2017). It also plays a crucial role in the implantation of the embryo where its dysregulation is linked to a reduction of embryo implantation rate. Lastly, it has been suggested that SGK1 exert a protective role during pregnancy regulating oxidative stress signals resulting from tissue remodelling (Salker et al., 2011).

2.1.3.2. *SGK1 in Human Cancer*

The PI3K/AKT/mTOR axis plays a pivotal role in the pathogenesis of cancer and the efficacy of anticancer therapies. Mutations in this pathway have been identified as a contributing factor in the development of several human malignancies, promoting cell proliferation and invasion and inhibiting apoptosis (Ghani, 2022). SGK1 is overexpressed in a range of human cancers, including prostate, lung, breast, ovarian, glioblastoma multiforme, myeloma and gastric cancers (Pan et al., 2019; Sang et al., 2020).

SGK1 has been demonstrated to stimulate the ubiquitination of p53, and its depletion has been shown to enhance cell proliferation and the transition from epithelial to mesenchymal cells (Lang & Stournaras, 2013; Sang et al., 2020) (Figure 12). In neoplastic transformation, SGK1 exerts its inhibitory effect on apoptosis through the phosphorylation of Foxo3a at threonine 32 and serine 315. This effect counteracts the Foxo3a-induced cell cycle arrest and apoptosis (Zhu et al., 2020).

In the context of tumour formation, SGK1 phosphorylates, activating, NF-kB, which in turn binds ORAI1 and STIM1 promoters, stimulating their transcription. SGK1 also downregulates the ubiquitin ligase NEDD4L, which is responsible for ORAI1 degradation. ORAI1 and STIM1 are components of the Calcium Release-Activated Calcium channel (CRAC). This channel plays a pivotal role in regulating cancer cell phenotype, angiogenesis and metastasis formation (Di Cristofano, 2017).

In prostate cancer, elevated levels of SGK1 correlate with the migration and invasion of tumour cells (Ghani, 2022). The androgen receptor (AR) is a transcriptional factor that plays a role in the development and progression of prostate cancer. It activates the response element motif of the SGK1 promoter, leading to SGK1 upregulation. Similarly, also glucocorticoid receptor (GR), which modulates SGK1 expression, has been shown to promote survival in prostate cancer and triple-negative breast cancer (Zhu et al., 2020).

In prostate cancer, inhibition of SGK1 and mTOR enhances autophagy causing cytotoxic and impeding cancer progression. Similarly, the inhibition of SGK1 exerts analogous effects on endometrial cancer and glioblastoma multiforme cells (Ghani, 2022).

In colorectal cancer (CRC), SGK1 induces cell proliferation through the nuclear accumulation and transcription inhibition of the tumour suppressor protein p27 (Liang et al., 2017). In intestinal cancers, SGK1 could be found downregulated, which may be due to the action of a transcriptional repressor on the SGK1 promoter. SGK1 is a component of an autoregulatory loop with p53, which modulates cell proliferation, survival and differentiation. p53 activates SGK1, which in turn enhances the ubiquitin ligase MDM2, resulting in the proteasomal degradation of p53. The interplay between SGK1 and p53 is further characterised by the observation that SGK1 is a target gene transcriptionally regulated by p53 and that p53 depletion is controlled by SGK1, thus establishing an autoregulatory loop between SGK1 and p53 (Amato et al., 2009). The SGK-p53 loop is a process which ultimately results in the degradation of p53 which, in the context of the colon, resulting in colonic tumorigenesis.

Furthermore, the kinase has been shown to enhance the clonogenic capacity of cancer cells depending on the p53 expression, regulating the tumour survival and growth (Lang, Perrotti, et al., 2010). Active Transcription Factor 3 (ATF3) plays a crucial role in DDR sensitising cells to radiation response. In this context, SGK1 mediated radio resistance in CRC downregulating ATF3 (Zhou et al., 2020).

SGK1 is also involved in chemoresistance and radioresistance in a number of other tumours, including breast cancer and gliomas. In particular, in gliomas, SGK1 induces chemoresistance by phosphorylating NDRG1 in response to alkylating agents such as temozolomide, which is the most widely used in the treatment of gliomas. In these tumours, high expression levels of NDRG1 have been shown to be predictive of poor response to alkylating agents, and the phosphorylation of NDRG1 by SGK1 confers drug resistance. The present findings suggest that NDRG1 is a potential predictive biomarker for temozolomide resistance, which could be overcome by inhibiting SGK1 (Talarico et al., 2016).

Given the different roles in many human tumours, SGK1 may serve as a potential biomarker for the evaluation of tumour type and grade, as well as for the prediction of prognostic factors in oncological patients (Cicenas et al., 2022; Pan et al., 2019).

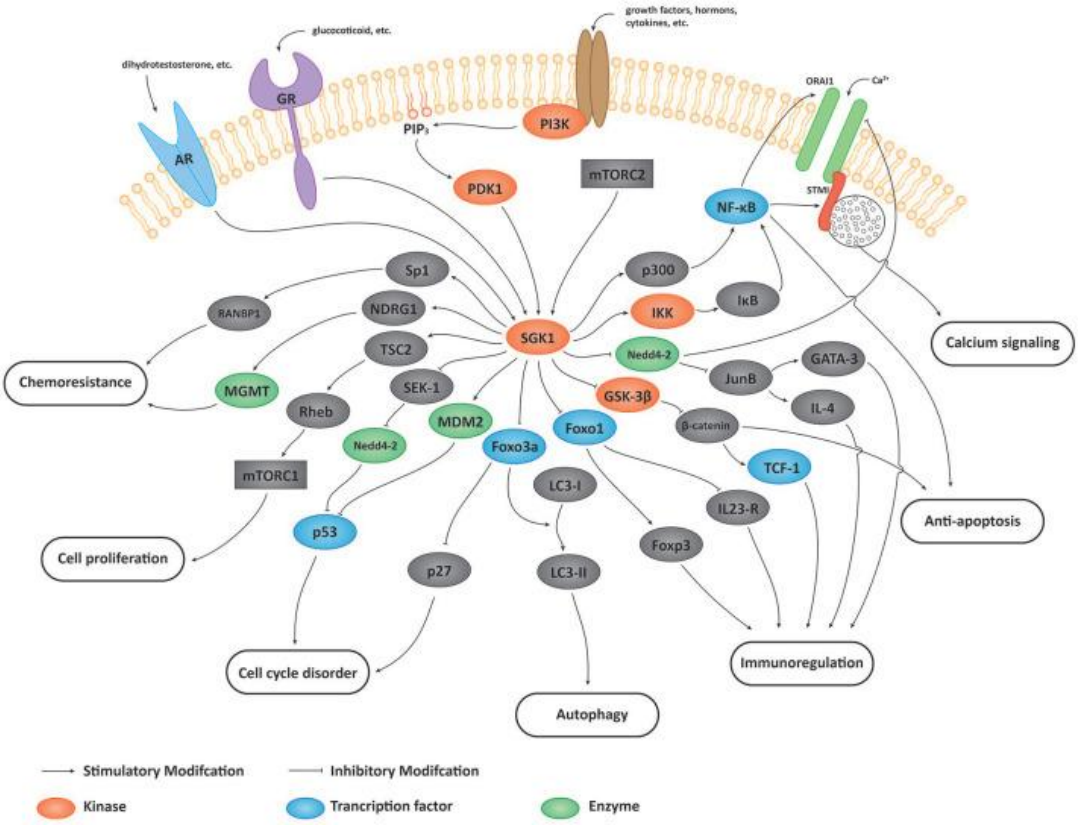

Figure 12. SGK1 Cancer-Related Signalling Pathways. (Zhu et al., 2020)

2.2. ELLAGITANNINS

In recent years, a correlation has been identified between phytochemicals and a reduced risk of chronic diseases, including cardiovascular disorders, diabetes and cancers. It has been demonstrated that a diet comprising a high proportion of phytochemicals is associated with a reduction in cancer-related mortality (Deng et al., 2019). Polyphenols constitute a class of phytochemicals composed by a promiscuous group of potent antioxidants, with Ellagitannins (ETs) representing a significant subgroup. ETs are hydrolysable polymers with a molecular weight ranging from 300 to 20,000 Da having the capacity to trap free radicals, including iron, and reduce oxidative stress. Their biological effects encompass antioxidant, antibacterial, anti-inflammatory, antihepatotoxic, antiatherosclerosis, and anticancer properties. ETs are the result of the secondary metabolism of dicotyledonous plants. They are present in higher concentration in fruit, especially pomegranates, berries, and nuts (Senobari et al., 2022). Chemically, ETs are built from a central sugar core, primarily glucose, which binds with ester bonds to gallic acid through C-C biaryl and C-O diaryl ether bonds. This results in an intra- and intermolecular phenolics oxidative coupling process. The oxidation process generates hexahydroxy diphenic acid (HHDP), which then binds with the sugar to form ETs (Aguilar-Zarate et al., 2018). It is estimated that there are more than 500 ETs, which can be divided into two principal groups: C-glucosidic ellagitannins, presenting an open-chain glucose residue, and dehydro-ellagitannins, which possess a HHDP moiety. The diversity of these compounds is due to the number of different monomers that are incorporated into their structure. The antioxidant properties and gut absorption of ETs are enhanced in accordance with the degree of polymerisation (Senobari et al., 2022). It is believed that the enzyme Ellagitannin acylhydrolase (EAH) plays a major role in the hydrolysis of ETs, generating Ellagic Acid (EA) and HHDP (Figure 13). However, the regulation of this process is poorly understood. ETs could be adsorbed directly into the bloodstream, where they are hydrolysed to EA, which is then transformed into biologically active and bioavailable metabolites, such as urolithins.

A substantial proportion of ETs are metabolised by the microbiota, consequently, ETs absorption is reduced and varies between individuals due to the presence of different microbiota in different individuals (Ismail et al., 2016; Senobari et al., 2022). The metabolic reactions result in the activation of ETs against free radicals, thereby exhibiting augmented antioxidant activity in comparison to their precursors. EA and its metabolites act as antioxidants, modulating the expression of enzymes involved in antioxidant defence, including nicotinamide adenine dinucleotide phosphate-oxidase and CYP-dependent phase-I enzymes (Usta et al., 2013).

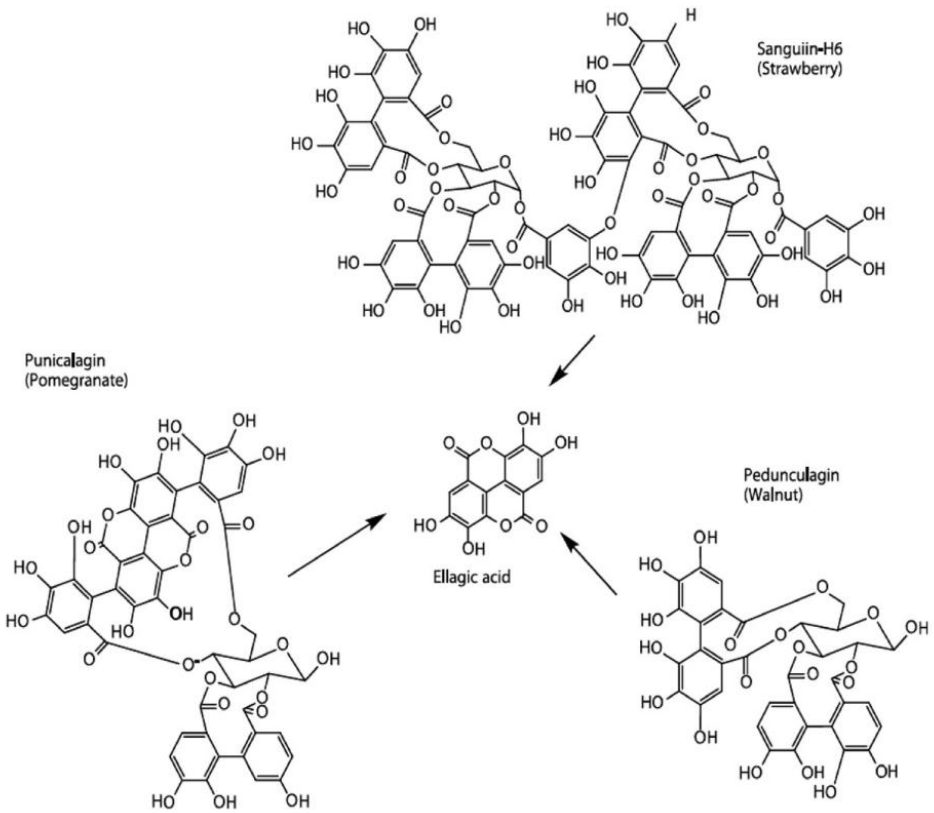

Figure 13. Structures of the major ETs derivatives. The three representative ETs derivatives from different plant sources. Ellagic acid serves as primary precursor of other ETs. (Usta et al., 2013)

2.2.1. Ellagitannins in Therapy

ETs have shown different chemopreventive and chemotherapeutic activities which are correlated with their antioxidant properties and iron-chelating capabilities (Ismail et al., 2016; Usta et al., 2013).

ETs derived from pomegranate have been observed to exert a therapeutic effect on a number of different types of cancer, including breast cancer, liver cancer, colon cancer, pancreatic cancer, uterine cancer, ovarian cancer, lymphoma, leukaemia, myeloma, lung cancer, prostate cancer, and others. In particular, these compounds facilitate cell cycle arrest in the G0/G1 phase of cancer stem cells (CSCs) in breast cancer, thereby reducing the number of cells in S phase and inhibiting proliferation. Additionally, pomegranate derivatives have been demonstrated to enhance the effects of tamoxifen in breast cancer cells (Wong et al., 2021). EA and gallic acid, another ET present in pomegranate, serve a similar function in colon cancer by downregulating DLK1, CD44, and the Wnt/β-catenin pathways (Senobari et al., 2022). In prostate cancer cell lines, pomegranate ETs promote anti-proliferative and pro-apoptotic effects inducing the activation of the apoptotic mediators BAX and BAK, as well as downregulating Bcl-2, Bcl-XL, cyclins, and cyclin-dependent kinases (Ismail et al., 2016).

EA is the most active compound in pomegranate extracts and has been linked to a wide range of beneficial properties, including anti-inflammatory, antifibrotic, anticancer, antimutagenic, immunomodulatory and anti-ageing effects. It has been suggested that EA regulates the cell cycle through the downregulation of Protein Kinase C signalling, which promotes malignancy progression in lymphomas. Furthermore, EA also acts as an inhibitor of DNA topoisomerases, which are implicated in the development of tumours (Ismail et al., 2016; Usta et al., 2013). Nitric oxide (NO) enhances the mitogen-activated protein kinase (MAPK) pathway, which regulates the production of inflammatory mediators. It has been shown that EA modulates NO production, activating the NF-κB pathway in

macrophages, thus affecting inflammatory response. Notably, the same process is mediated also by other ETs present in pomegranate (Baradaran Rahimi et al., 2020). Also, the proliferation, migration, and invasion of melanoma can be inhibited by EA, which mediates the downregulation of p-EGFR and vimentin and the upregulation of E-cadherin (F. Wang et al., 2020). EA also inhibits the proliferation and migration of gastric cancer cells by reducing the expression of Matrix MetalloProteinases 2 and 9 (MMP-2 and MMP-9), which play a pivotal role in regulating cell-matrix interactions (Cheshomi et al., 2022).

Punicalagin is another ETs and the largest known polyphenol exclusively found in pomegranates and, in lower concentration, in the leaves of *Terminalia catappa*. Several biological properties have been attributed to punicalagin, including anti-cancer and disease-modifying effects over a range of human pathologies. Punicalagin undergoes hydrolysis in EA which subsequently transformed into urolithins by the gut microbiota. Punicalagin and its metabolites have been demonstrated to induce a dose-dependent decrease in the DNA damage caused by different tumours (Berdowska et al., 2021). Punicalagin interacts with multiple targets in various types of cancers. As instance, it has been demonstrated to impede the progression and induce apoptosis of cervical cancer through downregulation of NF-κB, which plays a pivotal role in inflammatory processes (Berdowska et al., 2021; Sineh Sepehr et al., 2012). Punicalagin downregulates the same pathway also in prostate cancer inducing apoptosis. In ovarian cancer, punicalagin exerts a similar effect inhibiting the β-catenin pathway, thereby decreasing cell viability and migration. In lung cancer, it suppresses STAT3 pathway, impairing cell proliferation, arresting the cell cycle at the G1/S phases and inducing apoptosis (Berdowska et al., 2021) (Table 1).

The antioxidant and anti-inflammatory properties of punicalagin have been investigated for the treatment of neurodegenerative diseases. It has been shown that it reduces the production of radical oxygen species and enhances mitochondrial functions. Following treatment with punicalagin and EA, there was a notable reduction in both lipid peroxidation and the reduced glutathione level.

Additionally, punicalagin diminishes the expression of pro-apoptotic proteins, including BAX and caspase 3. Moreover, punicalagin promotes the expression and activity of Methionine sulfoxide reductase A (MsrA) in differentiated neuroblastoma cells. MsrA is a reductase that plays a pivotal role in the antioxidant defence. The effects of punicalagin on MsrA, thereby suggests a preventive role in neurodegenerative diseases (Reiterer et al., 2019; Tejada et al., 2017). Punicalagin was also evaluated for its effect in the treatment of Parkinson's and Alzheimer's diseases. It exerts a neuroprotective function in Parkinson's disease by reducing the levels of COX2, IL-18 and IL-1β in the brain, restoring mitochondrial activity and enhancing AMP-activated kinase (AMPK) phosphorylation. Punicalagin mediated neuroprotection is beneficial also in Alzheimer's disease, where it leads to the downregulation of IL-1β, IL-6 and TNF-α in the hippocampus (P. Chen et al., 2023; Tejada et al., 2017).

Pomegranate extracts have been employed to possess beneficial effects in the treatment of other medical conditions, including diabetes, malaria, intestinal infections and cardiovascular diseases (Keta et al., 2020). Pyroptosis, a form of programmed cell death, has been linked to an inflammatory response in the context of diabetic nephropathy. In a model of type 2 diabetes in mice, it has been demonstrated that punicalagin decreases the expression of caspase-1 and IL-1β, which are involved in the TXNIP/NLRP3 axis and the inflammatory cascade of pyroptosis in diabetic nephropathy (An et al., 2020).

Given the multiple beneficial effects of ETs proposed for human diseases, it is imperative to investigate this class of compound to elucidate the molecular mechanisms underlying the properties of these molecules and their potential applications. It is crucial to determine the targets, dosing, possible side effects, toxicity, and therapeutic effects of each single ET alone or in combination with conventional drugs (Ismail et al., 2016).

Table 1. Effects of Punicalagin on different human tumours. Continue in the next page. (Berdowska et al., 2021)

Cancer type	Upregulated factors	Downregulated factors	Effect
Lung carcinoma	Casp-3, 8 and 9, cytochrome C, cytosolic STAT-3, PARP-1, mitochondrial ROS	Jak-1, nuclear STAT-3, Bcl-2, cytosolic ROS	Induction of apoptosis via downregulation of STAT-3 pathway, cell cycle arrest in G1/S phase and inhibition of cell proliferation
Colon carcinoma	Cytochrome C, Casp-3 and 9, cyclin E	Cyclin A and B1, Bcl-XL, COX2, casp-3/7, 8 and 9 and Annexin A1	Cell cycle arrest in S phase, induction of apoptosis via mitochondrial pathway stimulation and suppression of inflammatory mechanisms
Cervical carcinoma	Bax, p53, Casp-3 and 9, cytosolic NF-ϰB-p65	nuclear NF-ϰB-p65 and Bcl-2	Induction of apoptosis via downregulation of NF-kB pathway and inhibition of cell proliferation
Glioblastoma astrocytoma	Cyclin E, Casp-3 and 9, PARP, AMPK-P, p27-P, LC3-II cleavage	Bcl-2, Cyclin A and B	Cell cycle arrest in G2/M phase, induction of apoptosis and autophagy
Osteosarcoma	Not evidence	IL-6, IL-8, P-IkBα and nucleolar NF-kβ-p65	Induction of apoptosis via downregulation of NF-kB pathway, reduction of invasion potential, cell proliferation
Ovarian cancer	Bax and TIMP2/3	Cyclin D1, Bcl-2, β-catenin, MMP2/9	Cell cycle arrest in G1 phase, downregulation of β-catenin pathway, induction of apoptosis and inhibition of cell viability and migration
Cervix epitheloid carcinoma	Bax and TIMP2/3	C-myc, Bcl-2, cyclin D1, β-catenin and MMP2/9	Suppression of cell proliferation and migration, promoting of cell cycle arrest in G1 phase, inhibition of β-catenin pathway. Induction of apoptosis

Breast adenocarcinoma	E-Cadherin	GOLPH3, N-Cadherin, MMP2/9	Suppression of migration via the regulation of GOLPH3, Epithelial-mesenchymal transition and cell viability
Papillary thyroid carcinoma	Beclin-1, P-ERK1/2, p38, LC3-II conversion, P-ATM, P-H2AX, p21, nuclear NF-kB-p65, IL-1β, IL-6, SA-β-Gal, cyclin-dependent kinase inhibitor	P-p62, p70, S6 and 4E-BP1	Induction of apoptosis, autophagy via MAPK activation and mTOR pathway inhibition. Induction of senescence, senescence-associated secretory phenotype (SASP) via the activation of NF-kB, cell death mediated by ATM-mediated DNA damage response

Abbreviation: GOLPH3 = Golgi phosphoprotein 3, LC3-II = Microtubule-associated protein light chain 3 II, SA-beta-Gal = Senescence-associated beta-galactosidase, TIMP2/3 = Tissue inhibitors of metalloproteinases 2 and 3

3. AIM OF THE WORK – 1st Part

In the majority of tumours, TMMs rely on telomerase activity. However, approximately 15% of cancers employ an alternative pathway known as ALT (Maciejowski & de Lange, 2017). ALT-positive cells exhibit elevated telomere recombination and heterogeneous, fluctuating telomere lengths. They also produce ECTCs, particularly C-circles and G-circles, which may arise from telomere trimming or act as self-replicating templates for telomere elongation. Another hallmark of ALT is the presence of APBs, specialized nuclear structures containing telomeric DNA and DNA repair/recombination proteins such as RPA, RAD51, RAD52, and BLM. These bodies are hypothesised to provide a "recombinogenic microenvironment" conducive to ALT activity (J.-M. Zhang et al., 2019, 2021). However, it remains unclear whether ALT DNA synthesis occurs specifically in APBs and whether APBs are essential for ALT DNA synthesis (Cesare & Reddel, 2010). Tumours that utilise the ALT mechanism are not susceptible to anti-telomerase therapies. Moreover, in some cases, the ALT process is activated as a backup in response to therapies that target telomerase (Gao & Pickett, 2022).

Human Pol λ, a member of the X-family of DNA polymerases, is involved in the repair of oxidative DNA damage and in NHEJ of DSBs (Bebenek et al., 2014). Given its similarity with other Pol-X members, Pol λ can be employed as a substitute for Pol β in BER and Pol μ in V(D)J recombination (Kaminski et al., 2021). Our laboratory recently uncovered a functional connection between Pol λ and the ALT pathway. In the ALT-positive human sarcoma cell line U2OS, Pol λ colocalizes with telomeric DNA, and its depletion leads to a significant reduction in APBs formation. Pol λ knockdown also impairs cell viability and induces the accumulation of TIFs, indicating elevated telomeric stress. Similar observations were made in the ALT-positive osteosarcoma cell line SAOS-2, but not in the telomerase-positive HeLa or BJ-hTert cells. These findings suggest that Pol λ may contribute to telomeric DNA synthesis during ALT (Mentegari et al., 2021).

Building on these findings, this project aims to further elucidate the role of Pol λ in the ALT mechanism, comparing its activity to that of other specialized DNA polymerases.

A major limitation in studying Pol λ's role in biological processes is the poor characterization of its interactors. To address this, we employed the BioID approach (D. I. Kim et al., 2014) to identify Pol λ-interacting proteins, particularly under DNA damage conditions. Identifying Pol λ interactors involved in telomere biology will open new avenues for investigating its role in ALT and may reveal novel therapeutic targets for ALT-associated cancers.

4. AIM OF THE WORK – 2nd Part

Approximately 1.7% of human genes encode for protein kinases, which, together with their phosphorylated targets, are essential components of signal transduction pathways regulating physiological and pathological cell processes (G Manning et al., 2002). Mutations in kinase genes play a crucial role in the pathogenesis of numerous diseases, including diabetes, inflammatory disorders, neurodegenerative diseases, metabolic syndromes, as well as cancer onset, progression, and resistance toward therapy (Krupa & Srinivasan, 2002; Middelbeek et al., 2010; Xerxa & Bajorath, 2024). As of 2024, the FDA has approved over 80 small-molecule kinase inhibitors targeting more than 20 different protein kinases, with 58 of these drugs approved specifically for cancer treatment (Roskoski, 2024).

SGK1 is a serine/threonine kinase involved in a variety of physiological and pathological contexts. SGK1 regulates key cellular processes, including proliferation, differentiation and survival. It plays a pivotal role in ion channel activity in the nervous system, contributing to memory formation. Dysregulation of SGK1 has been implicated in multiple diseases, including cancer, ischaemia, diabetes, diabetic neuropathy, hypertension, inflammation, and neurodegenerative disorders (Arteaga & Canessa, 2005; P. G. Howard et al., 2024; Lang & Stournaras, 2013). SGK1 is frequently overexpressed in various types of tumours including prostate, colorectal, breast, endometrial cancers, and glioblastoma where it promotes cell proliferation, invasion, and survival by activating the PI3K/AKT pathway and suppressing apoptosis (Cicenas et al., 2022; Ghani, 2022).

ETs are polyphenolic compounds that are abundant in pomegranate and exhibit diverse biological activities, including antioxidant, anti-inflammatory, antimicrobial, and anticancer properties (Senobari et al., 2022). Upon ingestion, ETs are metabolized by gut microbiota into EA, which is then converted into bioactive urolithins. The intestinal microbiota plays an essential role in ETs processing, limiting ETs bioavailability and making it subject to individual gut microbiota composition (Ismail et al., 2016). ETs have demonstrated therapeutic effects in several cancer types, including breast, liver, pancreatic, colon, uterine, ovarian, lung, prostate cancer, and haematological malignancies.

Although mechanisms of action are not fully understood, evidence suggests that EA exerts anticancer activity by inhibiting DNA topoisomerases, modulating PKC signalling, inducing cell cycle arrest in G0/G1, triggering apoptosis, and enhancing the efficacy of chemotherapeutics (Usta et al., 2013; Wong et al., 2021). Additionally, ETs have been proposed as active compounds in the treatment of other conditions, including diabetes, cardiovascular diseases, and neurodegeneration (Keta et al., 2020).

The aim of this work is to identify novel, potent, and selective SGK1 inhibitors, with a particular focus on ETs and their bioactive metabolites. To this end, this study employs an integrated pipeline encompassing in silico modelling, biochemical screening, and cellular assays to discover and validate new SGK1-targeting compounds. Through this work, we aim to contribute to the development of new therapeutic strategies targeting SGK1 for the treatment of cancer and potentially other SGK1-associated diseases.

5. MATERIALS AND METHODS – 1st Part

5.1. CELL CULTURE

5.1.1. Cells maintenance and treatment

U2-OS and SAOS-2 human osteosarcoma cells (ATCC) were cultured in Dulbecco's modified Eagle's Medium high glucose (DMEM, Euroclone), supplemented with 1X of L-glutamine (Euroclone), 1X of penicillin- streptomycin (Sigma-Aldrich) and 10% of fetal bovine serum (FBS from ThermoFisher), at 37°C and 5% CO2 in a humidified incubator. To enhance the biotinylation of proteins in BioID experiments, cells were grown with 50 μM of biotin at 37°C and 5% CO_2 in a humidified incubator for 16 hours. DNA damages in these clone cell lines were inducted using 25 μM etoposide (Sigma-Aldrich) and 500 μM hydroxyurea (Sigma-Aldrich) for 16 hours.

5.1.2. Cells transfections

For transient cellular transfections 2.5 x 10^5 cells were seeded into 6-well plates. The transfection mixture was prepared using Lipofectamine 2000 transfection reagent (Invitrogen) according to the manufacturer's protocol by adding 500 ng of pBirA and pBirA_Pol λ. Transfected cells were incubated at 37°C for 72 hours and then treated with the selection agent Geneticin (G418, Sigma-Aldrich).

5.1.3. Limiting dilution and clonal selection

Cells were seeded at 70% confluency in a 24-well plate and subsequently transfected with the pBirA and pBirA_Pol λ. Following a 48-hour incubation period, the cells were harvested and diluted until a density of 10 cells/ml was reached. 100 µl aliquot of the cellular suspension was plated in a 96-well plate at a density of 44 cells per well. The medium was DMEM, supplemented with 1 mg/ml of G418, which was used for the selection of a monoclonal population. The cells were monitored daily and expanded gradually until a sufficient number of cells had been obtained for validation by Western blotting. The cell colonies were selected in a medium containing G418 at a concentration of 1 mg/ml for a period of two weeks, after which they were maintained in complete DMEM with the addition of 200 µg/mL of G418.

5.1.4. RNA interference

5 x 10^5 cells were plated in a 100 mm dish and transfected using Lipofectamine RNAiMAX reagent (Invitrogen) according to the manufacturer's instructions. The efficiency of silencing was checked by Western blot analysis. The siRNA utilised are reported in Table 3.

5.2. CLONING

The Pol λ coding sequence used was in the plasmid pcDNA3-PolL developed previously by our laboratory. The PCR was performed according to recommended conditions for the Q5 High-Fidelity DNA polymerase (New England Biolabs, NEB) with 10 ng of vector.
The BirA_Polλ fusion protein was generated using the mycBioID2-13X Linker-MCS (#92308) plasmid (Figure 14), which was purchased from Addgene. This plasmid was designed by Kim et al. to possess a myc-tag, which was required for the detection of the resulting chimera, as well as an additional stretch of nucleotides situated between the multi-cloning site and the biotin ligase: 13X region. This resulted in the formation of an aminoacidic loop consisting of 13 repeats of glycine-serine sequences that confer higher flexibility to BirA. 2.5 μg of DNA of vector was digested with 10U/ul of HindIII and XhoI restriction enzymes (Promega) at 37 °C for 2 hours. The digested backbones were purified using an agarose gel by excising the agarose band corresponding to the proper molecular weight and melting it with the Nucleospin Gel and PCR Clean-UP (Macherey-Nagel) kit.
A high-fidelity PCR of pcDNA3-PolL was conducted using primers with protruding tails that included the corresponding digestion site (Table 2). Following PCR, the reaction was subjected to electrophoresis on an 1% agarose gel, and the DNA was extracted from the low-melting-temperature agarose along with the vector.
The DNA products were quantified and ligate in a ratio 1:3 vector: insert with T4 ligase (Promega) and incubated at 16 °C overnight. Subsequently, the ligated products were transformed into competent bacterial E. coli Top10 cells and incubated at 37°C for 24 hours. The resulting colonies were initially analysed by colony-PCR and subsequently by Sanger sequencing (Eurofins Genomics Europe Shared Services GmbH).

The resulting plasmid were purified with Mini-prep (Promega) and MIDI-prep (Machery-Nagel) kits following the manufacturer's instructions.

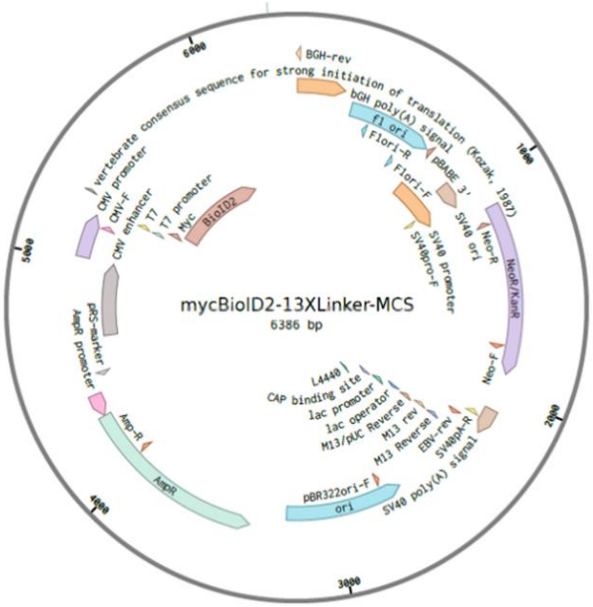

Figure 14: Map of BioID construct. Based on plasmid of Kim et al., 2014

5.3. BIOCHEMICAL TECHNIQUES

5.3.1. Western blot analysis

Cells were harvested using Trypsin EDTA (Euroclone), washed in DPBS (Euroclone), and then lysed in 1X COIP buffer (10 mM Tris HCl pH 7.6, 140 mM NaCl, 50 mM EDTA pH8, 0.5% NP-40), which was supplemented with a protease inhibitor cocktail (Sigma Aldrich) prior to use. The protein concentration was determined through the Bradford assay (Bio-Rad), which correlates the absorbance values with a calibration curve of the standard protein, Bovine Serum Albumin (BSA, Sigma-Aldrich). The proteins were subjected to electrophoresis using a 4–20% Mini-PROTEAN® TGX™ Precast Polyacrylamide Gel (Bio-Rad) in running buffer TGS1X buffer (240 mM Tris, 192 mM Glicine, 300 mM SDS). In the case of the control pull-down samples, the denaturation step was conducted by adding a biotin excess of 12.5 μM. Subsequently, the proteins were transferred to an Immuno-Blot nitrocellulose membrane (Bio-Rad, Transblot turbo transfer pack). The membranes were blocked for one hour at room temperature (RT) with 5% non-fat dried milk (Sigma-Aldrich) in 1X TBS (20 mM Tris HCl pH 7.5, 150 mM NaCl) for classical antibodies. Conversely, the detection of biotinylated proteins was conducted using a 1% BSA + 0.2% Triton X-100 (Applichem) blocking solution, which was incubated at room temperature for 10 minutes. The primary antibodies (Table 4) were incubated overnight at 4°C in a solution comprising 3% non-fat dried milk and 1X TBS-0.1% Tween (Fisher Bioreagents). The streptavidin-HRP was incubated for 1 hour at RT. Subsequently, the membranes were washed with TBS-T prior to the incubation of secondary antibodies (Table 4) for one hour at room temperature. This was conducted using HRP-conjugated antibodies diluted 1:3000 in 3% non-fat dried milk in TBS-T. For signal detection, the membranes were incubated with the chemiluminescence HRP substrate WESTER NOVA 2.0 (Cyanagen), or, for the detection of a weaker signal, with the WESTERN ηC ULTRA

2.0 (Cyanagen). The images were obtained using the ChemiDoc MP Imaging System (Bio-Rad). The intensity of the signal produced is directly proportional to the amount of protein detected on the membrane. The signals were quantified with Image Lab software (Bio-Rad).

5.3.2. Reverse transcription-quantitative PCR (qRT-PCR)

The primers used for the evaluation of DNA polymerase θ expression levels after its silencing by qRT-PCR are reported in Table 2.

Total RNA was extracted from cell pellets using the ReliaPrep™ RNA Miniprep System (Promega), following the manufacturer's instructions. RNA concentration and purity were assessed using a NanoDrop™ spectrophotometer. Reverse transcription was performed using the QuantiTect Reverse Transcription Kit (Qiagen). Specifically, 1 μg of RNA was retrotranscribed in a 14 μL reaction mix containing 1× Quantiscript RT Buffer, 1 μL of Quantiscript Reverse Transcriptase, and 1 μL of RT Primer Mix. The reactions were incubated at 42 °C for 15 minutes in a water bath, followed by 3 minutes at 95 °C in a dry block heater. RNA quantification was performed using the QuantiTect Sybr Green PCR kit (Qiagen). For each reaction, a 1:10 diluition of cDNA (or water for negative controls) was mixed with reaction mix (1X QuantiTect SYBR green PCR master mix, 0.5 μM pf each primer) in a total volume of 20 μl. Each sample was transferred into a 96-well PCR plate (Roche), sealed with optical adhesive film, centrifuged at 1000 × g for 1 minute, and analysed using a LightCycler® real-time PCR system (LC480, Roche).

5.3.3. Immunofluorescence (IF)

Biotinylation pattern validation

BioID clones were seeded on glass coverslips, which had been previously treated for 30 minutes with UV light and embedded in 2% gelatin (obtained from cold water fish skin, Sigma-Aldrich) in sterile DPBS, in order to improve cell adhesion. The cells were fixed by incubating them in 2% formaldehyde (PFA, Sigma-Aldrich) for 10 minutes at room temperature. Subsequently, the cells were permeabilised with Triton X-100 (0.25%) for a period of five minutes. Streptavidin conjugated with a fluorophore (Alexa fluor 488 dye, Invitrogen) diluted 1:500 in a blocking solution with 3% FBS in DPBS was added to each glass coverslip for a period of 2 hours at room temperature. The cell sample was treated with DAPI (Invitrogen) at a concentration of 1:100,000 for a period of 15 minutes at room temperature, with the objective of staining the DNA. Subsequently, the coverslips are mounted on slides with mounting solution (Aqua-Poly/Mount, Polyscience), stored in the dark for 1-2 hours at room temperature, and then transferred to 4°C in a cold room. Images were obtained using a 63x objective on a confocal microscope (Zeiss). The cell nuclei were visualised at 405 nm (DAPI) and at 488 nm (FITC). the images were analysed with FIJI software.

5.3.4. C-Circles Assay

$7.5x10^5$ U2OS and SAOS-2 were plated in a 100 mm dish and transfected with siRNA against Pol λ, Polμ, Polθ and scrambled siRNA. After one day of recovery, cells were harvested using trypsin-EDTA (Euroclone), washed in DPBS (Euroclone) and DNA extracted using the Nucleospin Tissue Kit (Machery-Nagel) according to the manufacturer's instructions. 30 ng of genomic DNA was digested at 37°C O/N with HinfI and RsaI (Thermo Fisher Scientific) and RNase A (Sigma-Aldrich) in Tango 1x buffer

(Thermo Fisher Scientific). The digested DNA was incubated with an amplification mix (0.2 mg/mL BSA, 0.1% Tween, 1 mM dNTPs (Euroclone)) supplemented with ϕ29 Pol and its reaction buffer (Thermo Fisher Scientific) for 8 hours at 30°C. The ϕ29 Pol was then inactivated by incubation at 70°C for 20 minutes. DNA samples were then spotted onto a nylon transfer membrane (GeneScreen Hybridisation Transfer Membrane, PerkinElmer) pre-hydrated in distilled H_2O for 10 minutes using a Bio-Dot Microfiltration Apparatus (Bio-Rad). The membrane was cross-linked on both sides with 254 nm UV radiation at 1200 J to covalently bind DNA to the membrane, washed twice in SSC2× (for 5 minutes with agitation. The membrane was then blocked in PerfectHyb Plus Hybridisation Buffer pre-hybridisation buffer preheated at 65° C for 2 hours (Sigma-Aldrich). The membrane was incubated with the C-rich 60-mer probe 5′ -CCC TAA CCC TAA CCC TAA CCC TAA CCC TAA CCC TAA CCC TAA-3' (biomers.net), labelled with T4 polynucleotide kinase (New England Biolabs) in the presence of γ32P-ATP (PerkinElmer), for 5 min at 65°C O/N. The labelled probe was purified using ILLUSTRA MICROSPIN G25columns (GE Healtcare). After washing, the membrane was dried and exposed to a phosphor screen for 40 minutes. The signal was detected by phosphor imaging (Typhoon, GE Healthcare).

5.3.5. Pull-Down assay

A total of 5 x 10^6 cells were seeded in a 150 mm dish with complete DMEM, supplemented with 200 μM of G418. Following a two-day incubation period, during which the cells reached 75% to 80% confluency, biotin was added to the medium for a 16-hour period. Following biotin treatment, the cells were washed and harvested using ice-cold PBS, then lysed in 1X ice-cold RIPA buffer, which was supplemented with protein inhibitors. To facilitate the digestion of nucleic acids, 1 μL of the enzyme benzonase (250 U/μL) was added to each sample. Dynabeads MyOne Streptavidin C1 beads (Invitrogen) were washed

with ice-cold RIPA buffer devoid of inhibitors. The 16-Tube SureBeads Magnetic Rack (Bio-Rad) was employed to facilitate the collection of all magnetic beads at the edge of the tube. Consequently, the magnetic beads were introduced into the clarified cell lysates. The tubes containing the cell lysate and the beads were incubated in a cold room at 4°C with rotation for a period of four hours. Once the affinity capture process was complete, the biotinylated proteins were collected using the magnetic rack, and the flowthrough was also recovered to monitor the unbound bait proteins as a control. The beads were then washed in RIPA buffer devoid of inhibitors and subsequently washed in 50 mM ice-cold ammonium bicarbonate (Sigma-Aldrich, ABC) before being pelleted with the magnetic rack. This washing procedure was necessary to ensure the removal of impurities from the beads. The beads were subsequently stored in 50 mM ABC, compatible with downstream MS analysis. Subsequent MS analyses were conducted by the Proteomics Unit Institute for Biomedical Technologies (ITB) of the National Research Council (CNR), led by Dr. Mauri and his team.

Protein extraction and enzymatic digestion

The beads were lysed, reduced/alkylated and subjected to enzymatic digestion with trypsin and Lys-C, using the Easy PepTM Mini MS Sample Prep Kit (Thermo Fisher Scientific). In accordance with the instructions provided in the kit, the peptides were generated, purified, and resuspended in 0.1% formic acid (Sigma-Aldrich) for subsequent LC-MS/MS analysis.

LC-MS/MS Analysis

Peptide mixtures were subjected to analysis using the Eksigent nanoLC-Ultra® 2D System (Eksigent), in conjunction with the cHiPLC-nanoflex system (Eksigent) in trap-elute mode. Two technical replicates were conducted for each condition, with the cHiPLC trap (200 μm x 500 μm ChromXP C18-CL, 3 μm, 120 Å, Eksigent) being injected and the loading pump operated in isocratic mode with 0.1% formic acid in water for 10 minutes at a flow

rate of 3 µL/min. Subsequently, the cHiPLC ten-port valve was engaged to elute the trapped mixture on a nano cHiPLC column (75 µm x 15 cm ChromXP C18-CL, 3 µm, 120 Å, Eksigent) through a 95-minute gradient of eluent B (eluent A, 0.1% formic acid in water; eluent B, 0.1% formic acid in acetonitrile) at a flow rate of 300 nL/min. The gradient was of a depth of 5-10% B for a period of three minutes, 10-25% B for 60 minutes, 25-40% B for five minutes, 40-95% B for five minutes, and 95% B for eight minutes. The eluted peptides were subjected to direct analysis on an Orbitrap Exploris 120 mass spectrometer (Thermo Fisher Scientific), which was equipped with an EASY-Spray ion source (Thermo Fisher Scientific). The EasySpray emitter (Thermo Fisher Scientific) (nanoflow 7 µm ID transfer line 20 µm x 50 cm) was held to 1.6 kV, while the ion transfer capillary was held at 220 °C, resulting in the desired EasySpray configuration. A data-dependent acquisition (DDA) was conducted, with precursor ions acquired within a mass-to-charge ratio range of 375–1,250 at a resolution (at m/z 200) of 60,000 full width at half maximum (FWHM). Precursor fragmentation was conducted at a resolution (at m/z 200) of 15,000 FWHM, employing the higher-energy collisional dissociation (HCD) method with a normalized collision energy (NCE) of 30 eV and a dynamic exclusion period of 20 seconds. The MS and MS/MS data were acquired in profile and centroid mode, respectively, with positive polarity and isotope exclusion enabled. The isolation width was set at 2 m/z, with the initial mass set at 120 m/z. The mass spectrometer scan functions and high-performance liquid chromatography solvent gradients were controlled by the Xcalibur data system, version 4.4 (Thermo Fisher Scientific), and the Eksigent Control Software, version 4.3 (Eksigent), respectively.

Data Handling

All raw data were subjected to a search against the Homo sapiens proteome database (74,842 entries), downloaded in March 2021 from Uniprot (www.uniprot.org) using the Sequest HT search engine, which is contained in Proteome Discoverer software, version 2.1 (Thermo Fisher Scientific). The following criteria were employed for the identification

of peptide sequences and related proteins: mass tolerances of ± 10 ppm for precursor ions and ± 0.02 Da for fragment ions; trypsin as the enzyme with a maximum of three missed cleavage tolerance; carbamidomethylation of cysteines as a fixed modification; methionine oxidation as a variable modification. The Percolator node was employed with a target-decoy strategy, resulting in a false discovery rate (FDR) of 1% (strict) and 5% (relaxed), based on q-values, with XCorr >1.2 and maximum deltaCN of 0.05 [Käll L, Canterbury JD, Weston J, Noble WS, MacCoss MJ]. The objective of this study is to develop a semi-supervised learning method for peptide identification from shotgun proteomics datasets. Nature Methods. [2007 Nov;4(11):923-5]. Only peptides with a minimum length of six amino acids and a rank of 1 were considered. The protein grouping and strict parsimony principles were applied.

Differential expression, linear discriminant analysis and PPI network

The protein lists obtained from the SEQUEST algorithm were aligned and compared using the average peptide spectrum matches (aPSM), which represents the average of all the spectra identified for a protein and, consequently, its relative abundance in each analysed condition. To identify proteins that were differentially expressed, the experimental conditions were pairwise compared, applying a threshold of 0.35 and 5 on the two MAProMa indexes, DAve (Differential Average) and DCI (Differential Confidence Index), respectively.

5.4. STATISTICAL ANALYSIS

All data were analysed and visualized using GraphPad Prism 9 (GraphPad Software). Densitometric quantification of Western blot bands was performed using Image Lab software (Bio-Rad).

6. MATERIALS AND METHODS – 2nd Part

6.1. CELL CULTURE

6.1.1. Cells maintenance

HEK293T cells of human embryonic kidney contains the SV40 T-antigen (ATCC) were cultured in Dulbecco's modified Eagle's Medium high glucose (DMEM, Euroclone), supplemented with 1X of L-glutamine (Euroclone), 1X of penicillin- streptomycin (Sigma-Aldrich) and 10% of fetal bovine serum (FBS from ThermoFisher Scientific), at 37°C and 5% CO2 in a humidified incubator.

6.2. IN SILICO ANALYSIS

A computational study was conducted by our collaborator, Prof. Manetti of the University of Siena, with the objective of identifying new inhibitors of SGK1. A ligand-based drug design approach was employed to generate a common-feature pharmacophoric model using the chemical structures of eight SGK-1 inhibitors (namely, compounds 1, 2, GSK650394, 3, 21g, EMD638683, SI113, 5), as identified through the software Phase of the Schrödinger suite.

6.3. IN IN VITRO KINASE INHIBITION ASSAYS

Recombinant human SGK1 (amino acids 60–end) (NCBI Gene ID: 6446) were purchased from Promega. The peptide substrate is included in the system purchased.

Assay conditions:

SGK1 reactions were performed in 10 µL using: 40mM Tris Ph 7.4; 20mM MgCl2; 0.1mg/ml BSA; 50µM DTT, 0.15 mM ATP, 5% DMSO, 10 ng of SGK1 and 1 µg/µl of peptide substrate (CKRPRAASFAE). All reactions were performed at 30 °C for 10 min. Reactions were stopped depleting the remaining ATP by adding 10 µl of ADP-Glo Reagent (Promega) for 40 minutes at 23°C shacking the tubes. 20 µl of Kinase Detection Reagent (Promega) were added and incubated for 60 minutes at room temperature. Luminescent signal was detected on a GloMax plate reader (Promega) in accordance to manufactures instructions. Time course experiment revealed linear generation of products up to 40 min of reaction. Titration of reaction substrates (ATP and peptide substrate) was performed and apparent affinities (Km) calculated according to Michaelis-Menten method (equation 1).

$$v = (V_{max} [PEP])/ (Km + [PEP]) \quad (1)$$

$Km_{(ATP)}$ = 121.5 +-8 µM

$Km_{(PEP)}$ = 6 +- 1.6 µM

IC50 values were obtained according to Equation 2, where v is the measured reaction velocity, V is the apparent maximal velocity in the absence of inhibitor, I is the inhibitor concentration, and IC50 is the 50% inhibitory concentration.

$$v = V/\{1+(I/IC50)\} \quad (2)$$

6.1. BIOCHEMICAL TECHNIQUES

6.1.1. Western blot analysis

Cells were harvested using Trypsin EDTA (Euroclone), washed in DPBS (Euroclone), and then lysed in 1X COIP buffer, which was supplemented with a protease inhibitor cocktail (Sigma-Aldrich) prior to use. The protein concentration was determined through the Bradford assay (Bio-Rad), which correlates the absorbance values with a calibration curve of the standard protein, bovine serum albumin (BSA, Sigma-Aldrich). The proteins were subjected to electrophoresis using a 4–20% precast polyacrylamide gel (Bio-Rad). In the case of the control pull-down samples, the denaturation step was conducted by adding a biotin excess of 12.5 μM. Subsequently, the proteins were transferred to an Immuno-Blot nitrocellulose membrane (Bio-Rad, Transblot turbo transfer pack). The membranes were blocked for one hour at room temperature (RT) with 5% non-fat dried milk (Sigma-Aldrich) in TBS-T. The primary antibodies (Table 4) were incubated overnight at 4°C in a solution comprising 3% non-fat dried milk and TBST. Subsequently, the membranes were washed with TBS-T prior to the incubation of secondary antibodies (Table 4) for one hour at room temperature. This was conducted using HRP-conjugated antibodies diluted 1:3000 in 3% non-fat dried milk in TBST. For signal detection, the membranes were incubated with the chemiluminescence HRP substrate WESTER NOVA 2.0 (Cyanagen), or, for the detection of a weaker signal, with the WESTERN ηC ULTRA 2.0 (Cyanagen). The images were obtained using the ChemiDoc MP Imaging System (Bio-Rad). The intensity of the signal produced is directly proportional to the amount of protein detected on the membrane.

6.1.2. Nanogels

To circumvent low membrane permeability due to high hydrophilicity of ellagitannins, the compounds were conveyed into cells using a nanogel matrix developed by our collaborators of University Politecnico of Milan led by Professor Mauri. Nanogels were synthesized according to the multi-step procedure previously developed (Mauri et al., 2016).

Nanogels were loaded with 10 µl of drug/mg, and the solution was spun at 5000-6000 rpm. After an incubation period of 20 minutes, the nanogels were diluted to the desired concentration and added to the cells.

6.1.3. Immunofluorescence (IF)

200 000 HEK 293T cells were seeded on glass coverslips, which had been previously treated for 30 minutes with UV light. After 24 hours, cells were treated for different time points with nanogels at 0.1, 0.5 and 1 mg/ml concentration of nanogel to define the concentration of nanogel to use. Otherwise, over a 24-hour period cells were treated with 0.5 mg/ml of nanogels with different time points at 2, 4, 6, and 8 hours to determine the incubation time of the particles. The cells were fixed with 4% PFA by incubating them in 2% formaldehyde for 10 minutes at room temperature. Subsequently, the cells were permeabilised with Triton X-100 (0.25%) for a period of five minutes. The cell sample was treated with DAPI (Invitrogen) at a concentration of 1:100,000 for a period of 15 minutes at room temperature, with the objective of staining the DNA. Subsequently, the coverslips are mounted on slides with mounting solution (Aqua-Poly/Mount, Polyscience), stored in the dark for 1-2 hours at room temperature, and then transferred to 4°C in a cold room. Images were obtained using a 63x objective on a confocal microscope (Zeiss). The cell nuclei were visualised at 405 nm (DAPI) and at 555 nm (TRITC).

6.1.4. FACS

200 000 HEK 293T cells were seeded for each well and harvested using Trypsin EDTA (Euroclone), centrifuged, and washed in DPBS (Euroclone) to remove cell culture medium and cellular debris. Following a second centrifugation, the cells were resuspended in DPBS or DAPI at a concentration of 1:50 000 (Invitrogen). Prior to fixing the cells, which had been resuspended in DPBS, with PBS-buffered 4% PFA, the cell nuclei were labelled with Zombie UV fixable viability staining (BioLegend, cat. no. 423107) in accordance with the manufacturer's datasheet. Thereafter, the samples were analysed using the BD FACS Lyric, with NG-positive fluorescence evaluated in the PE channel.

6.1. CELLULAR KINASE INHIBITION ASSAYS

To confirm the efficacy of the most prominent candidates, a BRET-based assay, namely NanoBRET™ TE Intracellular Kinase Assays (Promega), was performed in accordance with the manufacturer's protocol in HEK 293T cells. A total of 2×10^5 cells were seeded in each well of a 96-well white plate (Corning) using an assay medium composed of Opti-MEM (Thermo Fisher Scientific) and FBS. The inhibitors encapsulated within the nanogel were incubated for a period of six hours within the cells. The luminescent signal was detected on a GloMax plate reader (Promega) in accordance with the manufacturer's instructions.

Table 2. Primers sequences

Name	Sequence 5' → 3'
XhoI_Fw	CCATCTCGAGGATCCCAGGGGTATCTTGAAGGC
HindIII_Rv	CAGCAAGCTTTCACCAGTCCCGCTCAG
GAPDH_Fw	TGCACCACCAACTGCTTAGC
GAPDH_Rv	GGCATGGACTGTGGTCATGAG
Polθ_Fw	GGGGGCGTGGGGGAAGTAGAAT
Polθ_Rv	TGCCTATGGCTGCTGTCTGGGT

Table 3. List of SiRNA

Name	Sequence 5' → 3'
siPol λ, Ambion	CAAAAGUACUUGCAAAGAU
Scrambled control, Ambion	Silencer Select Negative Control siRNA #1
SiPolμ, Ambion	GCAUUUUCCGCCUACCACA
SiPolθ, IDT	AGCAUGAUAGCUAUU

Table 4. List of antibodies

Name	Dilution	Distributor
Anti-Pol λ	1:1000 in WB, 1:500 in IF	Santa Cruz Biotechnology
Anti-Pol θ	1:10000	Thermo Fisher Scientific
Anti-Pol μ	1:1000	Sigma-Aldrich
anti-myc tag	1:500 in WB, 1:250 in IF	Abcam
anti-actin	1:500	Santa Cruz Biotechnology
Anti-vinculin	1:10000	Millipore
Streptavidin-HRP	1:40000	Thermo Fisher Scientific
Anti-PML	1:250	Santa Cruz Biotechnology
Anti-NDRG1	1:1000	Cell Signalling
Anti- phospho-NDRG1	1:1000	Cell Signalling
Donkey-anti-goat-Alexa 488	1:500	Abcam
Donkey-anti-goat-Alexa 555	1:500	Abcam
Donkey-anti- rabbit-Alexa488	1:500	Abcam
Goat- anti-mouse-Alexa555	1:500	Abcam
Goat- anti- mouse-HRP	1:3000	Jackson ImmunoResearch
Goat- anti- rabbit-HRP	1:3000	Jackson ImmunoResearch

7. RESULTS – 1st part

7.1. ALT ACTIVITY AND POL Λ

A distinctive hallmark of ALT is the presence of Circular C-rich telomeric DNA (C-circles), which can be utilised to quantify ALT activity in a robust and effective manner through the C-circle assay. In this technique, C-circles are employed as a self-primer to perform a rolling circle amplification, thereby obviating the need for primer hybridisation and precluding the detection of non-ALT-specific telomeric DNA. The resulting amplification products thus provide a quantitative and responsive indicator of ALT activity (Henson et al., 2017). To ascertain the function of Pol λ in the ALT process, the levels of C-circles were examined following Pol λ silencing in U2OS and SAOS-2 cell lines. In both cell lines, an increase in C-circles was observed following Pol λ depletion, suggesting that Pol λ counteract ALT activity (Figure 15).

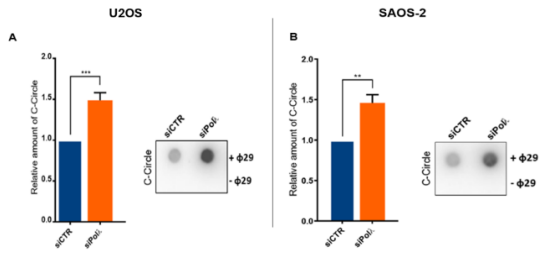

Figure 15. Pol λ silencing leads to an increase in C-circle levels. 20 ng of extracted DNA from U2OS **(A)** and SAOS-2 **(B)** cells were utilized as the template for rolling circle amplification with DNA polymerase ϕ29. The silencing of Pol λ leads to a significant increase in both ALT cell lines. The telomeric signal was normalised using an Alu probe. The error bars represent the mean and standard deviation. The uncoupled two-tailed T-test was used to calculate the p-value. *P<0.05, ***P<0.001

Pol μ and Pol θ share enzymatic activities with Pol λ, including template independent synthesis. Like Pol λ, Pol μ participates in NEHJ, while Pol θ is involved in MMEJ. The involvement of these two polymerases in ALT has been poorly explored. To elucidate their role in this pathway, a C-circles assay was conducted in U2OS and SAOS-2 following silencing of these factors (Figure 16-17). In this case, the depletion of Pol μ or Pol θ caused an increase in C-circle levels. Conversely, simultaneous silencing of Pol λ and Pol μ or Pol θ results in no additive effect in C-circle formation.

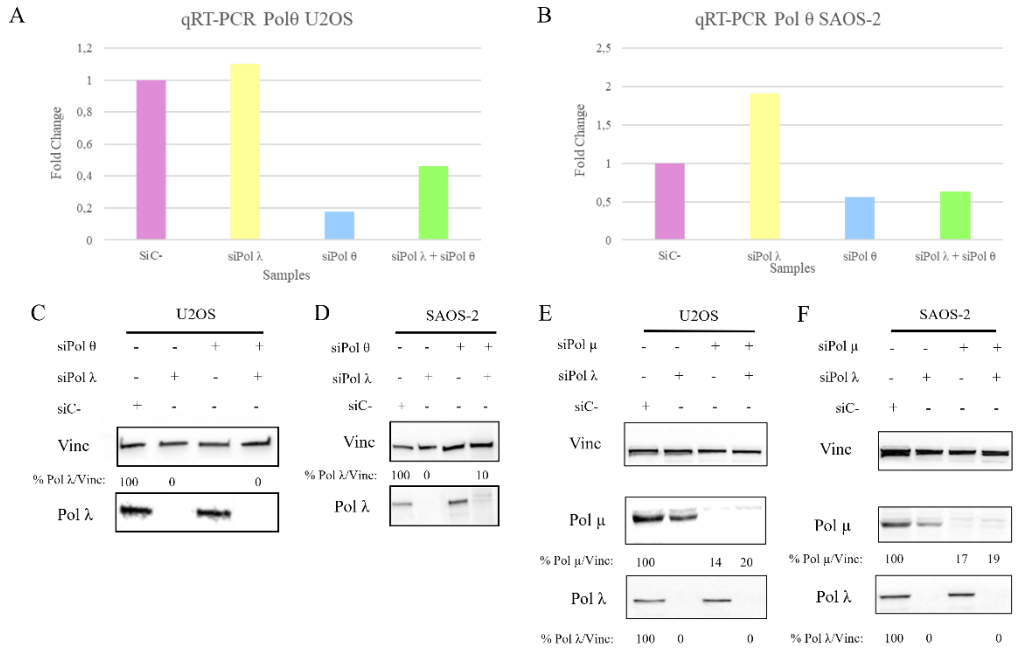

Figure 16. Validation of DNA polymerases silencing efficiency. (A-B) Lack of an effective α-Pol θ antibody required qRT-PCR experiments to evaluate Pol θ mRNA levels. Pol θ expression was normalized to GAPDH. **(C-F)** Pol λ and Pol μ protein levels were assessed using the respective antibodies. DNA polymerase/Vinculin signal ratio is reported.

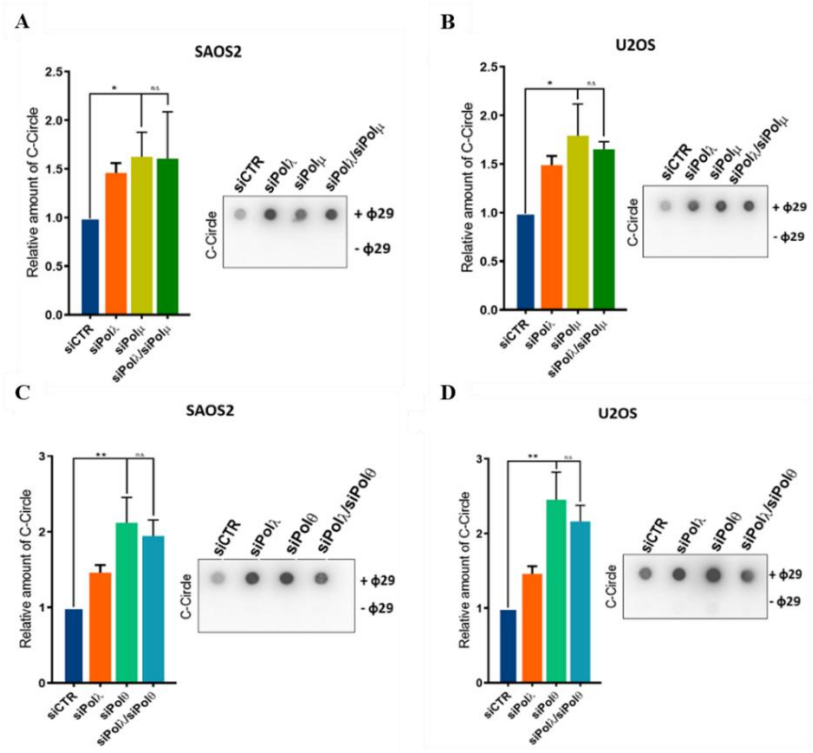

Figure 17. The depletion of Pol λ and Pol μ causes an increase in C-circle levels. 20 ng of extracted DNA from SAOS-2 **(A and C)** and U2OS **(B and D)** cells were utilised for the performance of rolling circle amplification with DNA polymerase ϕ29. The single silencing of each polymerase resulted in an increase in C-circles; however, the double depletion of Pol λ and Pol μ together or Pol λ and Pol θ together does not result in a further enhancement of the C-circles levels. The telomeric signal was then normalised using an Alu probe. The error bars represent the mean and standard deviation. The uncoupled two-tailed T-test was employed to calculate the p-value. *P<0.05, ***P<0.001

These results demonstrate that the studied Pols have similar roles on C-circle formation. This could underlie overlapping functions in ALT modulation, questioning the specific role of Pol λ in ALT.

To understand the specific role of Pol λ in the ALT pathway, it would be important to investigate its specific interaction partners. Unfortunately, Pol λ is transiently involved in multiple DNA repair pathways, making the identification of stable interactors particularly challenging. Moreover, available antibodies against Pol λ are not sufficiently selective, often recognizing other PolXs, and are poorly effective for immunoprecipitation-based approaches. For this reason, we decided to investigate the Pol λ interactome using a BioID approach.

7.2. EXPRESSION OF CLONED VECTORS

We cloned Pol λ cDNA within the BioID2 vector myc-BioID2-13XLinker-MCS, which expresses a myc-tag and a 13-amino acid linker between the BirA and the multicloning site. The gene was inserted using XhoI and HindIII restriction enzymes and sequence integrity was then tested by Sanger analysis (see Materials and Methods 5.2.; Figure 18).

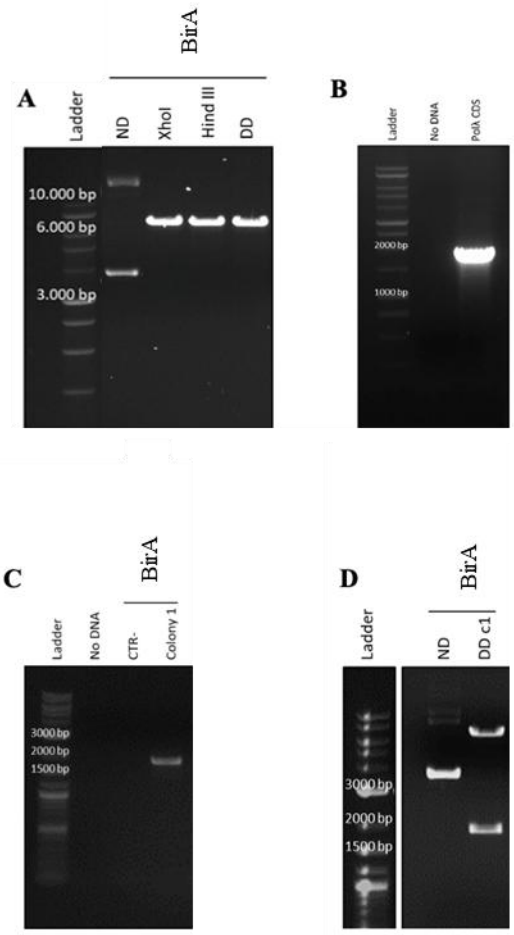

Figure 18. pBirA_Pol λ assembly and validation (A) Control digestion of construct BioID2-13X-MCS with the restriction enzymes XhoI and HindIII at 37°C for 2 hours. **(B)** Amplification of Pol λ from pcDNA3-Polλ plasmid. **(C)** PCR confirmation of BioID-2-P13X-Pol λ positive colonies after E. Coli Top10 transformation. **(D)** Control digestion with XhoI and HindIII from single colony DNA prep.

7.3. CELLULAR EXPRESSION OF CLONED VECTORS

Sequence validated constructs expressing BirA tagged Pol λ (pBirA_Pol λ) and the sole BirA (pBirA) were used to transiently transfect U2OS cells. After 48 and 72 hours, the expression was confirmed through WB analysis using anti-Myc antibodies (Figure 19). The expected signal at 50 and 100 kDa was observed for both BirA and BirA_Pol λ proteins.

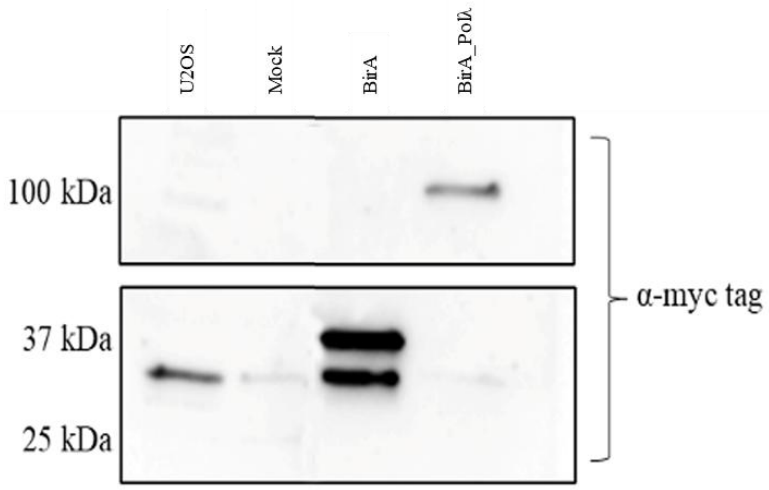

Figure 19. BirA and BirA_Pol λ expression in U2OS. U2OS: untreated cells; mock: only lipofectamine treated cells; BirA: U2OS transfected with pBirA; BirA_Polλ: U2OS transfected with pBirA_Polλ. In all samples, an unspecific band appeared at 35 kDa and was considered as a background signal

Subsequently, the activity of BirA was investigated by administering 50 μM of free biotin to transfected cells for 16 hours. The efficacy of biotinylation was determined by WB using HRP-conjugated streptavidin. A diffused biotinylation signal was observed in cells transfected with pBirA. Conversely, in cells expressing BirA_Pol λ a more specific biotinylation pattern was evident (Figure 20 A, compare BirA and BirA_Pol λ labelled lanes). This result corroborates the hypothesis that BirA biotinylates proteins that specifically interact with Pol λ, while the only BirA exhibits broader, unspecific activity. Moreover, a faint biotinylation pattern is present also in samples not treated with biotin. This is probably due to the presence of endogenous biotin. To verify the expression of the constructs, WB analysis using anti-myc antibodies was performed (Figure 20 B) and myc signal was properly detected in each condition.

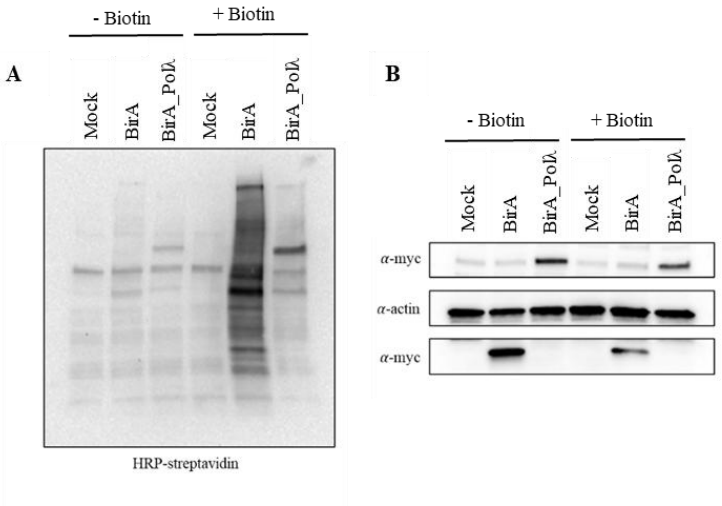

Figure 20. Biotinylation pattern of BirA and BirA_Pol λ. (A) WB analysis using streptavidin-HRP of protein extract of U2OS (mock) or U2OS transfected with pBirA or pBirA_Polλ in the absence and in the presence of biotin. **(B)** WB of the same samples to detect construct expression using α-myc antibody

After the validation of constructs expression and biotin ligation activity, we generated stable U2OS cell lines expressing BirA_Pol λ or BirA alone. A limiting dilution approach was used to select stable expressing clones. In this procedure, transfected cells were seeded at a density of 10 cells/mL in the presence of a selection agent. 15 clones for each construct were screened and analysed via WB to verify the expression of BirA and BirA_Pol λ (Figure 21).

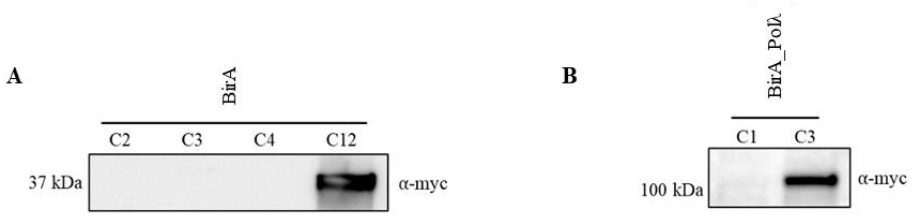

Figure 21. WB to verify the presence of the constructs in stable cell lines. (A) In BirA stable U2OS clones, in population C12 is identified the detection of a band at 49 KDa following incubation with an α-myc primary antibody. **(B)** In a BirA_Pol λ C3 colony, the signal at 117 KDa is recognisable due to the presence of the protein chimera

7.4. BIOTINYLATION PATTERN IN CELLS

To investigate BirA and BirA_Pol λ mediated biotinylation patterns, we studied proteins biotinylation through immunofluorescence analysis (IF) using streptavidin conjugated with the Alexa Fluor 488. The stable cell lines were treated with 50 μM of biotin to facilitate robust biotinylation. Confocal images revealed that in cells transfected with pBirA biotinylated proteins are present both in the cytoplasm and in the nucleus (Figure 22). This observation correlates well with the broad, unspecific biotinylation pattern observed by WB (Figure 20 A) and can be explained by the ability of BirA to diffuse through nuclear

pores. In contrast, proteins biotinylated by BirA_Pol λ were specifically localised to the cellular nucleus, consistently with the nuclear localization of Pol λ.

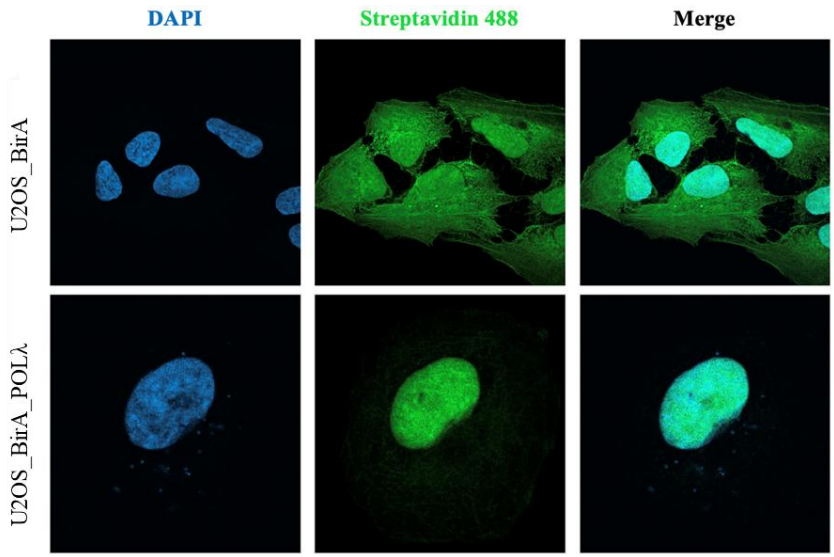

Figure 22. BirA_Pol λ biotinylated factors are localized in the nucleus. Confocal microscopy imaging of biotin-labelled proteins (green). DAPI is used to stain cellular nucleus (blue). In BirA stable cell line, the biotinylated factors are localised in both the cytoplasm and the nucleus. Conversely, the biotinylation pattern achieved by the BirA_Pol λ is specifically localised to the cellular nucleus

7.5. PULL-DOWN OF INTERACTING FACTORS FOR MS

To identify Pol λ interactors, clones expressing BirA and BirA_Pol λ were grown in the presence of 50 μM of free biotin for 16 hours and lysed. Biotinylated factors were precipitated using streptavidin coated beads and following trypsin digestion prior to Mass Spectrometry (MS) analysis.

A small amount of input, pull-down, and flow-through samples were conserved to check the biotinylation efficiency (Figure 23).

As for whole cell extract, input, pull down, and flow-through BirA_Pol λ samples showed a different biotinylation pattern in comparison with BirA alone. The signal detected in the flow-through fractions represents biotinylated proteins that have not been captured by streptavidin beads. In the case of BirA_Pol λ flow-through signal is weak, confirming that most of BirA_Pol λ interactors were successfully collected.

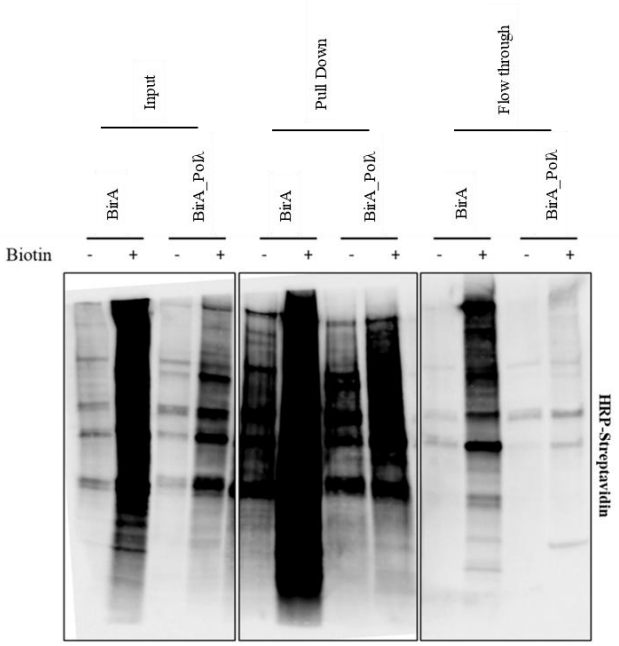

Figure 23. Biotinylation pattern of sample sent to MS analysis. Following the administration of biotin, the biotinylated proteins increased in BirA and BirA_Pol λ expressing cells in all fractions. In flow-through conditions, a percentage of unbound proteins are lost, specifically in BirA samples, due to saturation of the beads. In the pull-down fractions there was an enrichment of biotinylated proteins compared to the input sample

7.6. ANALYSIS OF POL Λ INTERACTOME

We decide to investigate Pol λ interactome and its variation under different conditions. In particular, we performed a BioID analysis of Pol λ in untreated U2OS clones, as well as after DSBs induction with etoposide or after induction of replication stress through administration of Hydroxyurea (HU). The unprocessed MS data were queried against the Homo sapiens proteome database from Uniprot to identify peptide sequences and related proteins (see section 5.3.4 in Materials and Methods).

In all conditions, we compared biotinylated factors obtained from cells expressing BirA alone and BirA_Pol λ, both of which had been with exogenous biotin. As an additional control, the same analysis was performed in the absence of biotin. In unperturbed condition, 131 proteins were found enriched in BirA_Pol λ. To analyse these factors, we used the DAve parameter, which indicates the differential ratio between two comparison terms for each condition: BirA vs BirA_Pol λ. Positive values indicate proteins enriched in the first comparison term, whereas negative values indicate the opposite. We considered only the interactors with a DAve value from 0.5, corresponding to an enrichment of 2.15-fold change (Figure 24). Among the identified proteins, only two factors known to interact with Pol λ were found: Ku70 and Ku80. These are essential components of NHEJ, forming the Ku70/80 heterodimer that recognises and binds the DNA broken ends, acting as a scaffold, protecting DNA ends from degradation, and recruiting other core NHEJ factors (Frit et al., 2019; Scully et al., 2019).

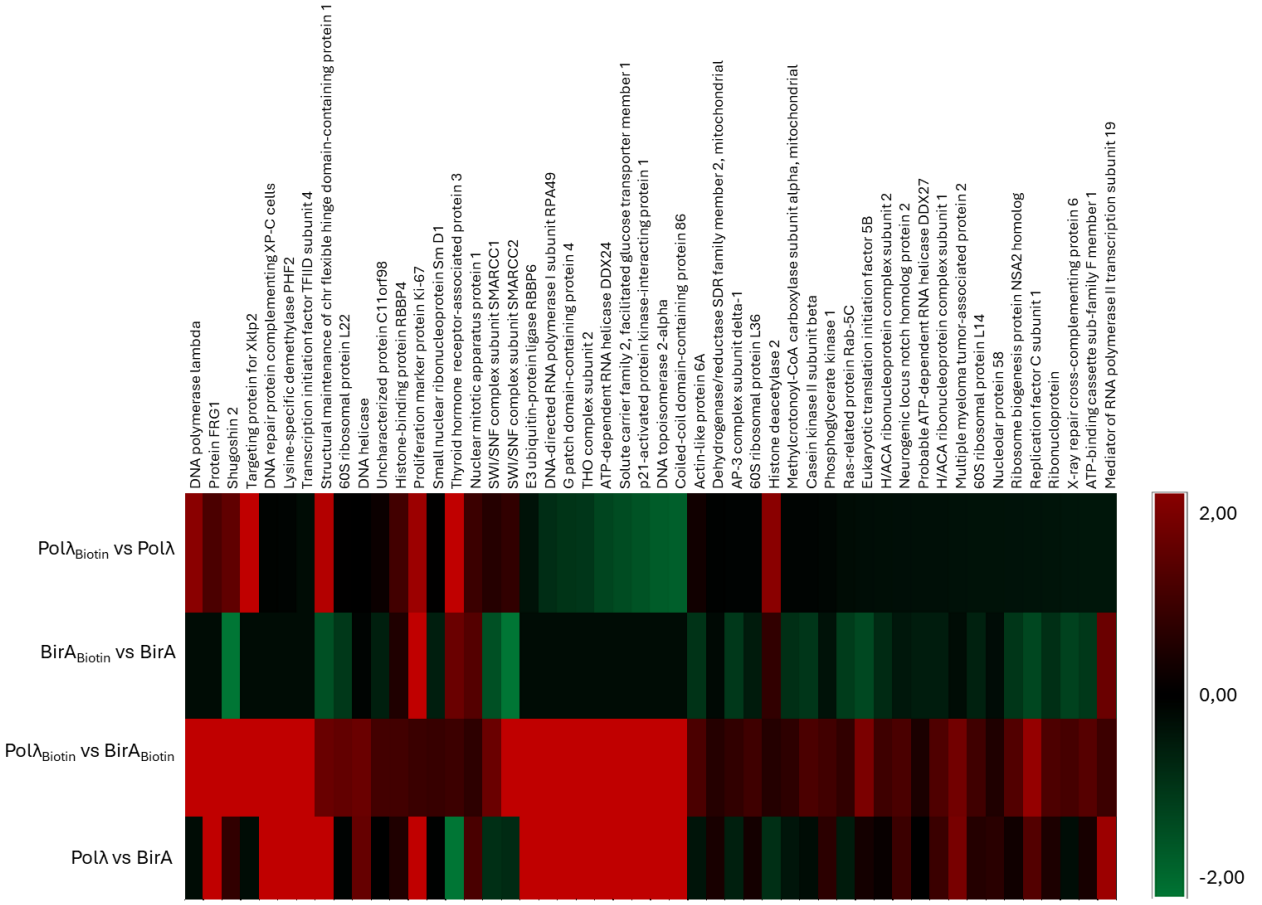

Figure 24. Heatmap of MS analysis. Proteins with negative Dave values are indicated in green, while positive Dave values are indicated in red. The DAve parameter, employed for the analysis of the heatmap, indicates the differential expression ratio between the two comparison terms for each condition. Positive values indicate that the protein is more highly expressed in the first comparison term, while negative values indicate the opposite.

Gene ontologies (GO) were performed using DAVID software. Biological Process (BP) analysis revealed that the majority of Pol λ interactors are implicated in cellular processes that well fit with known roles of Pol λ, such as DNA repair, replication processes, and telomere maintenance. However, the most representative biological processes identified are associated with nucleolar metabolism, while other BPs are related with RNA metabolism. Also KEGG pathways analysis identified DNA replication and DNA repair pathways associated with Pol λ interactors, including BER, NER and NHEJ pathways. However, also in this case, KEGG pathways related to nucleolar and RNA metabolism were identified (Figure 25 A, B and Table 5).

Accordingly, GO analysis of the Cellular Component Localization (CCL) identified nucleus, nucleoplasm, and nucleolus as the top-scoring components. Notably, telomeric regions are also ranked among the top 15 CCL terms, in accordance with the proposed role of Pol λ in telomere biology (Figure 25 C and Table 6).

It is noteworthy that previous researches have indicated that DNA repair proteins, in particular those involved in BER and c-NHEJ, are associated with the nucleolus until DNA damage occurs, causing their recruitment to the DNA lesions (Iarovaia et al., 2019; Ogawa & Baserga, 2017). After these preliminary results, a new set of immunofluorescence experiments was performed, utilising a reduced concentration of Streptavidin-488. This approach facilitated the observation of enhanced localisation of the fused protein, BirA_Pol λ interactors. As demonstrated in Figure 26, the interactors of the chimeric protein in an unperturbed state were found to localise in the nucleus, and in particular in the nucleolus of the stable cell line. Conversely, the interactome of only BirA construct was found to be present in all cell compartments. This represents a preliminary confirmation of the data obtained by MS, however, further investigation will be necessary to obtain a confirmation.

We then focused on the factors with the highest confidence values (DCI score above 100 and DAve score above 0.5) (Figure 27).

This selection resulted in the identification of 26 factors, which showed a high degree of interconnectivity based on STRING analysis. These findings provide further support for the data obtained from our BioID analysis, reinforcing the hypothesis of a shared interaction network with Pol λ.

Table 5. Gene Ontology of Biological Process. The BPs are sorted according to the p-value*. "Count" represents the number of factors involved in the BP (Follow in next pages)

Biological Process	**Count**	**P-value**
rRNA processing	14	4,99E-13
mRNA splicing, via spliceosome	14	5,31E-11
Transcription by RNA polymerase I	6	8,37E-08
Telomere maintenance via telomerase	6	1,37E-07
mRNA processing	12	1,44E-07
RNA splicing	11	1,83E-07
Chromatin looping	10	3,34E-07
Chromatin remodeling	20	4,89E-07
Ribosomal small subunit biogenesis	7	4,62E-06
DNA-templated transcription	7	1,71E-05
Transcription by RNA polymerase III	5	2,06E-05
Ribosome biogenesis	5	8,01E-05
snRNA pseudouridine synthesis	3	8,83E-05
Positive regulation of stem cell population maintenance	5	1,25E-04
Positive regulation of DNA-templated transcription	14	1,44E-04
Cytoplasmic translation	6	1,49E-04
rRNA pseudouridine synthesis	3	1,76E-04
RNA splicing, via transesterification reactions	4	3,33E-04
Regulation of G0 to G1 transition	4	3,33E-04
transcription by RNA polymerase II	8	3,49E-04
Positive regulation of transcription by RNA polymerase I	4	3,75E-04
Regulation of nucleotide-excision repair	4	4,21E-04
Transcription elongation by RNA polymerase I	3	6,09E-04
Regulation of mitotic metaphase/anaphase transition	4	8,37E-04

Ribosomal large subunit biogenesis	4	0,001074
Positive regulation of T cell differentiation	4	0,001161
Negative regulation of DNA-templated transcription	11	0,001181
Translation	7	0,001285
Transcription initiation at RNA polymerase I promoter	3	0,001291
Positive regulation of double-strand break repair	4	0,001555
RNA polymerase I preinitiation complex assembly	3	0,001573
Maturation of LSU-rRNA	3	0,00188
Positive regulation of myoblast differentiation	4	0,002024
Branched-chain amino acid catabolic process	3	0,002214
Regulation of cell fate specification	3	0,002574
Positive regulation of telomerase RNA localization to Cajal body	3	0,00296
DNA replication	5	0,00301
Regulation of G1/S transition of mitotic cell cycle	4	0,003205
Positive regulation of cell differentiation	4	0,004318
Telomere maintenance	4	0,004318
DNA repair	7	0,005172
Nucleosome disassembly	3	0,005794
Regulation of stem cell differentiation	3	0,007535
DNA duplex unwinding	4	0,008635
Double-strand break repair	4	0,009262
Spliceosomal complex assembly	3	0,010174
Cis assembly of pre-catalytic spliceosome	2	0,010889
Negative regulation of innate immune response	3	0,014783
snoRNA guided rRNA pseudouridine synthesis	2	0,01629
Nucleolar large rRNA transcription by RNA polymerase I	2	0,01629
Symbiont-mediated disruption of host cell PML body	2	0,01629
Short-chain fatty acid catabolic process	2	0,01629
Double-strand break repair via nonhomologous end joining	3	0,017365
Positive regulation of transcription by RNA polymerase II	14	0,018107
Negative regulation of proteasomal ubiquitin-dependent protein catabolic process	3	0,020123
Branched-chain amino acid metabolic process	2	0,021661
Endonucleolytic cleavage of tricistronic rRNA transcript (SSU-rRNA, 5,8S rRNA, LSU-rRNA)	2	0,021661
Positive regulation of protein kinase activity	3	0,025096

Cellular hyperosmotic salinity response	2	0,027003
DNA damage response	6	0,028252
L-leucine catabolic process	2	0,032317
Recombinational repair	2	0,032317
Translational initiation	3	0,036347
Plastid transcription	2	0,037601
Transcription by RNA polymerase V	2	0,037601
Transcription by RNA polymerase IV	2	0,037601
Telomerase RNA localization to Cajal body	2	0,037601
Negative regulation of cell differentiation	3	0,038791
Osteoblast differentiation	4	0,039192
Neural crest formation	2	0,042857
DNA ligation	2	0,042857
Negative regulation of macromolecule biosynthetic process	2	0,042857
RNA metabolic process	2	0,048085
R-loop processing	2	0,048085
Cellular response to X-ray	2	0,050284

***** The displayed p-values have been corrected for multiple testing within each category using the Benjamini-Hochberg procedure. P-value > 0.05.

Table 6. Gene Ontology of Cellular Component localization. The CLLs are sorted according to the p-value*. "Count" represents the number of factors localized in the specific CCL. (Follow in next page)

Cellular Component localization	Count	P-value
Nucleoplasm	74	2,15E-27
Nucleolus	47	1,18E-25
Chromosome	19	5,53E-15
RNA polymerase I complex	8	1,56E-13
Catalytic step 2 spliceosome	10	2,00E-09
U4/U6 x U5 tri-snRNP complex	8	3,59E-09
Fibrillar center	11	7,87E-09
Chromosome, telomeric region	11	2,87E-08
Nucleus	60	8,39E-08
Small-subunit processome	8	1,38E-07
U2-type precatalytic spliceosome	7	2,47E-07
box H/ACA scaRNP complex	4	5,69E-07
box H/ACA snoRNP complex	4	5,69E-07
box H/ACA telomerase RNP complex	4	1,42E-06
Nuclear speck	13	2,80E-06
Telomerase holoenzyme complex	5	4,98E-06
DNA-directed RNA polymerase complex	5	6,00E-06
U5 snRNP	5	8,50E-06
Ribonucleoprotein complex	10	1,36E-05
Cytosolic large ribosomal subunit	6	1,49E-05
Protein-containing complex	15	1,66E-05
npBAF complex	4	4,98E-05
RSC-type complex	4	7,60E-05
Spliceosomal complex	7	9,53E-05
RNA polymerase III complex	4	1,10E-04
SWI/SNF complex	4	5,22E-04
U2-type catalytic step 2 spliceosome	4	5,22E-04
Nuclear matrix	6	6,54E-04
sno(s)RNA-containing ribonucleoprotein complex	3	9,69E-04
Cajal body	5	9,77E-04

Site of DNA damage	4	0,001411
Kinetochore	6	0,001598
Protein-DNA complex	4	0,001615
Cytosol	45	0,001626
Cytosolic ribosome	5	0,001676
GBAF complex	3	0,002407
Brahma complex	3	0,002407
Nuclear lumen	3	0,002767
nBAF complex	3	0,003152
NuRD complex	3	0,003991
Preribosome, large subunit precursor	3	0,003991
Sin3-type complex	3	0,005944
Mitochondrial matrix	8	0,009091
Methylcrotonoyl-CoA carboxylase complex	2	0,010521
Ribosome	5	0,010937
Ku70:Ku80 complex	2	0,015741
Secretory granule lumen	4	0,023533
DNA replication factor C complex	2	0,026098
DNA-dependent protein kinase complex	2	0,026098
Protein kinase CK2 complex	2	0,031236
box C/D methylation guide snoRNP complex	2	0,031236
DNA-dependent protein kinase-DNA ligase 4 complex	2	0,036347
Chromatin	12	0,036895
Male germ cell nucleus	3	0,037624
Nonhomologous end joining complex	2	0,041431
B-WICH complex	2	0,041431
Nuclear telomere cap complex	2	0,046489
Chromosome, centromeric region	3	0,047522

***** The displayed p-values have been corrected for multiple testing within each category using the Benjamini-Hochberg procedure. P-value > 0.05.

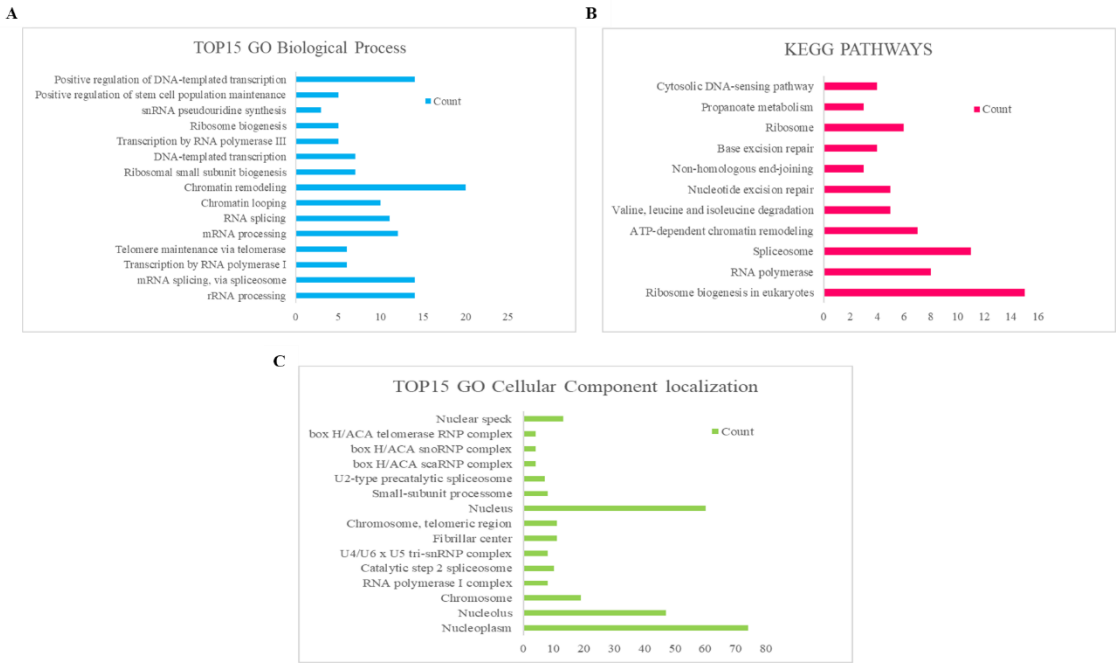

Figure 25. Gene Ontology analysis. The graphs show the 15 BPs with highest p-values among the pathways reported in Table 5 **(A),** the KEGG pathways **(B),** and the 15 CCLs with highest p-values among the pathways reported in Table 6 **(C).** The bars indicate the fold enrichment, which is called Count in DAVID software.

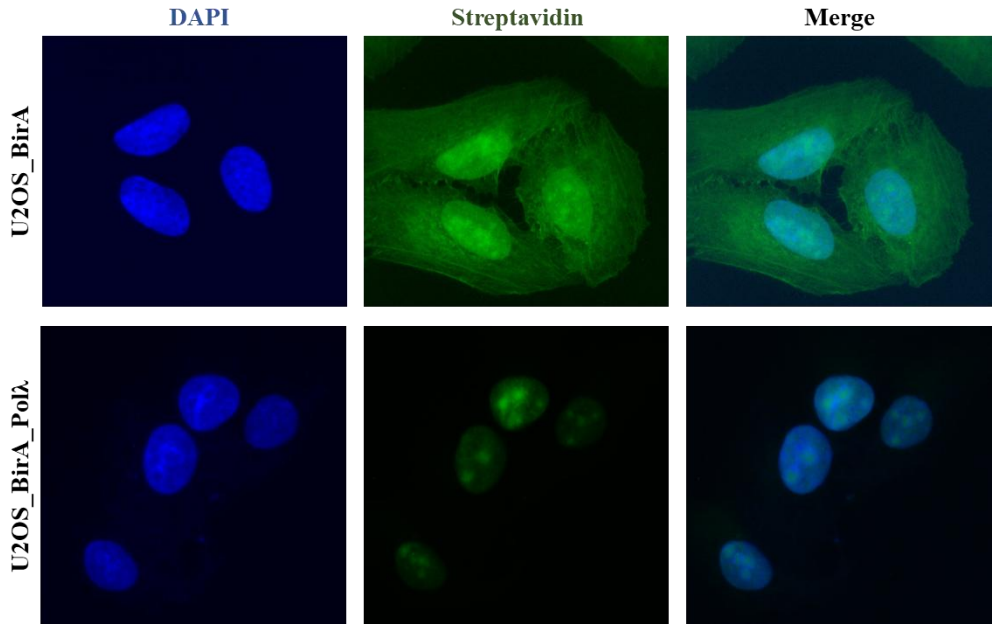

Figure 26. BirA_Pol λ interactors localize in nucleolus. Confocal microscopy imaging of biotin-labelled proteins (green). Nuclei were stained with DAPI (blue). BirA substrates localize in both the cytoplasm and the nucleus. BirA_Pol λ biotinylated substrates localized to the nucleolus

A

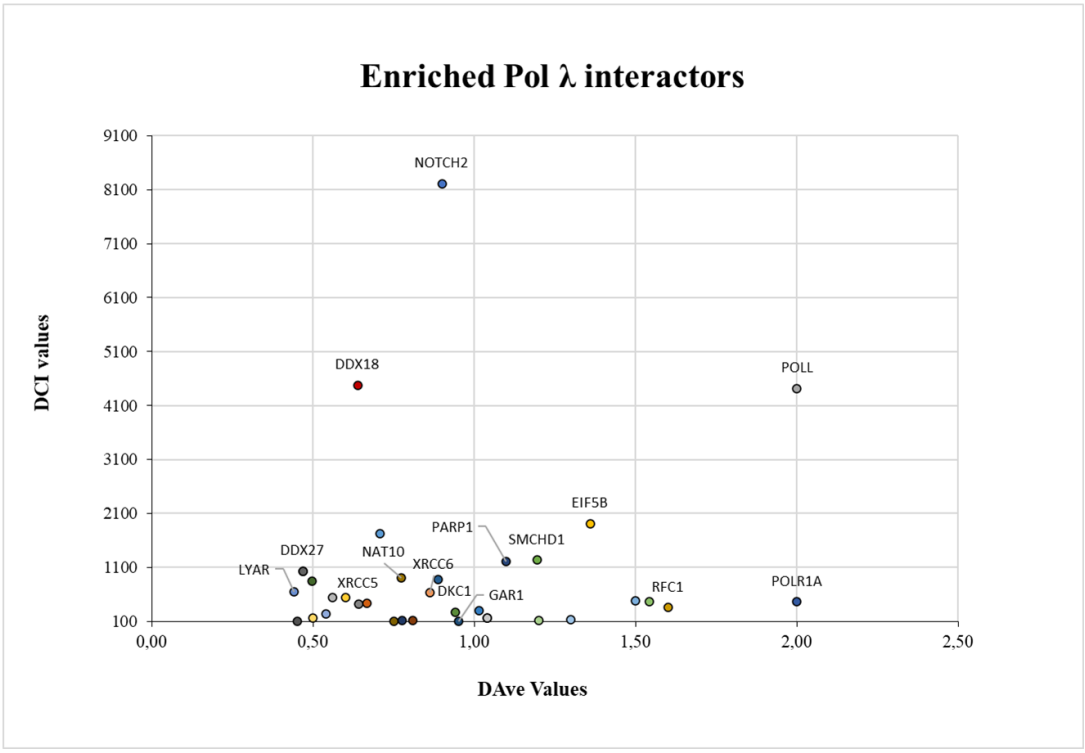
Enriched Pol λ interactors
DCI values
DAve Values
9100
8100
7100
6100
5100
4100
3100
2100
1100
100
0,00
0,50
1,00
1,50
2,00
2,50
NOTCH2
DDX18
POLL
EIF5B
PARP1
SMCHD1
DDX27
NAT10
XRCC6
LYAR
XRCC5
DKC1
GAR1
RFC1
POLR1A

B

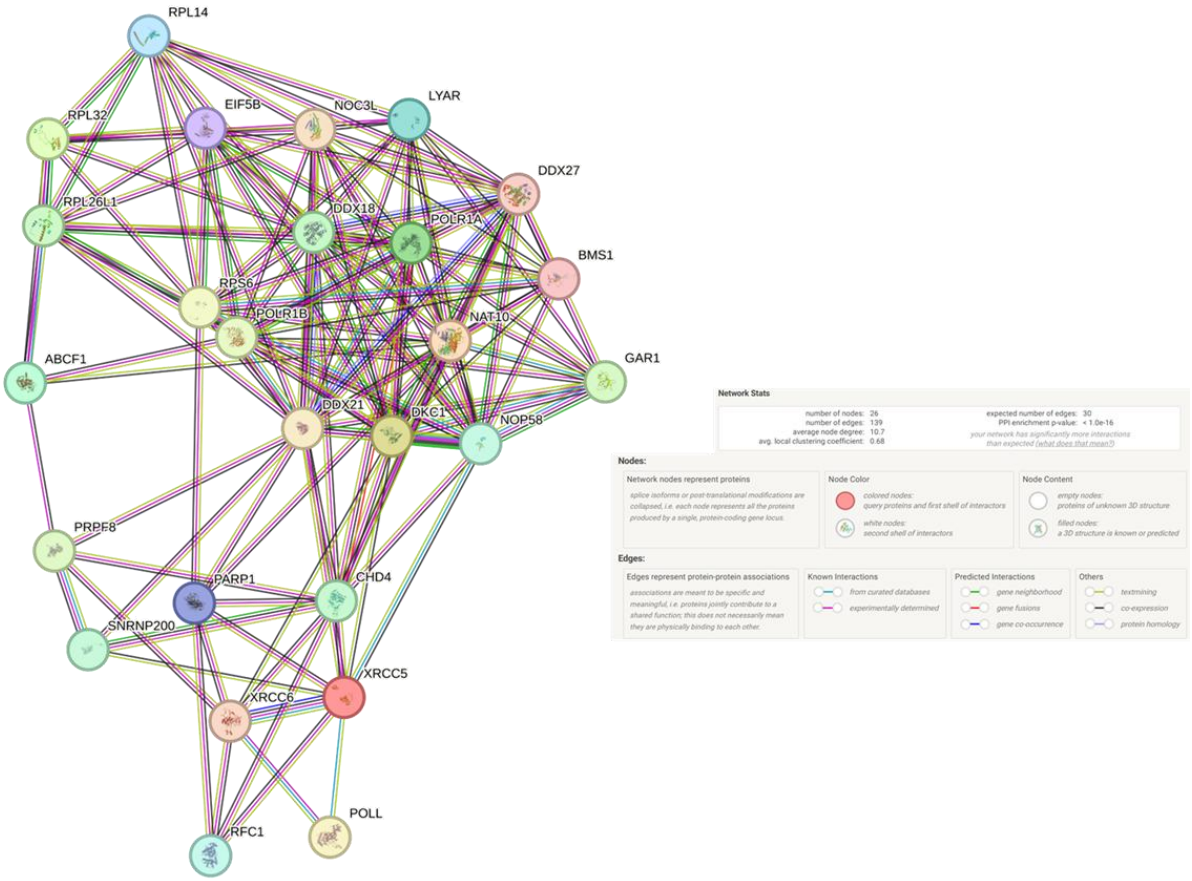

Figure 27. Pol λ interacting map. (A) Scatter plot of the first 26 interactors of Pol λ. The MS data were filtered for a DCI above 100 (Y axes), while Dave values are above 0.5 (X axes). **(B)** STRING interactome of the identified interactors

7.7. POL Λ INTERACTOME UPON DIFFERENT STRESS CONDITIONS

Being involved in DNA repair processes, Pol λ likely interacts with different factors in response to different DNA damages and/or cellular stress. For this reason, we decide to evaluate Pol λ interactome through BioID following treatment with etoposide or HU. Etoposide is a chemotherapeutic agent that induces transient DSBs through the inhibition of topoisomerase II, triggering NHEJ which in turn leads to the recruitment of Pol λ recruitment to the lesion site (Bax et al., 2019; Hande, 1998).

HU inhibits the Ribonucleotide Reductase (RNR), impairing dNTPs synthesis and arresting cells in S-phase (Musiałek & Rybaczek, 2021). Pol λ depletion leads to a reduced cell viability in ALT-positive cells, and this effect is enhanced following treatment with HU, thus suggesting a role for Pol λ in replicative stress response (Mentegari et al., 2021).

As in untreated conditions, biotin was administered to BirA and BirA_Pol λ U2OS clones, this time together with administration of 25 μM of etoposide or 500 μM of HU. Biotinylated factors were precipitated using streptavidin coated beads and identified as previously described.

Input, flow-through and pull-down samples were collected to verify the biotinylation pattern, revealing a differential biotinylated pathway among the two clones (Figure 28 A). We also investigated whether the DNA damage affects the biotinylation pattern. WB analysis of the input fraction was performed to validate the presence of DNA damage after treatment, using γH2AX as a marker of DNA lesion, revealing activation of DNA damage sensing after both etoposide and HU treatments (Figure 28 B). In both conditions, DNA damage did not affect the biotinylation pattern.

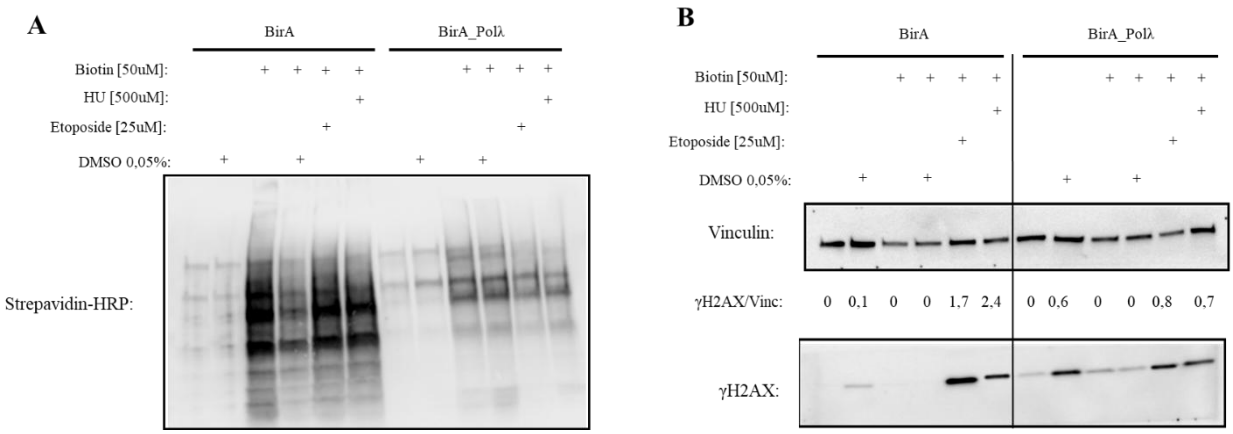

Figure 28. Biotinylation pattern and γH2AX activation following treatment with DNA damaging agents. (A) WB analysis using streptavidin-HRP of pull-down samples sent for MS analysis. BirA samples show a diffuse biotinylation pattern compared to the more specific pattern observed in cells stably expressing BirA_Pol λ. **(B)** WB of the same samples (input) using α-γH2AX antibody to evaluate DNA damage response. γH2AX/Vinculin signal is reported

MS analysis identified factors that interact with Pol λ also in unperturbed condition. These include the known Pol λ interactor Ku70/80, as well as BioID-identified RFC1, DDX27, and NAT10. In addition, new factors that specifically interact with Pol λ upon etoposide and/or HU administration were identified. In this case, BirA and BirA_Pol λ biotinylated factors were compared and filtered by DAve values for each treatment.

The proteins so identified were then divided into two categories: those that are enriched after treatment and those that lost their interaction with Pol λ after treatment. Again, GO was performed using DAVID. In unperturbed conditions, GO well matches the previous findings (data not shown).

Both etoposide and HU treatments result in a significant decrease in biotinylated factors associated with nucleolus and RNA metabolism, supporting the hypothesis that Pol λ, as

other DNA repair proteins, is recruited from the nucleolus in response to DNA damage (Figure 29 A, B, C and D, Tables 7, 8, 9, and 10).

As shown in Figure 30 A and B, DAVID analysis of the Cellular Component Localization (CCL) category following etoposide treatment reveals an increased enrichment of biotinylated factors localized to the nucleolus and chromatin. In addition, etoposide treatment alters the Biological Process (BP) category, highlighting terms such as "chromatin remodelling," "DNA repair," and "DNA duplex unwinding," all of which are associated with DDR.

A low number of factors enriched after HU treatment was identified. This could reflect a physiological condition in which Pol λ lose interactions after the treatment, or could be due to technical problems in the experiment. To overcome this issue, we plan to repeat this BioID analysis.

Table 7. Gene Ontology of Biological Process Reduced after Etoposide Treatment. The BPs are sorted according to the to p-value*. "Count" represents the number of factors involved in the BP. (Follow in next pages)

Biological Process Etoposide Reduced	Count	P-value*
Cytoplasmic translation	19	3,46E-23
Translation	23	1,49E-21
rRNA processing	14	8,11E-13
Ribosomal small subunit biogenesis	11	2,33E-11
Nucleosome assembly	10	1,38E-07
Negative regulation of DNA recombination	5	2,19E-06
Chromosome condensation	5	5,42E-06
Positive regulation of telomerase RNA localization to Cajal body	4	7,66E-05
Maturation of LSU-rRNA from tricistronic rRNA transcript (SSU-rRNA, 5,8S rRNA, LSU-rRNA)	4	1,14E-04
Telomere maintenance via telomerase	4	2,89E-04

Telomerase RNA localization to Cajal body	3	6,56E-04
Actomyosin structure organization	4	7,09E-04
Establishment of protein localization to chromatin	3	0,001116
Ribosomal large subunit biogenesis	4	0,001195
box C/D snoRNP assembly	3	0,001389
Ribosome biogenesis	4	0,00173
DNA repair	8	0,001824
Maturation of LSU-rRNA	3	0,002023
rRNA transcription	3	0,002382
Branched-chain amino acid catabolic process	3	0,002382
Positive regulation of telomere maintenance in response to DNA damage	3	0,003183
Regulation of DNA strand elongation	3	0,003624
Regulation of chromosome organization	3	0,004092
Actin filament-based movement	3	0,005654
Ribosomal large subunit assembly	3	0,006226
Heterochromatin formation	4	0,007068
Osteoblast differentiation	5	0,007695
DNA recombination	4	0,009552
Maturation of SSU-rRNA from tricistronic rRNA transcript (SSU-rRNA, 5,8S rRNA, LSU-rRNA)	3	0,010179
Regulation of double-strand break repair	3	0,010922
Protein stabilization	6	0,01351
Chromatin looping	5	0,015065
Nucleolar large rRNA transcription by RNA polymerase I	2	0,016901
snRNA pseudouridine synthesis	2	0,016901
Sex-chromosome dosage compensation	2	0,016901
snoRNA guided rRNA pseudouridine synthesis	2	0,016901
Skin development	3	0,021567
rRNA pseudouridine synthesis	2	0,022472
Negative regulation of transcription of nucleolar large rRNA by RNA polymerase I	2	0,022472
Positive regulation of plasma membrane repair	2	0,022472
Symbiont entry into host cell	4	0,022953
Positive regulation of protein import into nucleus	3	0,024696
Positive regulation of double-strand break repair via homologous recombination	3	0,024696

Regulation of DNA replication	3	0,025778
Embryo implantation	3	0,026878
snoRNA localization	2	0,028011
Mitochondrial ADP transmembrane transport	2	0,028011
Positive regulation of DNA repair	3	0,029136
Regulation of embryonic development	3	0,029136
RNA splicing	5	0,029301
Bundle of His cell-Purkinje myocyte adhesion involved in cell communication	2	0,033519
L-leucine catabolic process	2	0,033519
Regulation of DNA repair	3	0,044148
Neural crest formation	2	0,044443
Mitochondrial ATP transmembrane transport	2	0,044443
Negative regulation of transcription by RNA polymerase II	11	0,045197
Telomere maintenance	3	0,045506
Chromatin organization	5	0,047092
Postsynaptic neurotransmitter receptor internalization	2	0,049859

*The displayed p-values have been corrected for multiple testing within each category using the Benjamini-Hochberg procedure. P-value > 0.05.

Table 8. Gene Ontology of Cellular Component localization Reduced after Etoposide Treatment. The CCLs are sorted according to the p-value*. "Count" represents the number of factors localized in the specific CCL. (Follow in next page)

Cellular Component localization Etoposide Reduced	Count	P-value
Nucleolus	47	4,81E-25
Cytosolic ribosome	18	1,82E-21
Cytosolic large ribosomal subunit	14	5,49E-18
Ribosome	18	2,05E-17
Ribonucleoprotein complex	19	7,05E-15
Chromosome	18	1,36E-13
Nucleoplasm	56	1,20E-12
Nucleosome	13	2,01E-11
Nucleus	67	1,19E-10
Small-subunit processome	10	2,71E-10
Fibrillar center	12	6,57E-10
Focal adhesion	16	1,20E-08
Extracellular exosome	35	1,47E-08
Nuclear matrix	10	3,97E-08
Small ribosomal subunit	6	2,57E-07
box C/D methylation guide snoRNP complex	4	3,06E-06
Cytosolic small ribosomal subunit	6	3,92E-06
Telomerase holoenzyme complex	5	5,55E-06
Myosin II complex	5	1,30E-05
Euchromatin	6	2,53E-05
Cytosol	51	4,26E-05
Membrane	50	5,75E-05
Myosin II filament	3	8,70E-05
Myosin complex	5	1,12E-04
box H/ACA snoRNP complex	3	1,73E-04
box H/ACA scaRNP complex	3	1,73E-04
Myosin filament	4	2,21E-04
box H/ACA telomerase RNP complex	3	2,88E-04
Supramolecular fiber	3	4,30E-04

Granular component	3	6,01E-04
Barr body	3	6,01E-04
Rough endoplasmic reticulum	4	8,20E-04
sno(s)RNA-containing ribonucleoprotein complex	3	0,001022
Actomyosin	3	0,001273
Protein-containing complex	12	0,001342
Cytoplasm	48	0,001503
RNA polymerase I complex	3	0,002184
Melanosome	5	0,002479
Chromosome, telomeric region	6	0,002595
Synapse	10	0,003011
Ino80 complex	3	0,003754
Brush border	4	0,00385
Midbody	6	0,004041
Preribosome, large subunit precursor	3	0,004208
Nuclear envelope	6	0,00599
Nuclear chromosome	3	0,010037
Methylcrotonoyl-CoA carboxylase complex	2	0,01081
NuA4 histone acetyltransferase complex	3	0,013776
Ribosomal subunit	2	0,021504
Cytoplasmic side of plasma membrane	4	0,024687
R2TP complex	2	0,026808
RNA polymerase II transcription regulator complex	4	0,031196
Cytoplasmic side of rough endoplasmic reticulum membrane	2	0,032084
Pre-snoRNP complex	2	0,037331
Cornified envelope	3	0,042028
Zonula adherens	2	0,047741

***** The displayed p-values have been corrected for multiple testing within each category using the Benjamini-Hochberg procedure. P-value > 0.05.

Table 9. Gene Ontology of Biological Process Reduced after HU Treatment. The BPs are sorted according to the p-value*. "Count" represents the number of factors involved in the BP. (Follow in next page)

Biological Process HU Reduced	Count	P-value
Cytoplasmic translation	10	1,99E-10
rRNA processing	10	6,59E-09
Translation	11	3,22E-08
mRNA splicing, via spliceosome	9	1,93E-06
Osteoblast differentiation	7	2,67E-05
Chromatin remodeling	15	3,14E-05
Telomere maintenance via telomerase	4	1,25E-04
Regulation of circadian rhythm	5	1,83E-04
Circadian regulation of gene expression	5	2,43E-04
RNA splicing	7	2,47E-04
Ribosome biogenesis	4	7,67E-04
DNA-templated transcription	5	8,58E-04
Branched-chain amino acid catabolic process	3	0,001366
Positive regulation of transcription by RNA polymerase III	3	0,002945
Nucleosome disassembly	3	0,003597
Transcription by RNA polymerase I	3	0,003597
Transcription by RNA polymerase II	6	0,003675
Ribosomal small subunit biogenesis	4	0,004715
Entrainment of circadian clock by photoperiod	3	0,005081
Regulation of G0 to G1 transition	3	0,005081
Positive regulation of transcription by RNA polymerase I	3	0,00549
Chromatin looping	5	0,005727
Regulation of nucleotide-excision repair	3	0,005913
Cell division	7	0,005973
Transcription by RNA polymerase III	3	0,007267
Cis assembly of pre-catalytic spliceosome	2	0,008532
Glycogen metabolic process	3	0,008748
Regulation of mitotic metaphase/anaphase transition	3	0,009269
Ribosomal large subunit biogenesis	3	0,010913
Positive regulation of T cell differentiation	3	0,011488

snRNA pseudouridine synthesis	2	0,01277
snoRNA guided rRNA pseudouridine synthesis	2	0,01277
Positive regulation of double-strand break repair	3	0,013916
Positive regulation of myoblast differentiation	3	0,016545
rRNA pseudouridine synthesis	2	0,016991
Positive regulation of protein localization to cell cortex	2	0,021194
Positive regulation of blood-brain barrier permeability	2	0,021194
Mitochondrial ADP transmembrane transport	2	0,021194
Regulation of G1/S transition of mitotic cell cycle	3	0,022379
mRNA processing	5	0,023512
Nucleosome assembly	4	0,024284
L-leucine catabolic process	2	0,02538
Positive regulation of cell differentiation	3	0,027229
Transcription elongation by RNA polymerase I	2	0,029547
Transcription by RNA polymerase IV	2	0,029547
Transcription by RNA polymerase V	2	0,029547
Mitochondrial ATP transmembrane transport	2	0,033697
DNA repair	5	0,035757
Protein localization to cell-cell junction	2	0,03783
R-loop processing	2	0,03783
Postsynaptic neurotransmitter receptor internalization	2	0,03783
DNA topological change	2	0,041945
Response to aldosterone	2	0,046042
Establishment of endothelial intestinal barrier	2	0,046042
Protein dephosphorylation	3	0,048117

*P-values have been corrected for multiple testing within each category using the Benjamini-Hochberg procedure. P-value > 0.05.

Table 10. Gene Ontology of Cellular Component localization Reduced after HU Treatment. The CCLs are sorted according to the p-value*. "Count" represents the number of factors localized in the specific CCL (Follow in next page)

Cellular Component localization HU Reduced	Count	P-value
Nucleoplasm	50	6,31E-15
Nucleolus	30	8,96E-14
Chromosome	13	1,35E-09
Cytosolic large ribosomal subunit	8	4,44E-09
Cytosolic ribosome	9	5,78E-09
Nuclear matrix	9	6,72E-08
RNA polymerase I complex	5	1,85E-07
Nucleus	49	2,42E-07
Ribosome	9	3,62E-07
Telomerase holoenzyme complex	5	1,84E-06
Catalytic step 2 spliceosome	7	2,79E-06
Fibrillar center	8	3,10E-06
Protein-containing complex	14	4,78E-06
Chromosome, telomeric region	8	7,55E-06
Ribonucleoprotein complex	9	1,59E-05
Nucleosome	7	2,87E-05
Kinetochore	7	5,18E-05
Focal adhesion	10	6,97E-05
Extracellular exosome	23	7,79E-05
Box H/ACA snoRNP complex	3	9,98E-05
Box H/ACA scaRNP complex	3	9,98E-05
DNA-directed RNA polymerase complex	4	1,12E-04
Cytosol	40	1,40E-04
U5 snRNP	4	1,45E-04
Box H/ACA telomerase RNP complex	3	1,66E-04
Small-subunit processome	5	2,59E-04
PTW/PP1 phosphatase complex	3	3,46E-04
Nuclear speck	9	3,85E-04
B-WICH complex	3	4,61E-04

U4/U6 x U5 tri-snRNP complex	4	8,41E-04
npBAF complex	3	0,001473
Brahma complex	3	0,001473
RSC-type complex	3	0,001932
Membrane	36	0,002264
Nuclear chromosome	3	0,005896
Condensed chromosome	3	0,006316
SWI/SNF complex	3	0,006749
Synapse	8	0,007449
Methylcrotonoyl-CoA carboxylase complex	2	0,008209
Rough endoplasmic reticulum	3	0,008612
Melanosome	4	0,009073
U2-type precatalytic spliceosome	3	0,018024
Mitochondrial nucleoid	3	0,01871
Spliceosomal complex	4	0,0197
Endoplasmic reticulum	11	0,023364
Azurophil granule membrane	3	0,024584
Intercellular canaliculus	2	0,028442
Clathrin-coated endocytic vesicle membrane	3	0,034595
sno(s)RNA-containing ribonucleoprotein complex	2	0,036421
AP-2 adaptor complex	2	0,044335

*P-values have been corrected for multiple testing within each category using the Benjamini-Hochberg procedure. P-value > 0.05.

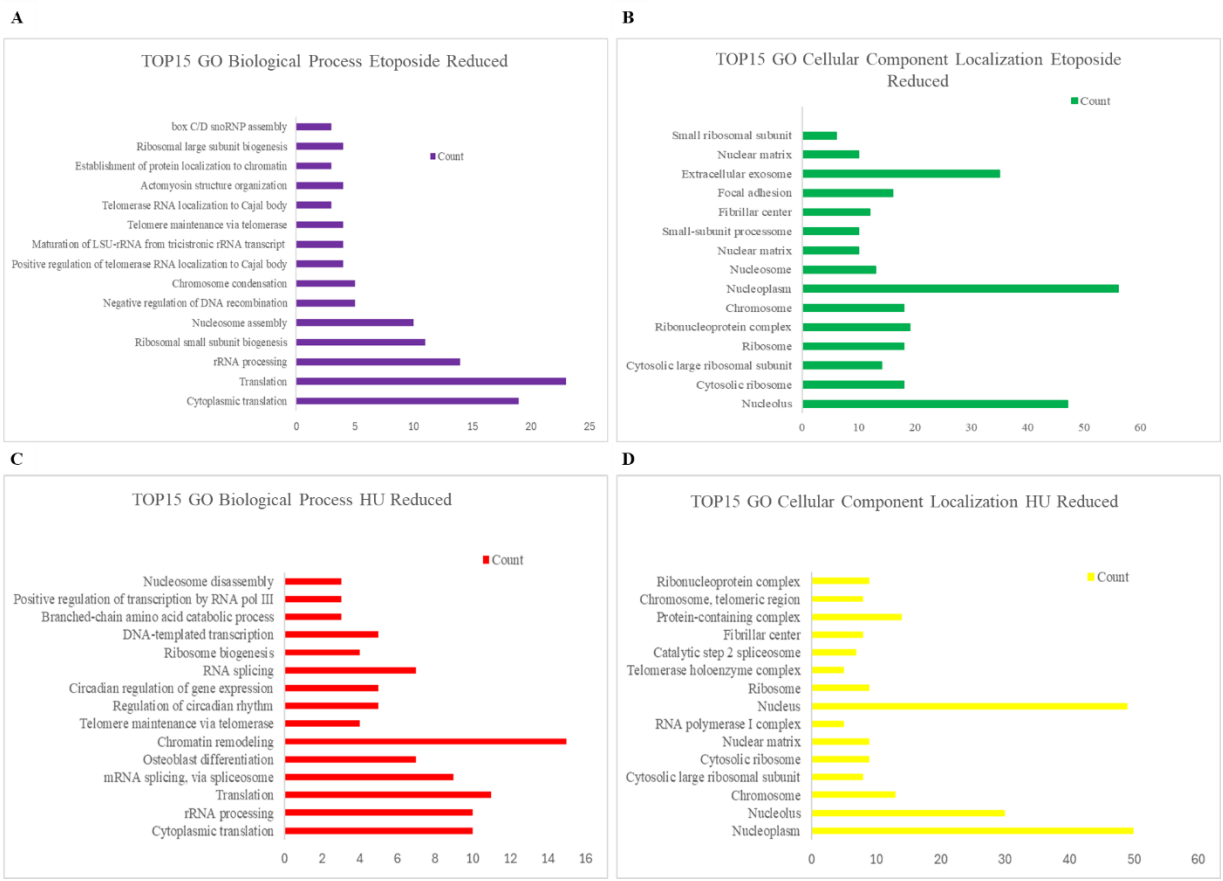

Figure 29. GO analysis of reduced factors following etoposide and HU treatment. Graphs of the biological processes **(A)** and cellular components **(B)** affected by factors that reduced interaction with Pol λ following etoposide DNA damage with the highest p-value of Tables 7 and 8. Graphs of the biological processes **(C)** and cellular components **(D)** affected by factors that decreased interaction with Pol λ following HU treatment with the highest p-value of Table 10 and 11. The bars indicate the fold enrichment, which is called Count in DAVID software

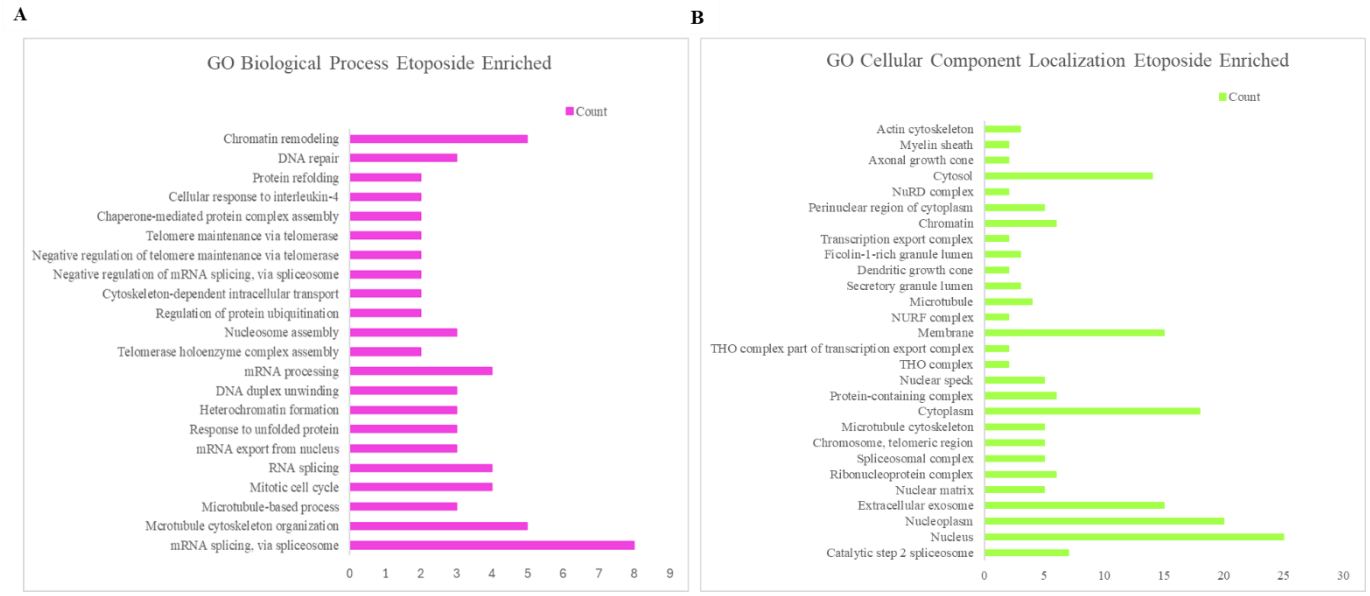

Figure 30. GO analysis of enriched factors following treatment with Etoposide. List of biological processes **(A)** and cellular components **(B)** affected by factors that increased interaction with Pol λ following etoposide treatment sorted by p-value. "Count" represents the number of factors localized in the specific CCL or involved in the BP

8. RESULTS – 2nd part

8.1. IDENTIFICATION OF TARGETS BY *IN SILICO* ANALYSIS

A computational study was conducted by our collaborator, Professor Manetti of the University of Siena, on new inhibitors of SGK1. A ligand-based drug design approach was employed to generate a common-feature pharmacophoric model using the chemical structures of eight SGK-1 inhibitors namely, compounds **1**, **2**, **GSK650394**, **3**, **21g**, **EMD638683**, **SI113**, **5** (Figure 31), as identified through the software Phase of the Schrödinger suite. Conversely, to consider the direct interactions between SGK1 and its small molecule inhibitors, the crystal structure of SGK1 in complex with **compound 1** was also employed to generate a structure-based pharmacophoric model that incorporates the excluded volumes (spatial regions occupied by amino-acidic portions and thus inaccessible to ligands). The two pharmacophores were then merged to obtain a hybrid model that could codify information from both the ligand- and the structure-based approaches. The resulting pharmacophoric hypothesis was constituted by a three-dimensional assembly of five chemical features, which included two hydrogen bond acceptors, one hydrogen bond donor, and two aromatic ring features (Figure 32). A pharmacophoric model was subsequently employed as a three-dimensional filter to conduct a virtual screening of a database comprising commercially available compounds, including those from DrugBank and NCI. The compounds that were deemed to be of potential interest during the virtual screening process were subsequently filtered to 19 compounds based on their alignment with the pharmacophore and the distinctiveness of their molecular structure. Within a hit-optimisation routine, different ellagitannins were collected, leading to the identification of compounds with a biological profile comparable to or superior to that of the reference compound.

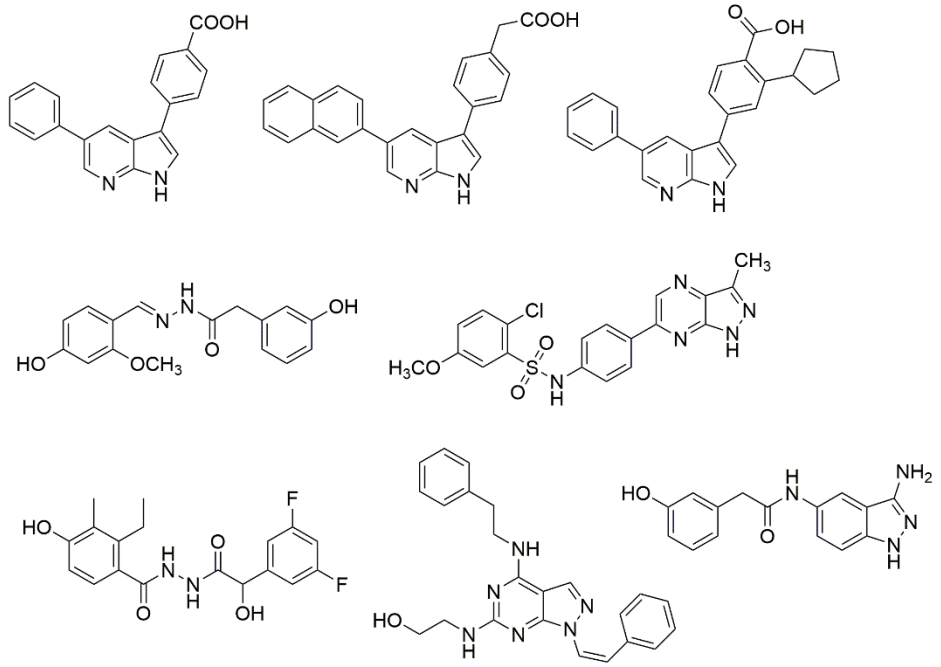

Figure 31. SGK1 compounds used for the generation of common feature pharmacophoric models. The chemical structures of compounds **1, 2, GSK650394, 3, 21g, EMD638683, SI113** and **5** are represented from left to right and from top to bottom, respectively. These compounds were employed in the ligand-based drug design approach to create a common-feature pharmacophoric model

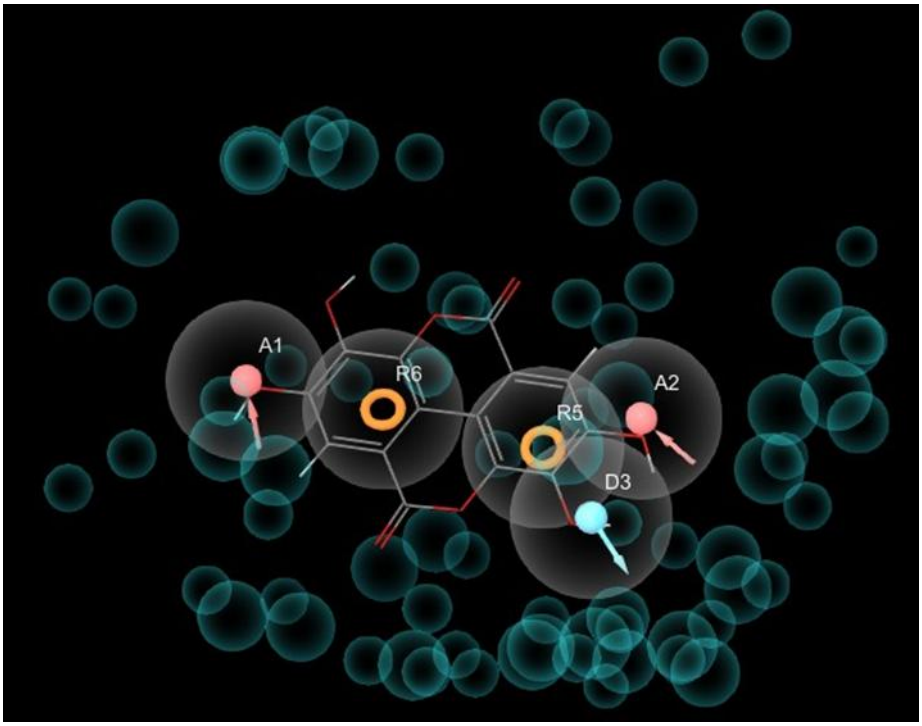

Figure 32. Graphical representation of the five-feature putative pharmacophoric model of SGK1 inhibitors (stick, atom-type notation). Two of the phenolic OH substituents are superposed to the hydrogen bond acceptor features (A1 and A2, respectively) of the model. Furthermore, the aromatic rings of the ligand correspond to the aromatic ring features (R5 and R6, respectively) of the pharmacophore. Finally, an additional phenolic OH group is superposed to the hydrogen bond donor feature of the model. The cyan spheres of variable size represent excluded volumes

8.2. ETs ARE POTENT INHIBITORS OF SGK1 *IN VITRO*

To validate the data obtained by the *in silico* prediction, we test the ability of the selected compounds to inhibit SGK1. Initially, a screening of different compounds was conducted at concentrations of 100 μM and 10 μM (Table 11). The majority of compounds inhibited SGK1, with only **FM_10**, **FM_11**, **FM_12**, and **FM_13** resulting not active. The potency of inhibition of the active molecules was determined by calculating ID50 values. **FM_8** and **FM_9** were active in the low-micromolar range (ID50: 1,27 and 2,2 μM, respectively). The remaning of the compounds showed ID50 values in the mid-nanomolar range (15,5 nM > ID50 > 68,3 nM). The four most active compounds were selected for further *in vitro* experimentation to investigate their selectivity toward SGK1. To this aim, the molecules were tested against a panel of kinases that included the tyrosine kinases Src and Abl, the SGK1 unrelated serine/threonine kinase CK1ε and SGK1 close homologous SGK2. This analysis was performed at two concentrations: 10 μM and 0,2 μM for each enzyme. All compounds shown null or modest inhibition towards tyrosine kinases and CK1ε (Figure 33 C, D, and E). On the other hand, all molecules inhibited SGK2 with potency comparable to SGK1. This is not surrendering giving the high homology of the active sites of the two kinases, indeed, they exhibit 80% sequence identity in kinase domain (J. Kim et al., 2021).

Table 11. Screening in vitro against SGK1. The different compounds were tested at two final concentrations in an in vitro assay, and it was observed that their inhibiting properties differed. Many of the selected molecules demonstrated activity at lower concentrations against SGK1. ND: not determined. The ID50 values were calculated using an exponential function and represent the mean of two replicates

ID	*residual activity (10µM)*	*IC50 (nM)* ±SD
	SGK1	
FM_1	1.3%	33.68 ± 13.93
FM_2	0%	29.38 ± 6.74
FM_3	10%	15.50 ± 4.09
FM_4	23.3%	29.15 ± 2.62
FM_5	11.8%	68.83 ± 12.16
FM_6	4.8%	62.94 ± 7.09
FM_7	4.7%	61.30 ± 16.19
FM_8	15%	1270 ± 910
FM_9	72.8%	2200 ± 1780
FM_10	68.3%	ND
FM_11	74.8%	ND
FM_12	87%	ND
FM_13	73.3%	ND

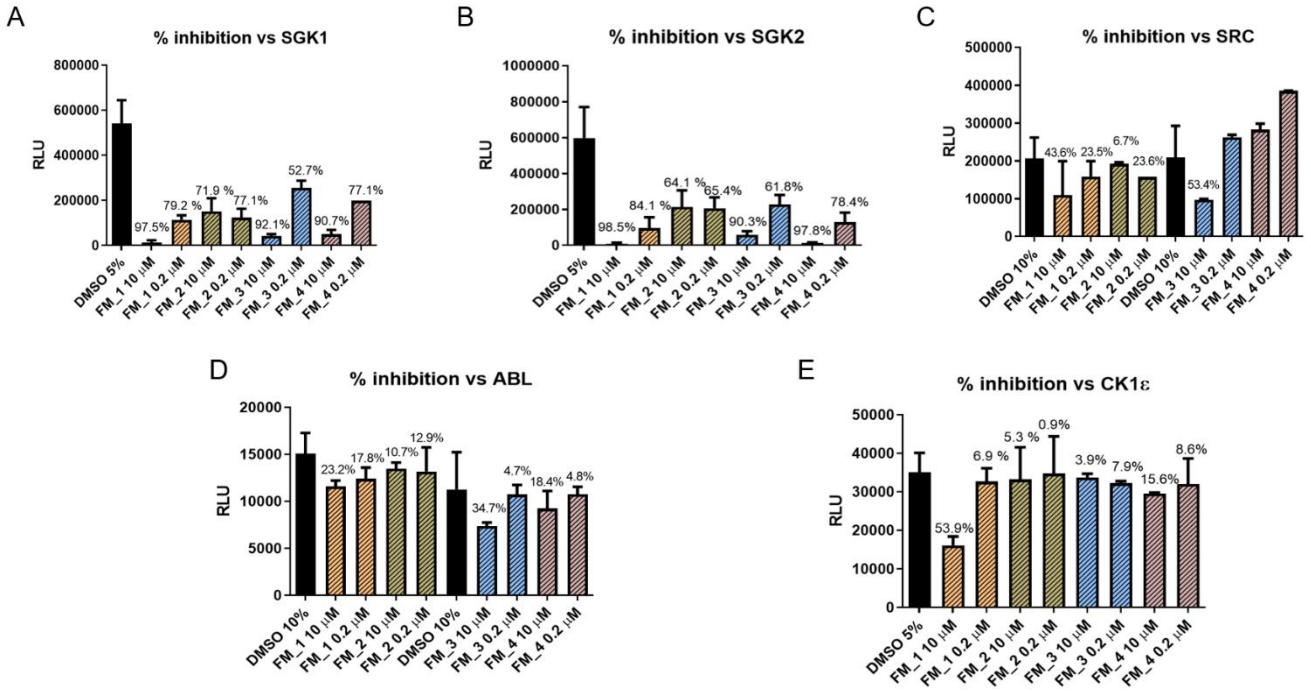

Figure 33. Selectivity of the 4 most potent compounds. Activity of **(A)** SGK1, **(B)** SGK2, **(C)** SRC, **(D)** ABL, **(E)** CK1ε at fix concentrations of compounds **FM_1**, **FM_2**, **FM_3**, **FM_4**. The percentage of inhibition (%) is indicated above graph bars. The discrepancy in the percentage of DMSO in the control samples is attributable to the specific assay conditions

8.2.1. FM Compounds are Competitive Inhibitors of SGK1

The subsequent step was to evaluate the mechanism of action of the most active compound **FM_1**. This was achieved by titrating the reaction substrates while maintaining at fixed concentrations **FM_1**. Variation of apparent affinity (Km) and maximal velocity of reaction (Vmax) was observed in the absence of inhibition or at different concentrations of **FM_1**. As reported in Figure 34 at increased concentration of **FM_1**, corresponds a decrease of the apparent affinity for ATP (increased Km) with no considerable alterations in the Vmax parameter. This is indicative of a competitive mechanism of action towards ATP, which is consistent with the *in silico* model, which was used to virtual screening the compounds by superimposing the chemical structure of small molecules on the ATP binding site.

A

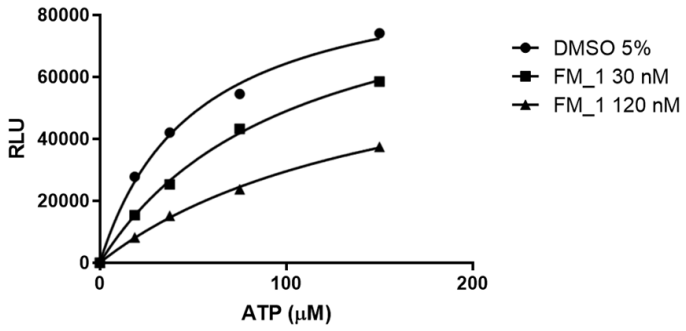

B

	DMSO 5%	FM_1 30 nM	FM_1 120 nM
Michaelis-Menten [2]			
Best-fit values			
Vmax	96702	99559	77039
Km	50.36	103.4	161.0
Std. Error			
Vmax	6090	5456	5354
Km	7.841	10.75	18.33

	DMSO 5%	FM_1 30 nM	FM_1 120 nM
R squared	0.9945	0.9984	0.9987

Figure 34. Mechanism of action of FM_1. (A) SGK1 activity varying FM_1 concentration at titrating ATP. **(B)** Table reporting max and Km parameters

8.3. TARGET INHIBITION IN CELL

SGK1 is activated *in trans* by other kinases. Therefore, it is not possible to evaluate its direct inhibition in cell following its phosphorylation status. Thus, to evaluate the potency of inhibition of the most active compounds identified *in vitro*, we initially decided to evaluate the levels of phosphorylation of NDRG1, a specific target of SGK1, in HEK 293T cells (Ackermann et al., 2011; Di Cristofano, 2017). Cells were treated with different concentration of **FM_1**, while SGK1 Inhibitor, a known SGK1 inhibitor (Cayman Chemical, item n. 25652), was used as reference compound. Figure 35 shows WB detection of total NDRG1, along with its phosphorylated form (P-NDRG1). Unfortunately, we did not observe a clear pattern of P-NDRG1 reduction upon **FM_1** administration. However, also SGK1 inhibitor did not affect P-NDRG1, as expected by effective SGK1 inhibition. We ascribe this unexpected finding to poor selectivity of the antibody targeting p-NDRG1. However, the presence of different hydroxyl groups in the chemical structure of the active compounds likely impairs their ability to permeate the cell membrane. For these reasons, we decide to exploit a nanoparticles delivery approach.

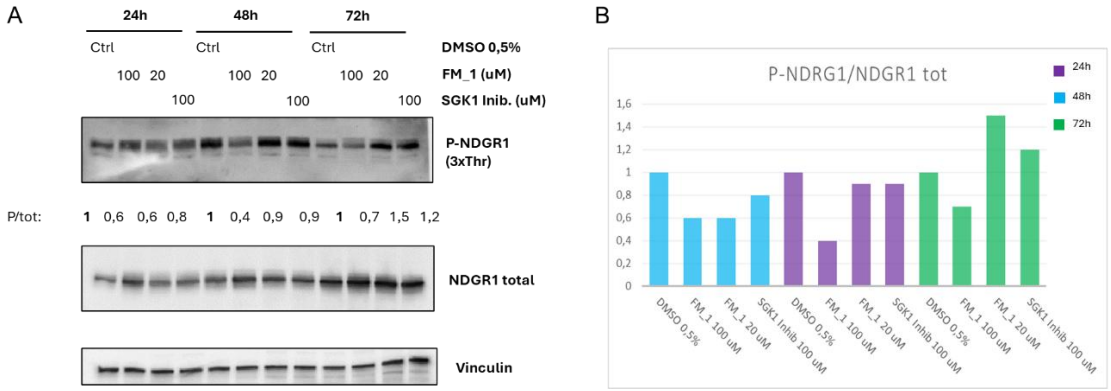

Figure 35. Ratio of NDRG1 phosphorylation after FM_1treatment. The FM_1 compound was observed to induce a reduction in the phosphorylation of NDRG1 at a concentration of 100 µM after 24, 48 and 72 hours. Conversely, the lower concentrations do not exert an inhibitory effect on the phosphorylation of NDRG1

8.3.1. Nanogel to Vehicular Compounds in cells

Given the high hydrophilicity of the active compounds, we decide to utilise nanogel (NG) to deliver the inhibitors directly in the cell cytoplasm. To this aim we opted for a NG composed by a matrix of polyethylene glycol (PEG) and linear polyethyleneimine (PEI) which has been developed by our collaborators at the University Politecnico of Milan. The PEG-PEI NG was conjugated with a chromophore (rhodamine B) to allow its detection and evaluate delivery efficiency. Such NG exhibits nano-scaffold representing the reference for cell uptake, offering a greater specific surface area than their bulk nano-system counterparts, facilitating interactions with physiological compartments and improving the stability and bioavailability of the cargo. The NG presented a size in the range of 20-500 nm, ensuring cell membrane crossing. PEG-PEI NGs have been tested to meet the criteria of biocompatibility, biodegradability and colloidal stability required for bio-application.

Drug loading was conducted using a sponge-like approach, adding drug solution to the dried NG to facilitate drug absorption and encapsulation within the NG meshes in accordance with its swelling behaviour. The release of the compounds in the solution occurs slowly, allowing NG internalization in the cell cytoplasm and the diffusion of the cargo molecules.

Initially, we evaluated the optimal concentration of NG to obtain high cellular internalisation without compromising cell viability in HEK 293T cells. Three distinct concentrations of two distinct nanogels (0.1, 0.5, and 1 mg/ml) were tested for 24 hours in HEK 293T cells. The two nanogels exhibit differences in their formulation, particularly in terms of their PEG molecules. Specifically, **NG_1** consists of a PEG8000 structure, while **NG_2** of a PEG2000 one. Entry of nanogels particles was verified through immunofluorescent microscopy and FACS analysis taking advantage of NGs rhodamine labelling. In the FACS analysis, the value of 10^3 of fluorescence intensity was selected as the threshold for "NG positivity." Cells that fall below this value were considered negative, while those that fall above it were identified as positive for NGs internalization. NGs accumulated in cell cytoplasm already when administered at a concentration of 0.1 mg/ml; however, the optimal result was obtained with a concentration of 0.5 mg/ml. No significant differences were observed between the two NGs in immunofluorescence (data not shown), while FACS analysis reported a small difference in internalisation, so we decided to use the nanogel called NG_1 (Figure 36).

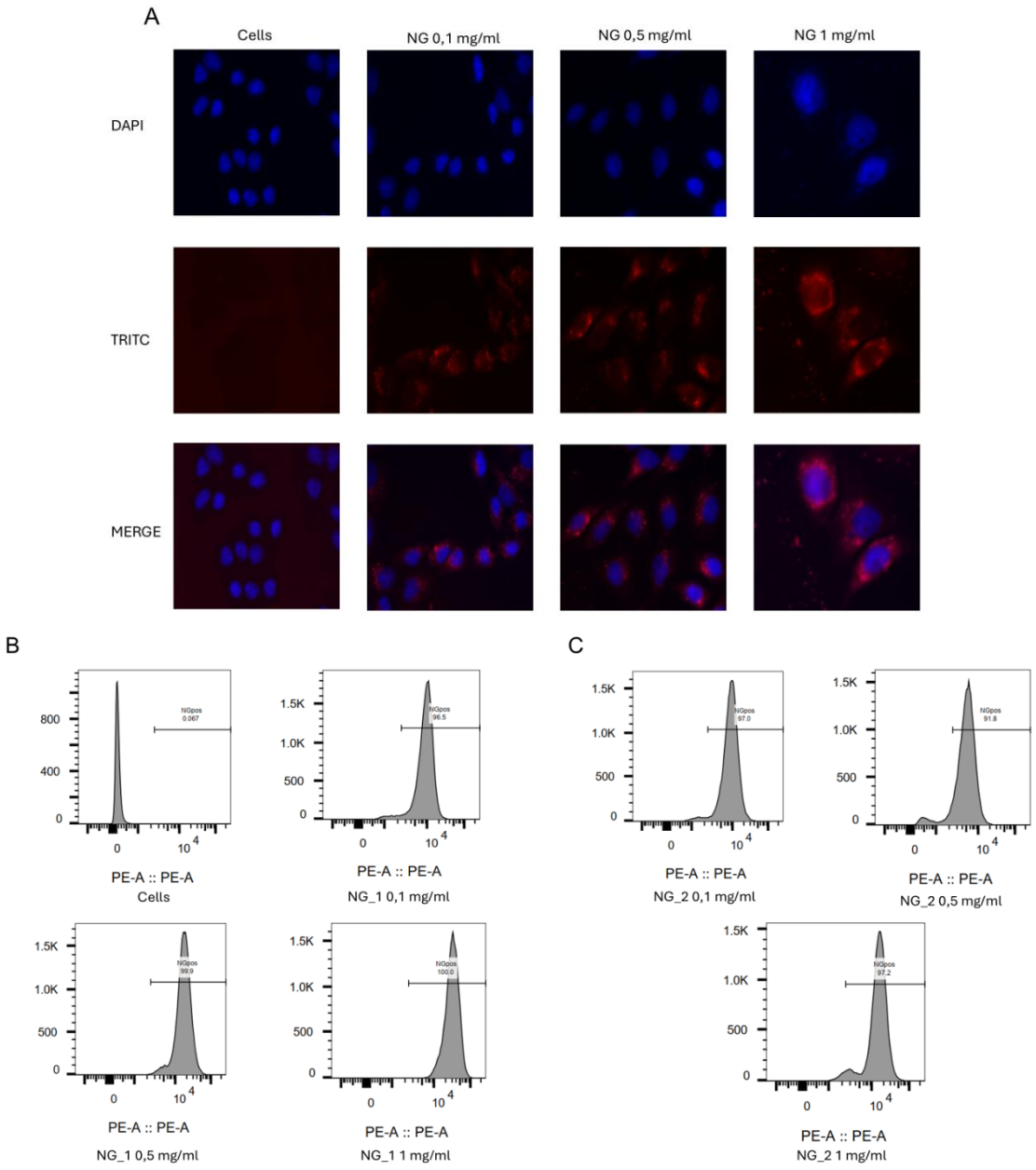

Figure 36. Internalization of NGs. HEK 293T cells were seeded onto coverslips and treated with different concentrations of NGs. (**A)** Cells were fixed, permeabilized and labelled with DAPI and treated with different amount of NG_1 conjugated with rhodamine. (The same results were obtained with NG_2, not shown). (**B and C)** FACS analysis internalization of rhodamine conjugated NG_1 and NG_2 respectively

To optimise the timing of cell entry, we follow **NG_1**'s accumulation in cells over a 24-hour period. As shown in Figure 37, **NG_1** accumulates in cells' the cytosol already after a two-hour of incubation. However, a considerable number of nanoparticles was observed outside the cells. The rate of nanogel uptake increases with the duration of the incubation, with the optimal result being achieved at six hours.

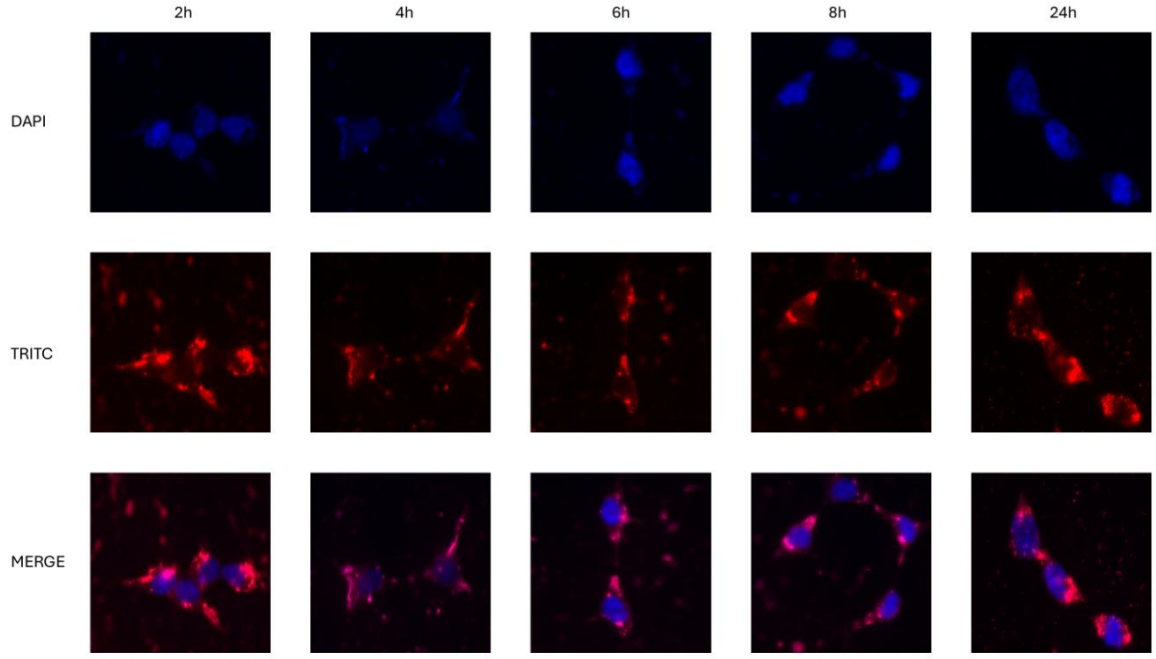

Figure 37. Timecourse of NG_1 cell entrance. HEK 293T cells treated with rhodamine conjugated NG_1

8.4. SGK1 CELLULAR ENGAGEMENT

A new set of WB experiments was conducted using **NG_1**, yet we were not able to distinguish a clear pattern of NDRG1 phosphorylation due to poor antibody selectivity toward the phosphorylated form.

To circumvent this problem, we opted for an alternative methodology based on a Bioluminescence Resonance Energy Transfer (BRET) approach developed by Promega.

In this system, SGK1 is ectopically expressed in HEK 293T. The ectopic kinase has been fused to the bright NanoLuc® luciferase. An SGK1 competitive compound labelled with a fluorochrome called Tracer is also added to the cells. The process of BRET is achieved by the non-radiative transfer of luminescence energy from the NanoLuc® luciferase to the SGK1-bound fluorescent tracer. The inhibitor competes with the tracer for SGK1 binding, thereby reducing the BRET signal in proportion to its affinity for the kinase (Figure 38).

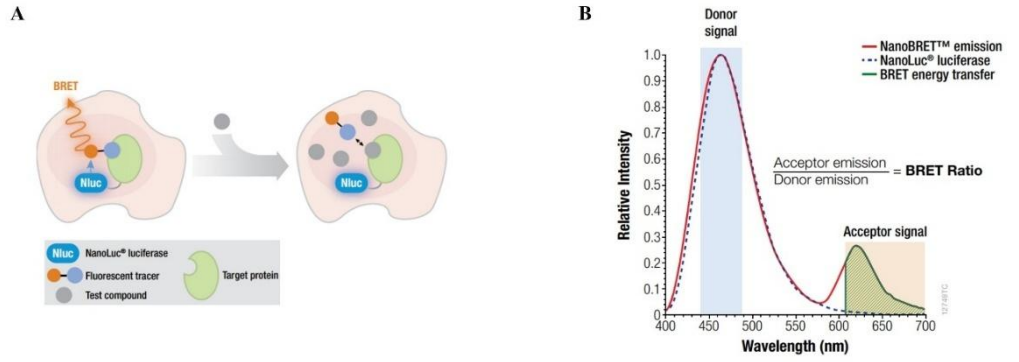

Figure 38. Illustration of the NanoBRET Target Engagement Assay. The fluorescent tracer binds to SGK1 fused with NanoLuc® luciferase. Luciferase signal (460 nm) excites the fluorophore bound to the tracer, generating a BRET signal (618 nm). Competing compounds displace the tracer, decreasing BRET signal proportionally to their affinity toward SGK1. (Adapted from Promega TM598)

The four most potent inhibitors were tested at 50 μM using **NG_1** as a carrier with an incubation period of six hours. The results indicate that **FM_3** inhibits almost completely SGK1 (Figure 39).

These results confirm that ETs potently inhibit SGK1 once penetrated the cell membrane. Therefore, to obtain an effective inhibition, ETs need delivery formulations. However, development of ETs derivatives using our *in silico* approach imposing better permeability features will allow to discover new, potent inhibitors with better pharmacological properties.

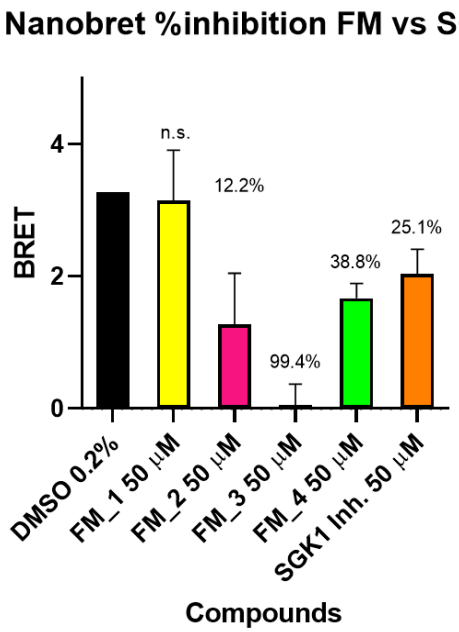

Figure 39. Inhibition of SGK1 in cells by FM compounds using NanoBRET™ Target Engagement Intracellular Kinase Assay. FM_3 is the most active compound in cells, giving an inhibition of 99%

9. DISCUSSION – 1st Part

DNA polymerases are essential for replicating and maintaining genomic integrity, playing central roles also in specialized pathways such as V(D)J recombination and the alternative lengthening of telomeres (ALT) mechanism (Hoitsma et al., 2020). Among them, the X-family polymerases (Pol β, Pol λ, Pol μ, and TdT) are specialized in short gap-filling synthesis and play a crucial role in several DNA repair pathways, including BER and NHEJ (Moon et al., 2014; W. Yang & Gao, 2018). Pol λ, in particular, exhibits remarkable enzymatic versatility, combining template-dependent polymerase, terminal transferase, polynucleotide synthetase, and dRP lyase activities. It plays key roles in multiple repair pathways, including DSB repair via NHEJ and MMEJ, and oxidative damage repair in BER (Maga et al., 2007). Moreover, Pol λ contributes to immune diversity playing a role in antibody gene rearrangement during V(D)J recombination (van Loon et al., 2017).

Recent work from our laboratory has shown that Pol λ plays a significant role in ALT positive cells (Mentegari et al., 2021). ALT is a TMM that is active in approximately 10-15% of human tumours. ALT positive tumours are characterized by common features including heterogeneous telomere lengths, elevated telomeric recombination, abundant ECTR, especially C-circles, and the presence of APBs (J. J. Lee et al., 2021). While the molecular mechanisms underlying ALT are not fully understood, it is now evident that DSBs derived by fork collapse act as the trigger for ALT. There are a number of proposed models of ALT process, however, the DNA polymerases involved in ALT remain unidentified (Hoang & O'Sullivan, 2020). In a previous study, our laboratory demonstrated that Pol λ is essential for C-circle regulation and colocalises with telomeric DNA in ALT cells. Silencing Pol λ led to impaired APB formation, decreased cell viability, and an increased TIFs, which are a hallmark of telomere stress (Mentegari et al., 2021).

Here, we further investigated the role of Pol λ in ALT by quantifying C-circle levels in Pol λ-silenced ALT-positive cell lines using a C-circle assay. We also evaluated the potential involvement of other accessory DNA polymerases, such as Pol θ and Pol μ. These polymerases have been identified as other possible candidates that could play a role in

replication during the ALT process. Our results showed increased C-circle accumulation upon silencing of all these polymerases, thus confirming their possible overlapping key role of all these enzymes in the ALT process.

Studying Pol λ biology presents specific challenges, primarily due to the limited availability of specific antibodies, largely because of its high sequence similarity with other X-family members, especially Pol β. Furthermore, another critical issue is that, like other DNA repair polymerases, Pol λ exploits its functions through transient interactions, complicating the identification of its interactors (Berdis, 2009).

To overcome this issue, we took advantage of the BioID2 proximity-labelling approach, which exploits the promiscuous activity of a mutated biotin ligase (BirA) to biotinylate proximity proteins at unspecific lysine residues within a range of 10 nm. In particular, we have cloned Pol λ in the BioID plasmid BioID2_13X, which expresses a 13 aa flexible linker between BirA and Pol λ, thus conferring high flexibility to the BirA moiety and enabling more contacts with Pol λ interactors.

To this aim we developed U2OS stable clones expressing BirA alone or BirA_Pol λ. Initially, we evaluated the biotinylation pattern of BioID2-Pol λ via WB finding that BirA_Pol λ exhibited a more specific biotinylation pattern in comparison to cells expressing the BirA alone. Confocal immunofluorescence analysis showed that while BirA alone labelled both nuclear and cytoplasmic proteins, BirA_Pol λ interactors were predominantly nuclear, consistent with Pol λ's role in DNA repair.

Given the role of Pol λ in DSB repair and in replication stress, we investigate the Pol λ interactome in unperturbed conditions, as well as upon treatment with Etoposide and HU. Etoposide is a chemotherapy drug that inhibits DNA topoisomerase II, thereby causing DSB. Hydroxyurea inhibits ribonucleotide reductase (RNR), thus reducing dNTPs pool causing replication stress (Montecucco et al., 2015; Musiałek & Rybaczek, 2021).

The biotinylated proteins have been pulled down through streptavidin conjugated beads and sent to MS analysis that was conducted by our collaborators at the ITB-CNR of Milan.

In all cases, the known Pol λ interactors Ku70 and Ku80 were identified, thus confirming that the tagged enzyme was effectively recruited in DSBs repair pathways, validating the physiological relevance of our construct.

In unperturbed condition, novel Pol λ interactors have been identified. Biotinylated proteins were analysed with the DAVID software. Enriched BP and, KEGG pathways were consistent with the role of Pol λ, including DNA repair and telomere maintenance, also confirming our findings on Pol λ role in ALT. Furthermore, the results of the CCL analysis are consistent with the established role of the Pol λ, with the nucleus ranking as the first category. However, DAVID analysis also revealed unexpected BP, with RNA metabolism categories having high scores. The same was true in cellular components, in which nucleolus ranks in the second position. Confocal IF also confirmed the nucleolar localisation of Pol λ interactors in unperturbed conditions. Recent literature has suggested that, in the absence of DNA damage, DNA repair proteins are sequestered at the cellular nucleolus, possibly as a regulatory mechanism, and are subsequently redirected to DNA damage by DDR (Iarovaia et al., 2019; Ogawa & Baserga, 2017). This behaviour has not been associated with Pol λ yet, but it would explain the enrichment of Pol λ interactors associated with RNA metabolism at nucleolus. This is also suggested by the observation that the presence of DNA damaging agents (both etoposide and HU) leads to a reduction of nucleolar and RNA metabolism-associated Pol λ-interacting factors.

Upon etoposide and HU treatment, the composition of biotinylated proteins changes dramatically. DAVID analysis highlight enrichment in BP and KEGG linked to DNA repair, DNA duplex unwinding, ATP-dependent activity acting on DNA and other processes, other than a reduction of interactors associated with RNA metabolism and nucleolus.

Notably, upon etoposide treatment, a greater number of enriched interactors were identified in comparison to HU treatment. This observation may reflect an essential function of Pol λ in DSBs repair rather than during replicative stress, in which it could play a more marginal role. New experiments using different DNA-damaging agents could provide deeper insights into the interaction network of Pol λ. Given that Pol λ exhibits all the enzymatic activities typical of the X-family, it has been hypothesized that it may substitute for other X-family polymerases in various DNA repair pathways. Investigating how the Pol λ interactome changes upon silencing of other repair polymerases could help validate this hypothesis.

A natural continuation of this study will be the validation of individual Pol λ interactors. In particular, it will be crucial to assess whether Pol λ is recruited to the nucleolus under unperturbed conditions, as this could unveil a poorly understood mechanism of DNA damage response regulation.

Similarly, validating Pol λ interactors involved in telomere metabolism and in the ALT pathway will be essential to better understand the role of this polymerase in these specific processes.

In conclusion, many hidden functions of human Pol λ remain to be discovered. Advancing our understanding of this enzyme may pave the way for its application as a pharmaceutical target, particularly in ALT-positive cancer cell lines and other diseases where targeting DNA repair proteins is essential.

10. DISCUSSION – 2nd Part

SGK1, a member of the AGC kinase family, is activated by glucocorticoids and is implicated in diverse cellular processes, including proliferation, apoptosis, ion channel regulation, and signal transduction (Webster et al., 1993). It plays a multifaceted role in immune modulation, notably in Th2 cell differentiation, and is critical in the nervous system for long-term potentiation and memory formation (P. G. Howard et al., 2024; R.-Q. Lu et al., 2022). SGK1 is also a key regulator of glucose homeostasis and has been associated with insulin secretion and β-cell function (C. Yang et al., 2020). Dysregulation or mutation of SGK1 contributes to a range of pathological conditions, including cancer, diabetes, inflammation, and neurodegenerative diseases such as Parkinson's and Alzheimer's, depression, and schizophrenia, through its regulation of BDNF (Kwon et al., 2021; Lang et al., 2009; Sarkar et al., 2023).

In cancer, SGK1 is overexpressed in several tumours, where promotes cell survival, invasion, proliferation, and resistance to chemotherapy and radiotherapy (Ghani, 2022; Sang et al., 2020). Given its central role in cancer, SGK1 has emerged as a promising therapeutic target and prognostic biomarker in oncology (Cicenas et al., 2022).

Recent studies suggest that phytochemicals such as ETs, found in pomegranates and berries, have shown significant antioxidant, antibacterial, anti-inflammatory, antihepatotoxic, antiatherosclerotic, anti-inflammatory, and anticancer activities (Senobari et al., 2022). ETs undergo metabolism by gut microbiota, which influences their bioavailability (Ismail et al., 2016). ETs in various types of cancer, including breast cancer, liver cancer, pancreatic cancer, colon cancer, uterine cancer, ovarian cancer, leukaemia, lymphoma, myeloma, lung cancer, prostate cancer, and others can induce apoptosis, inhibit cell proliferation, and enhance the efficacy of conventional therapies, such as tamoxifen (Usta et al., 2013; Wong et al., 2021). The precise mechanism through which these effects are produced remains to be elucidated (Ismail et al., 2016). Furthermore, they show potential in mitigating neuroinflammation and metabolic disorders, supporting their

relevance as complementary agents in therapeutic strategies (P. Chen et al., 2023; Keta et al., 2020).

Given the roles of SGK1 in different diseases and the effects of ETs in the same disorders, we sought to investigate the correlation between this kinase and these compounds. To this end, a computational study was conducted by our collaborator, Professor Manetti of the University of Siena, with the objective of identifying novel SGK1 inhibitors. Using a ligand-based drug design approach, the chemical structures of known SGK1 inhibitors were employed to develop a pharmacophoric model of SGK1 inhibitors. This was also implemented using the crystal structure of SGK1, resulting in a hybrid model that is capable of incorporating information from both the ligand- and structure-based approaches. We employed this *in silico* model as a three-dimensional filter to perform a virtual screening of a database of commercially available compounds, leading to the identification of 19 candidates with high biding scores, including several ellagitannins. These molecules were then validated through *in vitro* tests. Most of them resulted active towards SGK1, supporting the effectiveness of the *in silico* data. The calculated ID50 values span the micromolar to sub-micromolar range. The selectivity of the most potent inhibitors was assessed on an in-house panel of kinases including TK, STK and lipid kinases. All the hits showed a high degree of selectivity towards SGK1, yet they also exhibited similar inhibitory potency also towards SGK2. This is not surprising given the high degree of homology between the two proteins and the close conformation of their active sites. The mechanism of inhibition of the most potent compound (FM_1, ID50 nM) was investigated at steady state conditions. FM_1 clearly competes with ATP, once again confirming in silico prediction.

The hydrophilic nature of ETs limits spontaneous membrane permeabilization, making cellular uptake dependent on the presence of specific transporters, and thus, dependent on distinct ETs and cell type. Consequently, to evaluate target engagement within living cells, we opted for a delivery strategy using nanogels particles developed by Prof. Mauri's group

at the Politecnico of Milan. In particular, we used a NG composed of a matrix of polyethylene glycol (PEG) and linear polyethyleneimine (PEI) particles, which form a sponge-like nanostructure that can binds the cargo and cross the cellular membrane. These nanomaterials had already demonstrated to satisfy the criteria for bioapplication, specifically with regard to biocompatibility, biodegradability and colloidal stability. To this end, we took advantage of the NanoBRET Target Engagement Assay (Promega). This method relies on the expression of the target kinase conjugated with the Nanoluc luciferase and the administration of a known SKG1 inhibitor linked to a fluorescent moiety (Tracer). This latter absorbs the blue light generated by the luciferase, and emitted photons in the red spectrum. The displacement of the tracer by stronger SGK1 targeting compounds affect the BRET signal. Most of the ETs hits are coloured molecules that can absorb BRET signal, disturbing data acquisition. Luckily, being FM_3 (ID50 15.50 ± 4.09 nM) colourless in solution, it was evaluated in BRET experiment, showing outstanding activity, completely abolishing the BRET signal at 50 uM. Given the similar in vitro activity of other ETs hits identified, and their close related chemistry nature, it is possible to speculate they can also effectively target SGK1 in living cells.

Given the multifaceted roles of SGK1 in several cellular functions and diseases, it is unsurprising that it attracted considerable interest in medicinal chemistry for the development of SGK1 inhibitors. Several studies focused on the development and evaluation of small molecules targeting SGK1 exist. These molecules have been explored for their potential as neuroprotective and anti-hypertensive agents, for their ability to protect from cardiac damage after ischemia, and as anticancer agents and for their ability to protect from osteoarthritis. However, potent and selective inhibitors of SGK1 remain limited.

In this context, our findings represent a promising step forward in the identification of effective SGK1 inhibitors. However, the hydrophilic nature of ETs limits their ability to permeate cellular membranes, necessitating a detailed investigation of their uptake

mechanisms. It has been reported that ellagic acid (EA) and other ETs are detectable in the bloodstream, thus confirming their absorption through dietary intake (Cerdá et al., 2004). Future research focusing on the identification of the cellular transporters responsible for ETs uptake are required. At the same time, the chemical optimization of the hits described here would allow to identify potent inhibitors with better permeability. Nevertheless, the structural complexity of ETs presents a significant synthetic challenge. The resolution of the crystal structures of SGK1 in complex with active ETs will allow the improvement of the *in silico* models for a better rational design of novel derivatives.

11. REFERENCES

Ackermann, T. F., Boini, K. M., Beier, N., Scholz, W., Fuchß, T., & Lang, F. (2011). EMD638683, a Novel SGK Inhibitor with Antihypertensive Potency. *Cellular Physiology and Biochemistry*, *28*(1), 137–146. https://doi.org/10.1159/000331722

Ackerson, S. M., Romney, C., Schuck, P. L., & Stewart, J. A. (2021). To Join or Not to Join: Decision Points Along the Pathway to Double-Strand Break Repair vs. Chromosome End Protection. *Frontiers in Cell and Developmental Biology*, *Volume 9-*. https://www.frontiersin.org/journals/cell-and-developmental-biology/articles/10.3389/fcell.2021.708763

Aguilar-Zarate, P., Wong-Paz, J. E., Buenrostro-Figueroa, J. J., Ascacio, J. A., Contreras-Esquivel, J. C., & Aguilar, C. N. (2018). Ellagitannins: Bioavailability, Purification and Biotechnological Degradation. *Mini Reviews in Medicinal Chemistry*, *18*(15), 1244–1252. https://doi.org/10.2174/1389557517666170208144742

Albertella, M. R., Lau, A., & O'Connor, M. J. (2005). The overexpression of specialized DNA polymerases in cancer. *DNA Repair*, *4*(5), 583–593. https://doi.org/https://doi.org/10.1016/j.dnarep.2005.01.005

Amato, R., D'Antona, L., Porciatti, G., Agosti, V., Menniti, M., Rinaldo, C., Costa, N., Bellacchio, E., Mattarocci, S., Fuiano, G., Soddu, S., Paggi, M. G., Lang, F., & Perrotti, N. (2009). Sgk1 activates MDM2-dependent p53 degradation and affects cell proliferation, survival, and differentiation. *Journal of Molecular Medicine*, *87*(12), 1221–1239. https://doi.org/10.1007/s00109-009-0525-5

An, X., Zhang, Y., Cao, Y., Chen, J., Qin, H., & Yang, L. (2020). Punicalagin Protects Diabetic Nephropathy by Inhibiting Pyroptosis Based on TXNIP/NLRP3 Pathway. *Nutrients*, *12*(5). https://doi.org/10.3390/nu12051516

Arencibia, J. M., Pastor-Flores, D., Bauer, A. F., Schulze, J. O., & Biondi, R. M. (2013). AGC protein kinases: From structural mechanism of regulation to allosteric drug development for the treatment of human diseases. *Biochimica et Biophysica Acta (BBA) - Proteins and Proteomics*, *1834*(7), 1302–1321. https://doi.org/https://doi.org/10.1016/j.bbapap.2013.03.010

Arteaga, M. F., & Canessa, C. M. (2005). Functional specificity of Sgk1 and Akt1 on ENaC activity. *American Journal of Physiology. Renal Physiology*, *289*(1), F90-6. https://doi.org/10.1152/ajprenal.00390.2004

Baradaran Rahimi, V., Ghadiri, M., Ramezani, M., & Askari, V. R. (2020). Antiinflammatory and anti-cancer activities of pomegranate and its constituent, ellagic acid: Evidence from cellular, animal, and clinical studies. *Phytotherapy Research*, *34*(4), 685–720. https://doi.org/https://doi.org/10.1002/ptr.6565

Baranowski, B., Krysińska, M., & Gradowski, M. (2024). KINtaro: protein kinase-like database. *BMC Research Notes*, *17*(1), 50. https://doi.org/10.1186/s13104-024-06713-y

Barroso-González, J., García-Expósito, L., Hoang, S. M., Lynskey, M. L., Roncaioli, J. L., Ghosh, A., Wallace, C. T., de Vitis, M., Modesti, M., Bernstein, K. A., Sarkar, S. N., Watkins, S. C., & O'Sullivan, R. J. (2019). RAD51AP1 Is an Essential Mediator of Alternative Lengthening of Telomeres. *Molecular Cell*, *76*(1), 11-26.e7. https://doi.org/https://doi.org/10.1016/j.molcel.2019.06.043

Bax, B. D., Murshudov, G., Maxwell, A., & Germe, T. (2019). DNA Topoisomerase Inhibitors: Trapping a DNA-Cleaving Machine in Motion. In *Journal of Molecular Biology* (2019/07/10, Vol. 431, Issue 18, pp. 3427–3449). Elsevier. https://doi.org/10.1016/j.jmb.2019.07.008

Bebenek, K., Garcia-Diaz, M., Blanco, L., & Kunkel, T. A. (2003). The Frameshift Infidelity of Human DNA Polymerase λ: IMPLICATIONS FOR FUNCTION*. *Journal of Biological Chemistry*, *278*(36), 34685–34690. https://doi.org/https://doi.org/10.1074/jbc.M305705200

Bebenek, K., Pedersen, L. C., & Kunkel, T. A. (2014). Structure-function studies of DNA polymerase λ. *Biochemistry*, *53*(17), 2781–2792. https://doi.org/10.1021/bi4017236

Belousova, E. A., & Lavrik, O. I. (2015). DNA polymerases β and λ and their roles in cell. *DNA Repair*, *29*, 112–126. https://doi.org/https://doi.org/10.1016/j.dnarep.2015.02.001

Belova, L., Sharma, S., Brickley, D. R., Nicolarsen, J. R., Patterson, C., & Conzen, S. D. (2006). Ubiquitin–proteasome degradation of serum- and glucocorticoid-regulated kinase-1 (SGK-1) is mediated by the chaperone-dependent E3 ligase CHIP. *Biochemical Journal*, *400*(2), 235–244. https://doi.org/10.1042/BJ20060905

Berdis, A. J. (2009). Mechanisms of DNA Polymerases. *Chemical Reviews*, *109*(7), 2862–2879. https://doi.org/10.1021/cr800530b

Berdowska, I., Matusiewicz, M., & Fecka, I. (2021). Punicalagin in Cancer Prevention-Via Signaling Pathways Targeting. *Nutrients*, *13*(8). https://doi.org/10.3390/nu13082733

Bertocci, B., De Smet, A., Berek, C., Weill, J.-C., & Reynaud, C.-A. (2003). Immunoglobulin kappa light chain gene rearrangement is impaired in mice deficient for DNA polymerase mu. *Immunity*, *19*(2), 203–211. https://doi.org/10.1016/s1074-7613(03)00203-6

Bian, X., Xue, H., Jing, D., Wang, Y., Zhou, G., & Zhu, F. (2023). Role of Serum/Glucocorticoid-Regulated Kinase 1 (SGK1) in Immune and Inflammatory Diseases. *Inflammation*, *46*(5), 1612–1625. https://doi.org/10.1007/s10753-023-01857-8

Bienstock, R. J., Beard, W. A., & Wilson, S. H. (2014). Phylogenetic analysis and evolutionary origins of DNA polymerase X-family members. *DNA Repair*, *22*, 77–88. https://doi.org/10.1016/j.dnarep.2014.07.003

Biondi, R. M., & Nebreda, A. R. (2003). Signalling specificity of Ser/Thr protein kinases through docking-site-mediated interactions. *The Biochemical Journal*, *372*(Pt 1), 1–13. https://doi.org/10.1042/BJ20021641

Blasco, M. A. (2005). Telomeres and human disease: ageing, cancer and beyond. *Nature Reviews Genetics*, *6*(8), 611–622. https://doi.org/10.1038/nrg1656

Burke, J. E., Triscott, J., Emerling, B. M., & Hammond, G. R. V. (2023). Beyond PI3Ks: targeting phosphoinositide kinases in disease. *Nature Reviews. Drug Discovery*, *22*(5), 357–386. https://doi.org/10.1038/s41573-022-00582-5

Capra, M., Nuciforo, P. G., Confalonieri, S., Quarto, M., Bianchi, M., Nebuloni, M., Boldorini, R., Pallotti, F., Viale, G., Gishizky, M. L., Draetta, G. F., & Di Fiore, P. P. (2006). Frequent Alterations in the Expression of Serine/Threonine Kinases in Human Cancers. *Cancer Research*, *66*(16), 8147–8154. https://doi.org/10.1158/0008-5472.CAN-05-3489

Casamayor, A., Torrance, P. D., Kobayashi, T., Thorner, J., & Alessi, D. R. (1999). Functional counterparts of mammalian protein kinases PDK1 and SGK in budding yeast. *Current Biology*, *9*(4), 186–197. https://doi.org/10.1016/S0960-9822(99)80088-8

Cerdá, B., Espín, J. C., Parra, S., Martínez, P., & Tomás-Barberán, F. A. (2004). The potent in vitro antioxidant ellagitannins from pomegranate juice are metabolised into bioavailable but poor antioxidant hydroxy-6H-dibenzopyran-6-one derivatives by the colonic microflora of healthy humans. *European Journal of Nutrition*, *43*(4), 205–220. https://doi.org/10.1007/s00394-004-0461-7

Cesare, A. J., & Reddel, R. R. (2010). Alternative lengthening of telomeres: models, mechanisms and implications. *Nature Reviews Genetics*, *11*(5), 319–330. https://doi.org/10.1038/nrg2763

Chandramouly, G., Jamsen, J., Borisonnik, N., Tyagi, M., Calbert, M. L., Tredinnick, T., Ozdemir, A. Y., Kent, T., Demidova, E. V, Arora, S., Wilson, S. H., & Pomerantz, R. T. (2023). Polλ promotes microhomology-mediated end-joining. *Nature Structural & Molecular Biology*, *30*(1), 107–114. https://doi.org/10.1038/s41594-022-00895-4

Chapman-Smith, A., & Cronan, J. E. J. (1999). Molecular biology of biotin attachment to proteins. *The Journal of Nutrition*, *129*(2S Suppl), 477S-484S. https://doi.org/10.1093/jn/129.2.477S

Chen, C., Ha, B. H., Thévenin, A. F., Lou, H. J., Zhang, R., Yip, K. Y., Peterson, J. R., Gerstein, M., Kim, P. M., Filippakopoulos, P., Knapp, S., Boggon, T. J., & Turk, B. E. (2014). Identification of a major determinant for serine-threonine kinase phosphoacceptor specificity. *Molecular Cell*, *53*(1), 140–147. https://doi.org/10.1016/j.molcel.2013.11.013

Chen, P., Guo, Z., & Zhou, B. (2023). Neuroprotective Potential of Punicalagin, a Natural Component of Pomegranate Polyphenols: A Review. *JIN*, *22*(5), 113-null.

Cheshomi, H., Bahrami, A. R., Rafatpanah, H., & Matin, M. M. (2022). The effects of ellagic acid and other pomegranate (Punica granatum L.) derivatives on human gastric cancer AGS cells. *Human & Experimental Toxicology*, *41*, 9603271211064534. https://doi.org/10.1177/09603271211064534

Cho, K. F., Branon, T. C., Udeshi, N. D., Myers, S. A., Carr, S. A., & Ting, A. Y. (2020). Proximity labeling in mammalian cells with TurboID and split-TurboID. *Nature Protocols*, *15*(12), 3971–3999. https://doi.org/10.1038/s41596-020-0399-0

Cicenas, J., Meskinyte-Kausiliene, E., Jukna, V., Rimkus, A., Simkus, J., & Soderholm, D. (2022). SGK1 in Cancer: Biomarker and Drug Target. *Cancers*, *14*(10). https://doi.org/10.3390/cancers14102385

Crespan, E., Czabany, T., Maga, G., & Hübscher, U. (2012). Microhomology-mediated DNA strand annealing and elongation by human DNA polymerases λ and β on normal and repetitive DNA sequences. *Nucleic Acids Research*, *40*(12), 5577–5590. https://doi.org/10.1093/nar/gks186

Cross, T. G., Scheel-Toellner, D., Henriquez, N. V, Deacon, E., Salmon, M., & Lord, J. M. (2000). Serine/Threonine Protein Kinases and Apoptosis. *Experimental Cell Research*, *256*(1), 34–41. https://doi.org/https://doi.org/10.1006/excr.2000.4836

Deng, S., Shanmugam, M. K., Kumar, A. P., Yap, C. T., Sethi, G., & Bishayee, A. (2019). Targeting autophagy using natural compounds for cancer prevention and therapy. *Cancer*, *125*(8), 1228–1246. https://doi.org/10.1002/cncr.31978

Dewar, J. M., & Walter, J. C. (2017). Mechanisms of DNA replication termination. *Nature Reviews Molecular Cell Biology*, *18*(8), 507–516. https://doi.org/10.1038/nrm.2017.42

Di Cristofano, A. (2017). SGK1: The Dark Side of PI3K Signaling. *Current Topics in Developmental Biology*, *123*, 49–71. https://doi.org/10.1016/bs.ctdb.2016.11.006

Díaz-Talavera, A., Montero-Conde, C., Leandro-García, L. J., & Robledo, M. (2022). PrimPol: A Breakthrough among DNA Replication Enzymes and a Potential New Target for Cancer Therapy. *Biomolecules*, *12*(2). https://doi.org/10.3390/biom12020248

Dilley, R. L., & Greenberg, R. A. (2015). ALTernative Telomere Maintenance and Cancer. *Trends in Cancer*, *1*(2), 145–156. https://doi.org/10.1016/j.trecan.2015.07.007

Doksani, Y. (2019). The Response to DNA Damage at Telomeric Repeats and Its Consequences for Telomere Function. *Genes*, *10*(4), 318. https://doi.org/10.3390/genes10040318

Fiala, K. A., Duym, W. W., Zhang, J., & Suo, Z. (2006). Up-regulation of the Fidelity of Human DNA Polymerase λ by Its Non-enzymatic Proline-rich Domain *. *Journal of Biological Chemistry*, *281*(28), 19038–19044. https://doi.org/10.1074/jbc.M601178200

Frit, P., Ropars, V., Modesti, M., Charbonnier, J. B., & Calsou, P. (2019). Plugged into the Ku-DNA hub: The NHEJ network. *Progress in Biophysics and Molecular Biology*, *147*, 62–76. https://doi.org/https://doi.org/10.1016/j.pbiomolbio.2019.03.001

Gao, J., & Pickett, H. A. (2022). Targeting telomeres: advances in telomere maintenance mechanism-specific cancer therapies. *Nature Reviews Cancer*, *22*(9), 515–532. https://doi.org/10.1038/s41568-022-00490-1

García-Díaz, M., Bebenek, K., Sabariegos, R., Domínguez, O., Rodríguez, J., Kirchhoff, T., García-Palomero, E., Picher, A. J., Juárez, R., Ruiz, J. F., Kunkel, T. A., & Blanco, L. (2002). DNA polymerase lambda, a novel DNA repair enzyme in human cells. *The Journal of Biological Chemistry*, *277*(15), 13184–13191. https://doi.org/10.1074/jbc.M111601200

Ghani, M. J. (2022). SGK1, autophagy and cancer: an overview. *Molecular Biology Reports*, *49*(1), 675–685. https://doi.org/10.1007/s11033-021-06836-6

Ghosh, D., & Raghavan, S. C. (2021). 20 years of DNA Polymerase μ, the polymerase that still surprises. *The FEBS Journal*, *288*(24), 7230–7242. https://doi.org/https://doi.org/10.1111/febs.15852

Giardini, M. A., Segatto, M., da Silva, M. S., Nunes, V. S., & Cano, M. I. N. (2014). Chapter One - Telomere and Telomerase Biology. In R. T. B. T.-P. in M. B. and T. S. Calado (Ed.), *Telomeres in Health and Disease* (Vol. 125, pp. 1–40). Academic Press. https://doi.org/https://doi.org/10.1016/B978-0-12-397898-1.00001-3

Goldsmith, E. J., Akella, R., Min, X., Zhou, T., & Humphreys, J. M. (2007). Substrate and docking interactions in serine/threonine protein kinases. *Chemical Reviews*, *107*(11), 5065–5081. https://doi.org/10.1021/cr068221w

Hande, K. R. (1998). Etoposide: Four decades of development of a topoisomerase II inhibitor. *European Journal of Cancer*, *34*(10), 1514–1521. https://doi.org/10.1016/S0959-8049(98)00228-7

Hanks, S. K. (2003). Genomic analysis of the eukaryotic protein kinase superfamily: a perspective. *Genome Biology*, *4*(5), 111. https://doi.org/10.1186/gb-2003-4-5-111

HAYFLICK, L. (1965). THE LIMITED IN VITRO LIFETIME OF HUMAN DIPLOID CELL STRAINS. *Experimental Cell Research*, *37*, 614–636. https://doi.org/10.1016/0014-4827(65)90211-9

HAYFLICK, L., & MOORHEAD, P. S. (1961). The serial cultivation of human diploid cell strains. *Experimental Cell Research*, *25*, 585–621. https://doi.org/10.1016/0014-4827(61)90192-6

Henson, J. D., Lau, L. M., Koch, S., Martin La Rotta, N., Dagg, R. A., & Reddel, R. R. (2017). The C-Circle Assay for alternative-lengthening-of-telomeres activity. *Methods*, *114*, 74–84. https://doi.org/https://doi.org/10.1016/j.ymeth.2016.08.016

Hoang, S. M., & O'Sullivan, R. J. (2020). Alternative Lengthening of Telomeres: Building Bridges To Connect Chromosome Ends. *Trends in Cancer*, *6*(3), 247–260. https://doi.org/10.1016/j.trecan.2019.12.009

Hoitsma, N. M., Whitaker, A. M., Schaich, M. A., Smith, M. R., Fairlamb, M. S., & Freudenthal, B. D. (2020). Structure and function relationships in mammalian DNA polymerases. *Cellular and Molecular Life Sciences : CMLS*, *77*(1), 35–59. https://doi.org/10.1007/s00018-019-03368-y

Howard, M. J., & Wilson, S. H. (2017). Processive searching ability varies among members of the gap-filling DNA polymerase X family. *The Journal of Biological Chemistry*, *292*(42), 17473–17481. https://doi.org/10.1074/jbc.M117.801860

Howard, P. G., Zou, P., Zhang, Y., Huang, F., Tesic, V., Wu, C. Y.-C., & Lee, R. H.-C. (2024). Serum/glucocorticoid regulated kinase 1 (SGK1) in neurological disorders: pain or gain. *Experimental Neurology*, *382*, 114973. https://doi.org/https://doi.org/10.1016/j.expneurol.2024.114973

Iarovaia, O. V, Minina, E. P., Sheval, E. V, Onichtchouk, D., Dokudovskaya, S., Razin, S. V, & Vassetzky, Y. S. (2019). Nucleolus: A Central Hub for Nuclear Functions. *Trends in Cell Biology*, *29*(8), 647–659. https://doi.org/https://doi.org/10.1016/j.tcb.2019.04.003

Ismail, T., Calcabrini, C., Diaz, A. R., Fimognari, C., Turrini, E., Catanzaro, E., Akhtar, S., & Sestili, P. (2016). Ellagitannins in Cancer Chemoprevention and Therapy. *Toxins*, *8*(5). https://doi.org/10.3390/toxins8050151

Jain, R., Aggarwal, A. K., & Rechkoblit, O. (2018). Eukaryotic DNA polymerases. In *Current Opinion in Structural Biology* (Vol. 53, pp. 77–87). https://doi.org/10.1016/j.sbi.2018.06.003

Jang, H., Park, Y., & Jang, J. (2022). Serum and glucocorticoid-regulated kinase 1: Structure, biological functions, and its inhibitors. *Frontiers in Pharmacology*, *Volume 13*. https://www.frontiersin.org/journals/pharmacology/articles/10.3389/fphar.2022.1036844

Jiang, H., Li, L., Ma, T., Wang, R., Chen, X., Xu, K., Chen, C., Liu, Z., Wang, H., & Huang, L. (2024). Serine/Threonine Kinase (STK) 33 promotes the proliferation and metastasis of human esophageal squamous cell carcinoma via inflammation-related pathway. *Pathology - Research and Practice*, *254*, 155154. https://doi.org/https://doi.org/10.1016/j.prp.2024.155154

Johansson, E., & Dixon, N. (2013). Replicative DNA polymerases. *Cold Spring Harbor Perspectives in Biology*, *5*(6), a012799. https://doi.org/10.1101/cshperspect.a012799

Johnson, J. L., Yaron, T. M., Huntsman, E. M., Kerelsky, A., Song, J., Regev, A., Lin, T.-Y., Liberatore, K., Cizin, D. M., Cohen, B. M., Vasan, N., Ma, Y., Krismer, K., Robles, J. T., van de Kooij, B., van Vlimmeren, A. E., Andrée-Busch, N., Käufer, N. F., Dorovkov, M. V, … Cantley, L. C. (2023). An atlas of substrate specificities for the human serine/threonine kinome. *Nature*, *613*(7945), 759–766. https://doi.org/10.1038/s41586-022-05575-3

Johnson, L. N. (2009). Protein kinase inhibitors: contributions from structure to clinical compounds. *Quarterly Reviews of Biophysics*, *42*(1), 1–40. https://doi.org/DOI: 10.1017/S0033583508004745

Kalaivani, R., Reema, R., & Srinivasan, N. (2018). Recognition of sites of functional specialisation in all known eukaryotic protein kinase families. *PLoS Computational Biology*, *14*(2), e1005975. https://doi.org/10.1371/journal.pcbi.1005975

Kaminski, A. M., Bebenek, K., Pedersen, L. C., & Kunkel, T. A. (2020). DNA polymerase mu: An inflexible scaffold for substrate flexibility. *DNA Repair*, *93*, 102932. https://doi.org/10.1016/j.dnarep.2020.102932

Kaminski, A. M., Chiruvella, K. K., Ramsden, D. A., Bebenek, K., Kunkel, T. A., & Pedersen, L. C. (2024). DNA polymerase λ Loop1 variant yields unexpected gain-of-function capabilities in nonhomologous end-joining. *DNA Repair*, *136*, 103645. https://doi.org/https://doi.org/10.1016/j.dnarep.2024.103645

Kaminski, A. M., Kunkel, T. A., Pedersen, L. C., & Bebenek, K. (2021). Structural Insights into the Specificity of 8-Oxo-7,8-dihydro-2'-deoxyguanosine Bypass by Family X DNA Polymerases. *Genes*, *13*(1). https://doi.org/10.3390/genes13010015

Kent, T., & Clynes, D. (2021). Alternative Lengthening of Telomeres: Lessons to Be Learned from Telomeric DNA Double-Strand Break Repair. *Genes*, *12*(11). https://doi.org/10.3390/genes12111734

Keta, O. D., Deljanin, M., Petković, V. D., Zdunić, G., Janković, T., Živković, J., Fira, A. R., Petrović, I. M., & \vSavikin, K. (2020). Pomegranate (Punica granatum L.) Peel Extract: Potential Cytotoxic Agent Against Different Cancer Cell Lines. *Records of Natural Products*. https://api.semanticscholar.org/CorpusID:218941676

Kido, K., Yamanaka, S., Nakano, S., Motani, K., Shinohara, S., Nozawa, A., Kosako, H., Ito, S., & Sawasaki, T. (2020). AirID, a novel proximity biotinylation enzyme, for analysis of protein-protein interactions. *ELife*, *9*. https://doi.org/10.7554/eLife.54983

Kim, D. I., Birendra, K. C., Zhu, W., Motamedchaboki, K., Doye, V., & Roux, K. J. (2014). Probing nuclear pore complex architecture with proximity-dependent biotinylation. *Proceedings of the National Academy of Sciences of the United States of America*, *111*(24), E2453-61. https://doi.org/10.1073/pnas.1406459111

Kim, D. I., Jensen, S. C., Noble, K. A., Kc, B., Roux, K. H., Motamedchaboki, K., & Roux, K. J. (2016). An improved smaller biotin ligase for BioID proximity labeling. *Molecular Biology of the Cell*, *27*(8), 1188–1196. https://doi.org/10.1091/mbc.E15-12-0844

Kim, J., Kim, D., Jung, H., Lee, J., & Hong, V. S. (2021). Identification and Kinetic Characterization of Serum- and Glucocorticoid-Regulated Kinase Inhibitors Using a Fluorescence Polarization–Based Assay. *SLAS Discovery*, *26*(5), 655–662. https://doi.org/https://doi.org/10.1177/24725552211002465

kinase.com. (n.d.). http://kinase.com/web/current/

Krokan, H. E., & Bjørås, M. (2013). Base excision repair. *Cold Spring Harbor Perspectives in Biology*, *5*(4), a012583. https://doi.org/10.1101/cshperspect.a012583

Krupa, A., & Srinivasan, N. (2002). The repertoire of protein kinases encoded in the draft version of the human genome: atypical variations and uncommon domain combinations. *Genome Biology*, *3*(12), RESEARCH0066. https://doi.org/10.1186/gb-2002-3-12-research0066

Kuznetsova, A. A., Fedorova, O. S., & Kuznetsov, N. A. (2022). Structural and Molecular Kinetic Features of Activities of DNA Polymerases. *International Journal of Molecular Sciences*, *23*(12). https://doi.org/10.3390/ijms23126373

Kwon, O.-C., Song, J.-J., Yang, Y., Kim, S.-H., Kim, J. Y., Seok, M.-J., Hwang, I., Yu, J.-W., Karmacharya, J., Maeng, H.-J., Kim, J., Jho, E.-H., Ko, S. Y., Son, H., Chang, M.-Y., & Lee, S.-H. (2021). SGK1 inhibition in glia ameliorates pathologies and symptoms in Parkinson disease animal models. *EMBO Molecular Medicine*, *13*(4), e13076. https://doi.org/10.15252/emmm.202013076

Lang, F., Görlach, A., & Vallon, V. (2009). Targeting SGK1 in diabetes. *Expert Opinion on Therapeutic Targets*, *13*(11), 1303–1311. https://doi.org/10.1517/14728220903260807

Lang, F., Perrotti, N., & Stournaras, C. (2010). Colorectal carcinoma cells—Regulation of survival and growth by SGK1. *The International Journal of Biochemistry & Cell Biology*, *42*(10), 1571–1575. https://doi.org/https://doi.org/10.1016/j.biocel.2010.05.016

Lang, F., & Stournaras, C. (2013). Serum and glucocorticoid inducible kinase, metabolic syndrome, inflammation, and tumor growth. *Hormones*, *12*(2), 160–171. https://doi.org/10.14310/horm.2002.1401

Lang, F., Stournaras, C., Zacharopoulou, N., Voelkl, J., & Alesutan, I. (2018). Serum- and glucocorticoid-inducible kinase 1 and the response to cell stress. *Cell Stress*, *3*(1), 1–8. https://doi.org/10.15698/cst2019.01.170

Lang, F., Strutz-Seebohm, N., Seebohm, G., & Lang, U. E. (2010). Significance of SGK1 in the regulation of neuronal function. *The Journal of Physiology*, *588*(Pt 18), 3349–3354. https://doi.org/10.1113/jphysiol.2010.190926

Lange, S. S., Takata, K., & Wood, R. D. (2011). DNA polymerases and cancer. *Nature Reviews. Cancer*, *11*(2), 96–110. https://doi.org/10.1038/nrc2998

Lee, J. J., Lee, J., & Lee, H. (2021). Alternative paths to telomere elongation. *Seminars in Cell & Developmental Biology*, *113*, 88–96. https://doi.org/https://doi.org/10.1016/j.semcdb.2020.11.003

Lee, K.-H., Kim, D.-Y., & Kim, W. (2021). Regulation of Gene Expression by Telomere Position Effect. *International Journal of Molecular Sciences*, *22*(23). https://doi.org/10.3390/ijms222312807

Liang, X., Lan, C., Jiao, G., Fu, W., Long, X., An, Y., Wang, K., Zhou, J., Chen, T., Li, Y., Xu, J., Huang, Q., Xu, B., & Xiao, J. (2017). Therapeutic inhibition of SGK1 suppresses colorectal cancer. *Experimental & Molecular Medicine*, *49*(11), e399. https://doi.org/10.1038/emm.2017.184

Lieber, M. R. (2023). Pol X DNA polymerases contribute to NHEJ flexibility. *Nature Structural & Molecular Biology*, *30*(1), 5–8. https://doi.org/10.1038/s41594-022-00904-6

Lu, R.-Q., Zhang, Y.-Y., Zhao, H.-Q., Guo, R.-Q., Jiang, Z.-X., & Guo, R. (2022). SGK1, a Critical Regulator of Immune Modulation and Fibrosis and a Potential Therapeutic Target in Chronic Graft-Versus-Host Disease. *Frontiers in Immunology*, *13*, 822303. https://doi.org/10.3389/fimmu.2022.822303

Lu, W., Zhang, Y., Liu, D., Songyang, Z., & Wan, M. (2013). Telomeres-structure, function, and regulation. *Experimental Cell Research*, *319*(2), 133–141. https://doi.org/10.1016/j.yexcr.2012.09.005

Lue, N. F., Chan, J., Wright, W. E., & Hurwitz, J. (2014). The CDC13-STN1-TEN1 complex stimulates Pol α activity by promoting RNA priming and primase-to-polymerase switch. *Nature Communications*, *5*(1), 5762. https://doi.org/10.1038/ncomms6762

Maciejowski, J., & de Lange, T. (2017). Telomeres in cancer: tumour suppression and genome instability. *Nature Reviews. Molecular Cell Biology*, *18*(3), 175–186. https://doi.org/10.1038/nrm.2016.171

Maga, G., Villani, G., Crespan, E., Wimmer, U., Ferrari, E., Bertocci, B., & Hübscher, U. (2007). 8-oxo-guanine bypass by human DNA polymerases in the presence of auxiliary proteins. *Nature*, *447*(7144), 606–608. https://doi.org/10.1038/nature05843

Maltseva, E. A., Rechkunova, N. I., & Lavrik, O. I. (2023). Non-Catalytic Domains of DNA Polymerase λ: Influence on Enzyme Activity and Its Regulation. *Doklady. Biochemistry and Biophysics*, *512*(1), 245–250. https://doi.org/10.1134/S1607672923700382

Manning, G, Whyte, D. B., Martinez, R., Hunter, T., & Sudarsanam, S. (2002). The Protein Kinase Complement of the Human Genome. *Science*, *298*(5600), 1912–1934. https://doi.org/10.1126/science.1075762

Manning, Gerard, Plowman, G. D., Hunter, T., & Sudarsanam, S. (2002). Evolution of protein kinase signaling from yeast to man. *Trends in Biochemical Sciences*, *27*(10), 514–520. https://doi.org/https://doi.org/10.1016/S0968-0004(02)02179-5

Mauri, E., Moroni, I., Magagnin, L., Masi, M., Sacchetti, A., & Rossi, F. (2016). Comparison between two different click strategies to synthesize fluorescent nanogels for therapeutic applications. *Reactive and Functional Polymers*, *105*, 35–44. https://doi.org/https://doi.org/10.1016/j.reactfunctpolym.2016.05.007

May, D. G., Scott, K. L., Campos, A. R., & Roux, K. J. (2020). Comparative Application of BioID and TurboID for Protein-Proximity Biotinylation. *Cells*, *9*(5). https://doi.org/10.3390/cells9051070

Mazzucco, G., Huda, A., Galli, M., Piccini, D., Giannattasio, M., Pessina, F., & Doksani, Y. (2020). Telomere damage induces internal loops that generate telomeric circles. *Nature Communications*, *11*(1), 5297. https://doi.org/10.1038/s41467-020-19139-4

Medvedev, K. E., Schaeffer, R. D., Pei, J., & Grishin, N. V. (2023). Pathogenic mutation hotspots in protein kinase domain structure. *Protein Science : A Publication of the Protein Society*, *32*(9), e4750. https://doi.org/10.1002/pro.4750

Melnikova, I., & Golden, J. (2004). Targeting protein kinases. *Nature Reviews Drug Discovery*, *3*(12), 993–994. https://doi.org/10.1038/nrd1600

Mendez-Bermudez, A., Giraud-Panis, M.-J., Ye, J., & Gilson, E. (2020). Heterochromatin replication goes hand in hand with telomere protection. *Nature Structural & Molecular Biology*, *27*(4), 313–318. https://doi.org/10.1038/s41594-020-0400-1

Mentegari, E., Bertoletti, F., Kissova, M., Zucca, E., Galli, S., Tagliavini, G., Garbelli, A., Maffia, A., Bione, S., Ferrari, E., Fagagna, F. d'Adda di, Francia, S., Sabbioneda, S., Chen, L.-Y., Lingner, J., Bergoglio, V., Hoffmann, J.-S., Hübscher, U., Crespan, E., & Maga, G. (2021). A Role for Human DNA Polymerase λ in Alternative Lengthening of Telomeres. *International Journal of Molecular Sciences*, *22*(5), 2365. https://doi.org/10.3390/ijms22052365

Mentegari, E., Kissova, M., Bavagnoli, L., Maga, G., & Crespan, E. (2016). DNA Polymerases λ and β: The Double-Edged Swords of DNA Repair. *Genes*, *7*(9), 57. https://doi.org/10.3390/genes7090057

Middelbeek, J., Clark, K., Venselaar, H., Huynen, M. A., & van Leeuwen, F. N. (2010). The alpha-kinase family: an exceptional branch on the protein kinase tree. *Cellular and Molecular Life Sciences : CMLS*, *67*(6), 875–890. https://doi.org/10.1007/s00018-009-0215-z

Montecucco, A., Zanetta, F., & Biamonti, G. (2015). Molecular mechanisms of etoposide. *EXCLI Journal*, *14*, 95–108. https://doi.org/10.17179/excli2015-561

Moon, A. F., Garcia-Diaz, M., Batra, V. K., Beard, W. A., Bebenek, K., Kunkel, T. A., Wilson, S. H., & Pedersen, L. C. (2007). The X family portrait: structural insights into biological functions of X family polymerases. *DNA Repair*, *6*(12), 1709–1725. https://doi.org/10.1016/j.dnarep.2007.05.009

Moon, A. F., Pryor, J. M., Ramsden, D. A., Kunkel, T. A., Bebenek, K., & Pedersen, L. C. (2014). Sustained active site rigidity during synthesis by human DNA polymerase μ. *Nature Structural & Molecular Biology*, *21*(3), 253–260. https://doi.org/10.1038/nsmb.2766

Muñoz-Espín, D., & Serrano, M. (2014). Cellular senescence: from physiology to pathology. *Nature Reviews Molecular Cell Biology*, *15*(7), 482–496. https://doi.org/10.1038/nrm3823

Muoio, D., Laspata, N., & Fouquerel, E. (2022). Functions of ADP-ribose transferases in the maintenance of telomere integrity. *Cellular and Molecular Life Sciences : CMLS*, *79*(4), 215. https://doi.org/10.1007/s00018-022-04235-z

Musiałek, M. W., & Rybaczek, D. (2021). Hydroxyurea-The Good, the Bad and the Ugly. *Genes*, *12*(7). https://doi.org/10.3390/genes12071096

Nguyen, T. H. D., Collins, K., & Nogales, E. (2019). Telomerase structures and regulation: shedding light on the chromosome end. *Current Opinion in Structural Biology*, *55*, 185–193. https://doi.org/https://doi.org/10.1016/j.sbi.2019.04.009

Ogawa, L. M., & Baserga, S. J. (2017). Crosstalk between the nucleolus and the DNA damage response. *Molecular BioSystems*, *13*(3), 443–455. https://doi.org/10.1039/c6mb00740f

Pan, H., Lv, W., Li, Z., & Han, W. (2019). SGK1 protein expression is a prognostic factor of lung adenocarcinoma that regulates cell proliferation and survival. *International Journal of Clinical and Experimental Pathology*, *12*(2), 391–408.

Pearce, L. R., Komander, D., & Alessi, D. R. (2010). The nuts and bolts of AGC protein kinases. *Nature Reviews Molecular Cell Biology*, *11*(1), 9–22. https://doi.org/10.1038/nrm2822

Ray, S., Breuer, G., DeVeaux, M., Zelterman, D., Bindra, R., & Sweasy, J. B. (2018). DNA polymerase beta participates in DNA End-joining. *Nucleic Acids Research*, *46*(1), 242–255. https://doi.org/10.1093/nar/gkx1147

Reddel, R. R. (2014). Telomere maintenance mechanisms in cancer: clinical implications. *Current Pharmaceutical Design*, *20*(41), 6361–6374. https://doi.org/10.2174/1381612820666140630101047

Reha-Krantz, L. J. (2010). DNA polymerase proofreading: Multiple roles maintain genome stability. *Biochimica et Biophysica Acta*, *1804*(5), 1049–1063. https://doi.org/10.1016/j.bbapap.2009.06.012

Reiterer, M., Schmidt-Kastner, R., & Milton, S. L. (2019). Methionine sulfoxide reductase (Msr) dysfunction in human brain disease. *Free Radical Research*, *53*(11–12), 1144–1154. https://doi.org/10.1080/10715762.2019.1662899

Riegel, K., Vijayarangakannan, P., Kechagioglou, P., Bogucka, K., & Rajalingam, K. (2022). Recent advances in targeting protein kinases and pseudokinases in cancer biology. *Frontiers in Cell and Developmental Biology*, *10*. https://www.frontiersin.org/journals/cell-and-developmental-biology/articles/10.3389/fcell.2022.942500

Rose, A. M., Goncalves, T., Cunniffe, S., Geiller, H. E. B., Kent, T., Shepherd, S., Ratnaweera, M., O'Sullivan, R. J., Gibbons, R. J., & Clynes, D. (2023). Induction of the alternative lengthening of telomeres pathway by trapping of proteins on DNA. *Nucleic Acids Research*, *51*(13), 6509–6527. https://doi.org/10.1093/nar/gkad150

Roskoski Jr., R. (2022). Properties of FDA-approved small molecule protein kinase inhibitors: A 2022 update. *Pharmacological Research*, *175*, 106037. https://doi.org/https://doi.org/10.1016/j.phrs.2021.106037

Roskoski, R. (2024). Properties of FDA-approved small molecule protein kinase inhibitors: A 2024 update. *Pharmacological Research*, *200*, 107059. https://doi.org/https://doi.org/10.1016/j.phrs.2024.107059

Rosso, I., Jones-Weinert, C., Rossiello, F., Cabrini, M., Brambillasca, S., Munoz-Sagredo, L., Lavagnino, Z., Martini, E., Tedone, E., Garre', M., Aguado, J., Parazzoli, D., Mione, M., Shay, J. W., Mercurio, C., & d'Adda di Fagagna, F. (2023). Alternative lengthening of telomeres (ALT) cells viability is dependent on C-rich telomeric RNAs. *Nature Communications*, *14*(1), 7086. https://doi.org/10.1038/s41467-023-42831-0

Roux, K. J., Kim, D. I., Raida, M., & Burke, B. (2012). A promiscuous biotin ligase fusion protein identifies proximal and interacting proteins in mammalian cells. *The Journal of Cell Biology*, *196*(6), 801–810. https://doi.org/10.1083/jcb.201112098

Roy, S., Vivoli Vega, M., & Harmer, N. J. (2019). Carbohydrate Kinases: A Conserved Mechanism Across Differing Folds. In *Catalysts* (Vol. 9, Issue 1). https://doi.org/10.3390/catal9010029

Rozpędek, W., Pytel, D., Nowak-Zduńczyk, A., Lewko, D., Wojtczak, R., Diehl, J. A., & Majsterek, I. (2019). Breaking the DNA Damage Response via Serine/Threonine Kinase Inhibitors to Improve Cancer Treatment. In *Current Medicinal Chemistry* (Vol. 26, Issue 8, pp. 1425–1445). https://doi.org/http://dx.doi.org/10.2174/0929867325666180117102233

Salker, M. S., Christian, M., Steel, J. H., Nautiyal, J., Lavery, S., Trew, G., Webster, Z., Al-Sabbagh, M., Puchchakayala, G., Föller, M., Landles, C., Sharkey, A. M., Quenby, S., Aplin, J. D., Regan, L., Lang, F., & Brosens, J. J. (2011). Deregulation of the serum- and glucocorticoid-inducible kinase SGK1 in the endometrium causes reproductive failure. *Nature Medicine*, *17*(11), 1509–1513. https://doi.org/10.1038/nm.2498

Samavarchi-Tehrani, P., Samson, R., & Gingras, A.-C. (2020). Proximity Dependent Biotinylation: Key Enzymes and Adaptation to Proteomics Approaches*. *Molecular & Cellular Proteomics*, *19*(5), 757–773. https://doi.org/https://doi.org/10.1074/mcp.R120.001941

Sang, Y., Kong, P., Zhang, S., Zhang, L., Cao, Y., Duan, X., Sun, T., Tao, Z., & Liu, W. (2020). SGK1 in Human Cancer: Emerging Roles and Mechanisms. *Frontiers in Oncology*, *10*, 608722. https://doi.org/10.3389/fonc.2020.608722

Sarkar, N., Singh, A., Kumar, P., & Kaushik, M. (2023). Protein kinases: Role of their dysregulation in carcinogenesis, identification and inhibition. *Drug Research*, *73*(4), 189–199. https://doi.org/10.1055/a-1989-1856

Sawyer, T. K., Wu, J. C., Sawyer, J. R., & English, J. M. (2013). Protein kinase inhibitors: breakthrough medicines and the next generation. *Expert Opinion on Investigational Drugs*, *22*(6), 675–678. https://doi.org/10.1517/13543784.2013.804509

Schopp, I. M., Amaya Ramirez, C. C., Debeljak, J., Kreibich, E., Skribbe, M., Wild, K., & Béthune, J. (2017). Split-BioID a conditional proteomics approach to monitor the composition of spatiotemporally defined protein complexes. *Nature Communications*, *8*, 15690. https://doi.org/10.1038/ncomms15690

Schwab, M., Lupescu, A., Mota, M., Mota, E., Frey, A., Simon, P., Mertens, P. R., Floege, J., Luft, F., Asante-Poku, S., Schaeffeler, E., & Lang, F. (2008). Association of SGK1 Gene Polymorphisms with Type 2 Diabetes. *Cellular Physiology and Biochemistry*, *21*(1–3), 151–160. https://doi.org/10.1159/000113757

Scully, R., Panday, A., Elango, R., & Willis, N. A. (2019). DNA double-strand break repair-pathway choice in somatic mammalian cells. *Nature Reviews. Molecular Cell Biology*, *20*(11), 698–714. https://doi.org/10.1038/s41580-019-0152-0

Sears, R. M., May, D. G., & Roux, K. J. (2019). BioID as a Tool for Protein-Proximity Labeling in Living Cells. *Methods in Molecular Biology (Clifton, N.J.)*, *2012*, 299–313. https://doi.org/10.1007/978-1-4939-9546-2_15

Senobari, Z., Karimi, G., & Jamialahmadi, K. (2022). Ellagitannins, promising pharmacological agents for the treatment of cancer stem cells. *Phytotherapy Research*, *36*(1), 231–242. https://doi.org/https://doi.org/10.1002/ptr.7307

Seol, J. H., Shim, E. Y., & Lee, S. E. (2018). Microhomology-mediated end joining: Good, bad and ugly. In *Mutation Research - Fundamental and Molecular Mechanisms of Mutagenesis* (2017/07/16, Vol. 809, pp. 81–87). https://doi.org/10.1016/j.mrfmmm.2017.07.002

Shay, J. W. (2016). Role of Telomeres and Telomerase in Aging and Cancer. *Cancer Discovery*, *6*(6), 584–593. https://doi.org/10.1158/2159-8290.CD-16-0062

Shay, J. W., & Wright, W. E. (2019). Telomeres and telomerase: three decades of progress. *Nature Reviews Genetics*, *20*(5), 299–309. https://doi.org/10.1038/s41576-019-0099-1

Sineh Sepehr, K., Baradaran, B., Mazandarani, M., Khori, V., & Shahneh, F. Z. (2012). Studies on the Cytotoxic Activities of Punica granatum L. var. spinosa (Apple Punice) Extract on Prostate Cell Line by Induction of Apoptosis. *ISRN Pharmaceutics*, *2012*, 547942. https://doi.org/10.5402/2012/547942

Sobinoff, A. P., & Pickett, H. A. (2017). Alternative Lengthening of Telomeres: DNA Repair Pathways Converge. *Trends in Genetics*, *33*(12), 921–932. https://doi.org/https://doi.org/10.1016/j.tig.2017.09.003

Sohn, E. J., Goralsky, J. A., Shay, J. W., & Min, J. (2023). The Molecular Mechanisms and Therapeutic Prospects of Alternative Lengthening of Telomeres (ALT). *Cancers*, *15*(7). https://doi.org/10.3390/cancers15071945

Sommer, E. M., Dry, H., Cross, D., Guichard, S., Davies, B. R., & Alessi, D. R. (2013). Elevated SGK1 predicts resistance of breast cancer cells to Akt inhibitors. *The Biochemical Journal*, *452*(3), 499–508. https://doi.org/10.1042/BJ20130342

Stroik, S., & Hendrickson, E. A. (2020). Telomere replication-When the going gets tough. *DNA Repair*, *94*, 102875. https://doi.org/10.1016/j.dnarep.2020.102875

Sun, H., Ma, L., Tsai, Y.-F., Abeywardana, T., Shen, B., & Zheng, L. (2023). Okazaki fragment maturation: DNA flap dynamics for cell proliferation and survival. *Trends in Cell Biology*, *33*(3), 221–234. https://doi.org/10.1016/j.tcb.2022.06.014

Svilar, D., Goellner, E. M., Almeida, K. H., & Sobol, R. W. (2011). Base excision repair and lesion-dependent subpathways for repair of oxidative DNA damage. *Antioxidants & Redox Signaling*, *14*(12), 2491–2507. https://doi.org/10.1089/ars.2010.3466

Talarico, C., Dattilo, V., D'Antona, L., Menniti, M., Bianco, C., Ortuso, F., Alcaro, S., Schenone, S., Perrotti, N., & Amato, R. (2016). SGK1, the New Player in the Game of Resistance: Chemo-Radio Molecular Target and Strategy for Inhibition. *Cellular Physiology and Biochemistry*, *39*(5), 1863–1876. https://doi.org/10.1159/000447885

Taylor, S. S., & Kornev, A. P. (2011). Protein kinases: evolution of dynamic regulatory proteins. *Trends in Biochemical Sciences*, *36*(2), 65–77. https://doi.org/https://doi.org/10.1016/j.tibs.2010.09.006

Tejada, S., Setzer, W. N., Daglia, M., Nabavi, S. F., Sureda, A., Braidy, N., Gortzi, O., & Nabavi, S. M. (2017). Neuroprotective Effects of Ellagitannins: A Brief Review. *Current Drug Targets*, *18*(13), 1518–1528. https://doi.org/10.2174/1389450117666161005112002

Torkamani, A., Verkhivker, G., & Schork, N. J. (2009). Cancer driver mutations in protein kinase genes. *Cancer Letters*, *281*(2), 117–127. https://doi.org/10.1016/j.canlet.2008.11.008

Truong, L. N., Li, Y., Shi, L. Z., Hwang, P. Y.-H., He, J., Wang, H., Razavian, N., Berns, M. W., & Wu, X. (2013). Microhomology-mediated End Joining and Homologous Recombination share the initial end resection step to repair DNA double-strand breaks in mammalian cells. *Proceedings of the National Academy of Sciences*, *110*(19), 7720–7725. https://doi.org/10.1073/pnas.1213431110

Turner, K. J., Vasu, V., & Griffin, D. K. (2019). Telomere Biology and Human Phenotype. *Cells*, *8*(1), 73. https://doi.org/10.3390/cells8010073

Ubersax, J. A., & Ferrell Jr, J. E. (2007). Mechanisms of specificity in protein phosphorylation. *Nature Reviews Molecular Cell Biology*, *8*(7), 530–541. https://doi.org/10.1038/nrm2203

Uchiyama, Y., Takeuchi, R., Kodera, H., & Sakaguchi, K. (2009). Distribution and roles of X-family DNA polymerases in eukaryotes. *Biochimie*, *91*(2), 165–170. https://doi.org/https://doi.org/10.1016/j.biochi.2008.07.005

Udroiu, I., & Sgura, A. (2019). Alternative Lengthening of Telomeres and Chromatin Status. *Genes*, *11*(1). https://doi.org/10.3390/genes11010045

Usta, C., Ozdemir, S., Schiariti, M., & Puddu, P. E. (2013). The pharmacological use of ellagic acid-rich pomegranate fruit. *International Journal of Food Sciences and Nutrition*, *64*(7), 907–913. https://doi.org/10.3109/09637486.2013.798268

van Loon, B., Hübscher, U., & Maga, G. (2017). Living on the Edge: DNA Polymerase Lambda between Genome Stability and Mutagenesis. *Chemical Research in Toxicology*, *30*(11), 1936–1941. https://doi.org/10.1021/acs.chemrestox.7b00152

van Loon, B., Woodgate, R., & Hübscher, U. (2015). DNA polymerases: Biology, diseases and biomedical applications. *DNA Repair*, *29*, 1–3. https://doi.org/https://doi.org/10.1016/j.dnarep.2015.04.001

Visnes, T., Grube, M., Hanna, B. M. F., Benitez-Buelga, C., Cázares-Körner, A., & Helleday, T. (2018). Targeting BER enzymes in cancer therapy. *DNA Repair*, *71*, 118–126. https://doi.org/https://doi.org/10.1016/j.dnarep.2018.08.015

Wang, F., Chen, J., Xiang, D., Lian, X., Wu, C., & Quan, J. (2020). Ellagic acid inhibits cell proliferation, migration, and invasion in melanoma via EGFR pathway. *American Journal of Translational Research*, *12*(5), 2295–2304.

Wang, M., Xue, Y., Shen, L., Qin, P., Sang, X., Tao, Z., Yi, J., Wang, J., Liu, P., & Cheng, H. (2019). Inhibition of SGK1 confers vulnerability to redox dysregulation in cervical cancer. *Redox Biology*, *24*, 101225. https://doi.org/10.1016/j.redox.2019.101225

Wang, Y., Sušac, L., & Feigon, J. (2019). Structural Biology of Telomerase. *Cold Spring Harbor Perspectives in Biology*, *11*(12). https://doi.org/10.1101/cshperspect.a032383

Webster, M. K., Goya, L., Ge, Y., Maiyar, A. C., & Firestone, G. L. (1993). Characterization of sgk, a novel member of the serine/threonine protein kinase gene family which is transcriptionally induced by glucocorticoids and serum. *Molecular and Cellular Biology*, *13*(4), 2031–2040. https://doi.org/10.1128/mcb.13.4.2031-2040.1993

Wong, T. L., Strandberg, K. R., Croley, C. R., Fraser, S. E., Nagulapalli Venkata, K. C., Fimognari, C., Sethi, G., & Bishayee, A. (2021). Pomegranate bioactive constituents target multiple oncogenic and oncosuppressive signaling for cancer prevention and intervention. *Seminars in Cancer Biology*, *73*, 265–293. https://doi.org/https://doi.org/10.1016/j.semcancer.2021.01.006

Wu, Y., Zou, Y., Song, C., Cao, K., Cai, K., Chen, S., Zhang, Z., Geng, D., Zhang, N., Feng, H., Tang, M., Li, Z., Sun, G., Zhang, Y., Sun, Y., & Zhang, Y. (2024). The role of serine/threonine protein kinases in cardiovascular disease and potential therapeutic methods. *Biomedicine & Pharmacotherapy*, *177*, 117093. https://doi.org/https://doi.org/10.1016/j.biopha.2024.117093

Xerxa, E., & Bajorath, J. (2024). Data-oriented protein kinase drug discovery. *European Journal of Medicinal Chemistry*, *271*, 116413. https://doi.org/https://doi.org/10.1016/j.ejmech.2024.116413

Yamtich, J., & Sweasy, J. B. (2010). DNA polymerase family X: function, structure, and cellular roles. *Biochimica et Biophysica Acta*, *1804*(5), 1136–1150. https://doi.org/10.1016/j.bbapap.2009.07.008

Yang, C., Li, J., Sun, F., Zhou, H., Yang, J., & Yang, C. (2020). The functional duality of SGK1 in the regulation of hyperglycemia. *Endocrine Connections*, *9*(7), R187–R194. https://doi.org/10.1530/EC-20-0225

Yang, W., & Gao, Y. (2018). Translesion and Repair DNA Polymerases: Diverse Structure and Mechanism. *Annual Review of Biochemistry*, *87*, 239–261. https://doi.org/10.1146/annurev-biochem-062917-012405

Yoon, J.-H., Basu, D., Sellamuthu, K., Johnson, R. E., Prakash, S., & Prakash, L. (2021). A novel role of DNA polymerase λ in translesion synthesis in conjunction with DNA polymerase ζ. *Life Science Alliance*, *4*(4). https://doi.org/10.26508/lsa.202000900

Zhang, J.-M., Genois, M.-M., Ouyang, J., Lan, L., & Zou, L. (2021). Alternative lengthening of telomeres is a self-perpetuating process in ALT-associated PML bodies. *Molecular Cell*, *81*(5), 1027-1042.e4. https://doi.org/https://doi.org/10.1016/j.molcel.2020.12.030

Zhang, J.-M., Yadav, T., Ouyang, J., Lan, L., & Zou, L. (2019). Alternative Lengthening of Telomeres through Two Distinct Break-Induced Replication Pathways. *Cell Reports*, *26*(4), 955-968.e3. https://doi.org/10.1016/j.celrep.2018.12.102

Zhang, L., Luo, B., Lu, Y., & Chen, Y. (2023). Targeting Death-Associated Protein Kinases for Treatment of Human Diseases: Recent Advances and Future Directions. *Journal of Medicinal Chemistry*, *66*(2), 1112–1136. https://doi.org/10.1021/acs.jmedchem.2c01606

Zhang, T., Zhang, Z., Shengzhao, G., Li, X., Liu, H., & Zhao, Y. (2019). Strand break-induced replication fork collapse leads to C-circles, C-overhangs and telomeric recombination. *PLoS Genetics*, *15*(2), e1007925–e1007925. https://doi.org/10.1371/journal.pgen.1007925

Zhao, Shengyuan, Tadesse, S., & Kidane, D. (2021). Chapter Four - Significance of base excision repair to human health. In U. Weyemi & L. B. T.-I. R. of C. and M. B. Galluzzi (Eds.), *Chromatin and Genomic Instability in Cancer* (Vol. 364, pp. 163–193). Academic Press. https://doi.org/https://doi.org/10.1016/bs.ircmb.2021.05.002

Zhao, Shuang, Wang, F., & Liu, L. (2019). Alternative Lengthening of Telomeres (ALT) in Tumors and Pluripotent Stem Cells. *Genes*, *10*(12), 1030. https://doi.org/10.3390/genes10121030

Zhou, C., Xiao, W., Jiang, T., Guo, Z., Li, M., Chang, H., Wu, Y., Chen, M., Shi, M., Xu, W., & Gao, Y. (2020). Targeting SGK1 enhances the efficacy of radiotherapy in locally advanced rectal cancer. *Biomedicine & Pharmacotherapy*, *125*, 109954. https://doi.org/https://doi.org/10.1016/j.biopha.2020.109954

Zhu, R., Yang, G., Cao, Z., Shen, K., Zheng, L., Xiao, J., You, L., & Zhang, T. (2020). The prospect of serum and glucocorticoid-inducible kinase 1 (SGK1) in cancer therapy: a rising star. *Therapeutic Advances in Medical Oncology*, *12*, 1758835920940946. https://doi.org/10.1177/1758835920940946